Трудности сейсмической инверсии и построения сейсмических изображении

Advanced seismic processing and imaging

(Part I)

By Evgeny Landa

Petergof - 2015

Acknowledgments

This course contains contribution of many friends and colleagues and it is often inspired by work of others: ***Sergey Goldin, Sergey Fomel, Vladimir Glogovsky, Tijmen Jan Moser, Tury Taner, Albert Tarantola, Tad Ulrych…***

To all of them I am greatly thankful.

I want to acknowledge several companies that provided me with field examples illustrating applications of different non-conventional imaging methods: TOTAL, GII, Geomage, TEEC, Petrologic, Landmark, Shell

Чем определяется удача в науке? В первую очередь - это выдающиеся учителя.

В науке есть те, которые пробивают стены, а есть другие, которые потом в течении 100 лет расчищают осколки

Sergey Goldin

Нет ничего постыдного быть игнорантом, то есть не знать чего либо. Но очень опасно быть игнорантом наполовину - то есть претендовать, что ты знаешь все

Tury Taner

Все люди имеют мозг: разной формы и размера. Но только немногие имеют УМ (познавательные и аналитические способности). Ум как правило сочетается с душой.

Tad Ulrych

Наблюденные данные не могут предсказать модель. Они могут только отрицать неправильные модели.

Albert Tarantola

Одномерная обратная задача может быть решена путем бурения одной скважины

Vladimir Glogovsky

Многому я научился у своих наставников, еще большему — у своих товарищей, но больше всего — у своих учеников.

Talmud

In this course:

- I do not pretend to teach you a part of seismic that is known pretty well.
- I will not tell you about a subject that has been very thoroughly analyzed.
- I will not propose or describe a new completely developed algorithms or numerical schemes for seismic imaging or inversion.
- I will not compare different methods and algorithms.

The course has a conceptual character and I will try as accurately as I can to describe new ideas, new visions, new dreams (why not!) which hopefully can lead to substantial progress in both resolution and reliability of seismic exploration.

О понимании

- Я постараюсь объяснить вещи так, чтобы вы смогли понять. Но может случиться , что вы не поймете то, что я буду рассказывать.
- Моя задача сделать так, чтобы вы не ушли, чтобы вы остались.
- Если это поможет... Я тоже не все понимаю. Никто не понимает всего...

Есть много причин, почему мы можем не понять рассказчика:

- Его язык плохой - он не говорит того, что думает или рассказывает наоборот
- Рассказчик использует слова не в их обычном смысле ("работа", "энергия", "свет")
- Когда рассказчик описывает как Природа работает, вы не понимаете ***почему*** Природа работает именно так (никто не понимает этого)
- После того, как рассказчик говорит что либо, мы просто не верим ему. Или мы просто не любим то, что он говорит

Концептуальный характер курса не позволяет мне представить многие вещи в строгой математической формулировке. Да это и не является моей целью. Попробую объяснить это на примере (по Фейнману):

"Когда то давно индейцы Майя интересовались восходом и закатом планеты Венера... Для вычислений, они придумали систему "палочек и точек", чтобы представлять числа и они имели правила для вычислений и предсказаний... В те далекие дни только священники Майя могли делать такие сложные расчеты. Как бы священник сегодня объяснил бы нам, что такое вычитание. Он мог бы либо научить нас их преставлению чисел с помощью точек и палочек, и их правилам... или он мог бы рассказать нам, что он в принципе делает: "Допустим мы хотим вычесть 236 из 584. Сначала, мы отсчитываем 584 фасоли и кладем их в горшок. Потом вынимаем 236 фасолей... В конце мы считаем оставшиеся в горшке фасоли..." Вы можете сказать: "Как примитивно, считать фасоли..." Священник мог бы ответить: "Поэтому мы имеем правила для точек и палочек. Правила эти сложны, но эффективны... Важно то, что нет разницы относительно результата: мы можем предсказать появление Венеры считая фасоли (что долго, но легко объяснимо) или используя сложные правила (что намного быстрее, но требует годы обучения)"

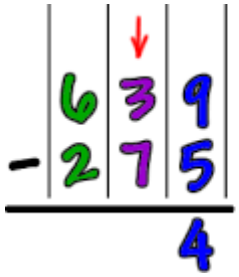

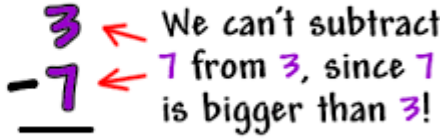

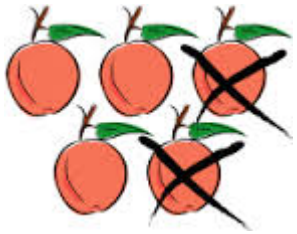

In memory of my teacher and friend
Sergey Goldin

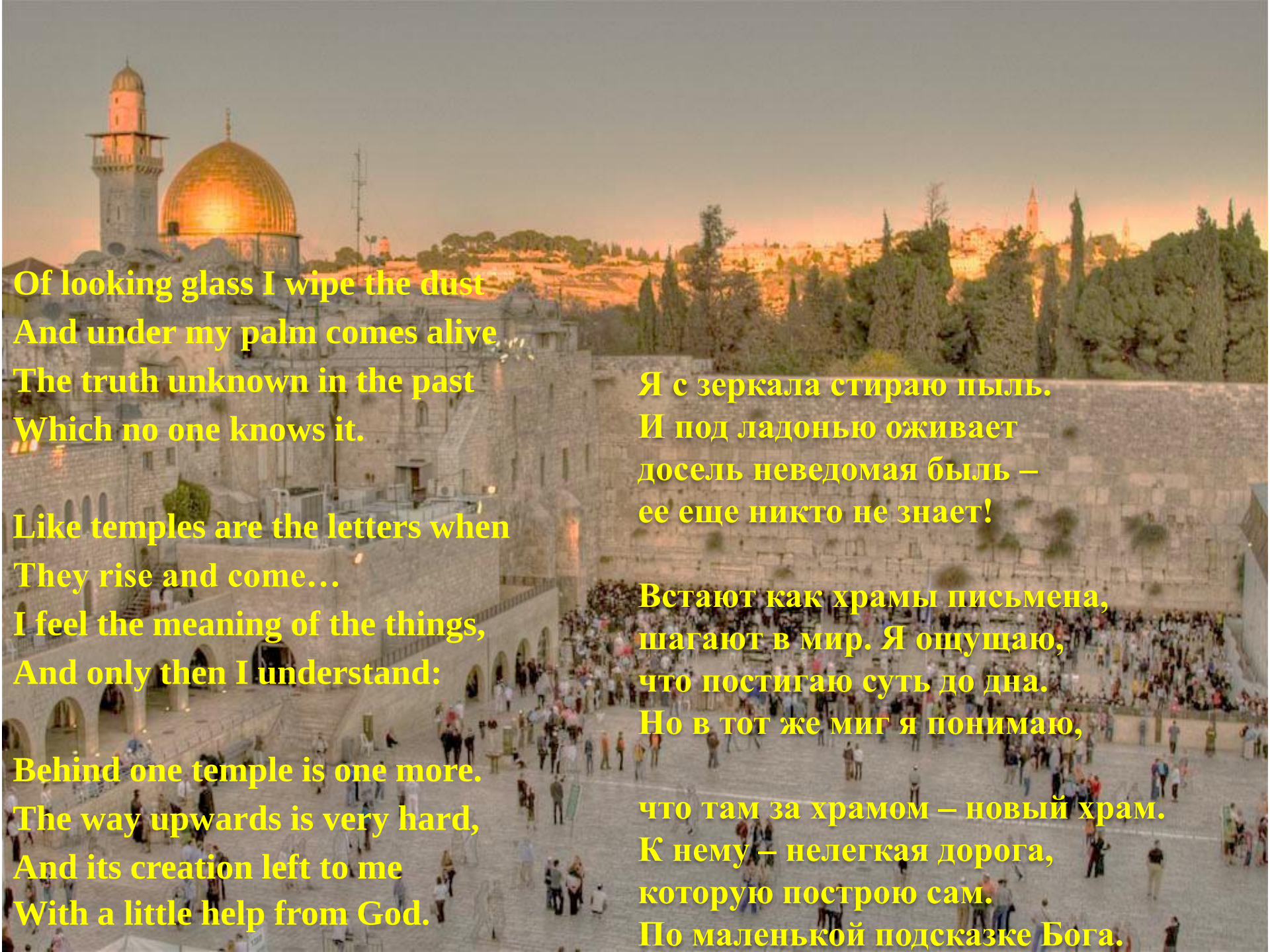

Of looking glass I wipe the dust
And under my palm comes alive
The truth unknown in the past
Which no one knows it.

Like temples are the letters when
They rise and come…
I feel the meaning of the things,
And only then I understand:

Behind one temple is one more.
The way upwards is very hard,
And its creation left to me
With a little help from God.

Я с зеркала стираю пыль.
И под ладонью оживает
досель неведомая быль –
ее еще никто не знает!

Встают как храмы письмена,
шагают в мир. Я ощущаю,
что постигаю суть до дна.
Но в тот же миг я понимаю,

что там за храмом – новый храм.
К нему – нелегкая дорога,
которую построю сам.
По маленькой подсказке Бога.

“Birds and Frogs”

Бывают учёные-птицы, а бывают и учёные-лягушки. Птицы парят в вышине и обозревают обширные пространства математики, сколько видит глаз. Наслаждение им доставляют понятия, которые сводят наши размышления воедино и позволяют совместно рассматривать задачи, возникающие в разнообразных элементах пейзажа. Лягушки же копошатся далеко внизу в грязи и видят только растущие поблизости цветы. Для них наслаждение — внимательно разглядывать конкретные объекты; задачи они решают последовательно, одну за другой.

Математика сложна и прекрасна потому, что птицы привносят в неё широкий взгляд, а лягушки — замысловатые детали. Математика сочетает в себе общность принципов и глубину структур, что делает её и великим искусством, и важной наукой. Было бы глупо утверждать, что птицы лучше лягушек, ибо видят дальше, или что лягушки лучше птиц, ибо проницают глубже. Мир математики широк и глубок, и для его изучения нужны и птицы, и лягушки.

Freeman Dyson

Goldin’s legacy

FROM STATISTICS TO DETERMINISM AND DUALITY

- Бедные эмпирические данные приводят к очень упрощенным статистическим моделям и отсутствию статистического анализа экспериментальных данных

- "В конце концов можно научить обезьяну строить функцию правдоподобия“

- Сейсмический сигнал состоит в основном из функции источника, среды распространения и условий приема. Эти компоненты обычно рассматриваются как чисто детерминистические.

- Движение в сторону чистого детерминизма тоже неверно. Когда детерминизм выполнил свою функцию и помеха должна быть принята во внимание, статистика необходима.

- Ричард Фейнман, в своей знаменитой классификации науки, поставил геофизику на 11 (почти самую высокую) ступень сложности, охарактеризовав её как "непрерывный спектр неоднородностей".

- Чистый детерминизм и описание среды с помощью гладких кусочно-непрерывных функции не соответствует этому определению.

FORMALISM AND OVERCOMING UNCERTAINTY

- Насколько обратная геофизическая задача может быть формализована?
- Применение определенного решения задачи построения сейсмического изображения - это область интерпретации, которая не относится к математической теории.
- Разрыв между неизвестной геологической ситуацией и известным модельным решением может быть заполнена только если мы понимаем, что невозможно полностью формализовать обратную задачу
- Является ли степень использования математики показателем зрелости науки?
- Математика помогает выполнять вещи эффективно

EFFICIENCY AND UNDERSTANDING

- Для многих ученых цель любого исследования - это получение новых данных
- Наука не ограничивается новыми знаниями. Необходимо, чтобы наука улучшала что либо в человеческой жизни и повседневной деятельности человека
- Новые методы часто предлагаются талантливыми людьми с хорошей интуицией, но в то же время без ясного физического видения и понимания
- Эффективность не необходима для понимания

«Наука – баба веселая и паучьей серьезности не терпит»
Тимофеев-Рессовскии

Наука как сфера человеческой деятельности

- **Н**аука – это люди
- **Н**аучные традиции, научные школы создаются медленно; достаточно двух деградирующих поколений, чтобы потерять
- **Н**аука – это игра; игровое поле – семинары
- **Ф**акт становится научным результатом, когда он проинтерпретирован научным сообществом

- **Н**аука - лучшии вид человеческой деятельности; в научном творчестве человек может достигнуть максимальной свободы

- **М**ожно ли говорить об особенных моральных качествах ученых? Ученый может ошибаться, но его заблуждения должны быть искренними

- **С**ергей Гольдин: качество, прежде всего, присущее материальному миру – сложность

- **Р**ичард Фейнман - фундаментальные законы физики могуть быть описаны разными путями; в этом отображение простоты фундаментальных законов

Goldin’s legacy

- **О**бычно мы наблюдаем не отдельные простые явления, а сложный феномен взаимодействия простых идей

- « **Н**е та сложность, которая похожа на высокую гладкую стену, а скорее скала, где всегда найдешь место, куда поставить ногу, и подняться на полметра выше… »

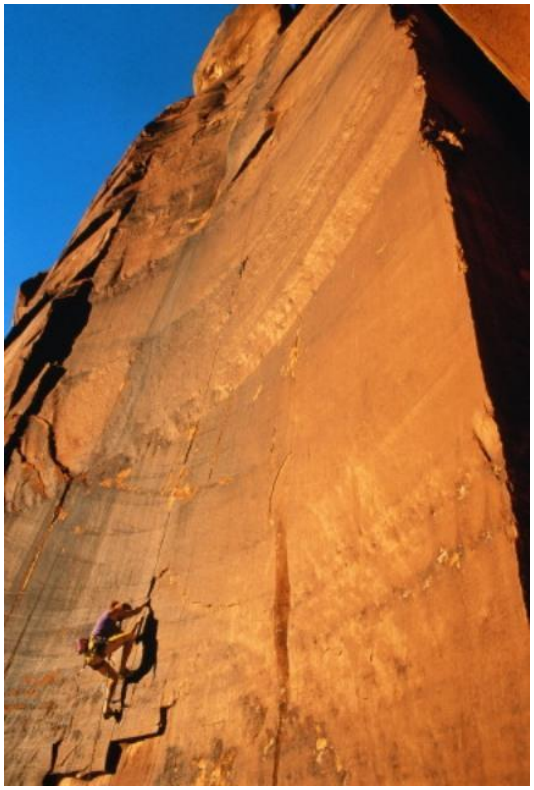

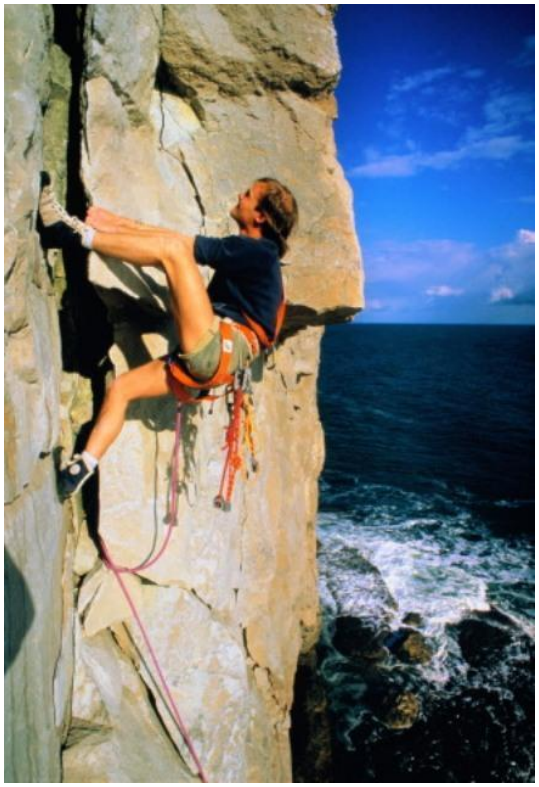

Content

- **Non-CMP based processing**
- **Velocity model building by recursive prestack datuming**
- **Diffraction imaging**
- **Pitfalls and challenges in seismic inversion**
- **Quantum seismic imaging: is it possible?**

Preamble

While depth imaging plays an increasing role in seismic exploration, prestack data analysis and imaging in time domain remain important issues in processing and interpretation. Time imaging provides sufficient information for a variety of subsurface models of moderate complexity. Moreover, for more complex models that request the use of prestack depth migration, time imaging usually constitutes a key first step.

Time vs. Depth Imaging

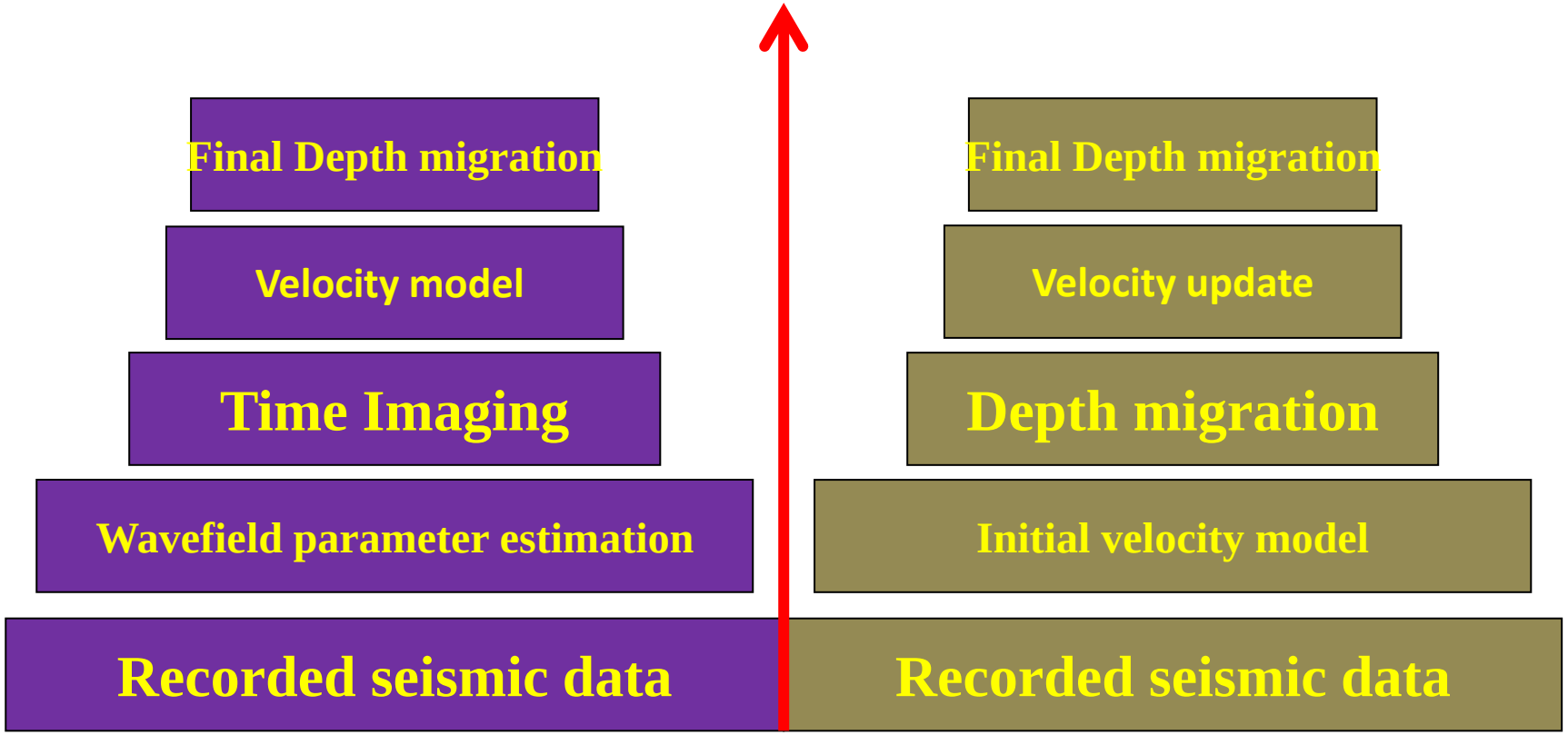

Decomposition of the total wavefield into body waves is one of the fundamental principles of the seismic reflection method

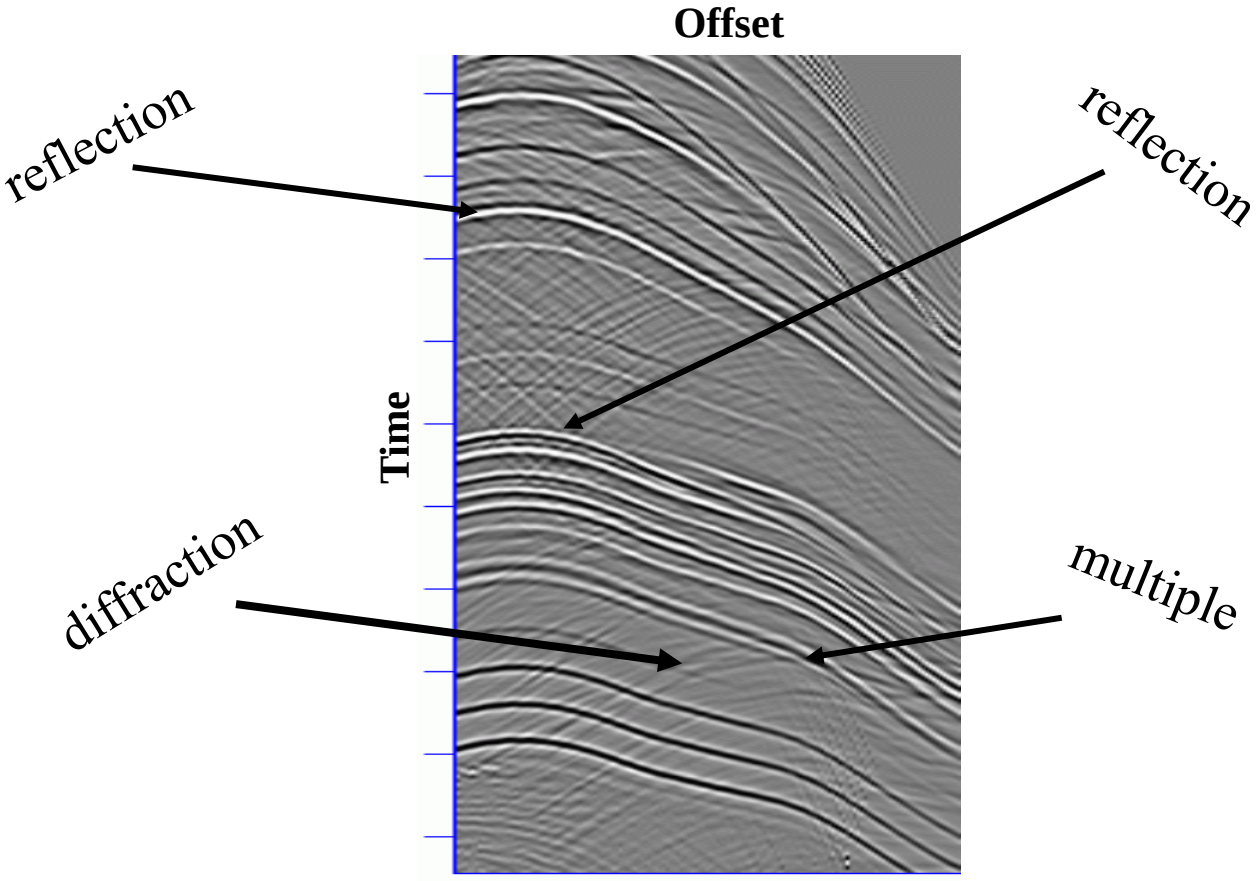

Correlation

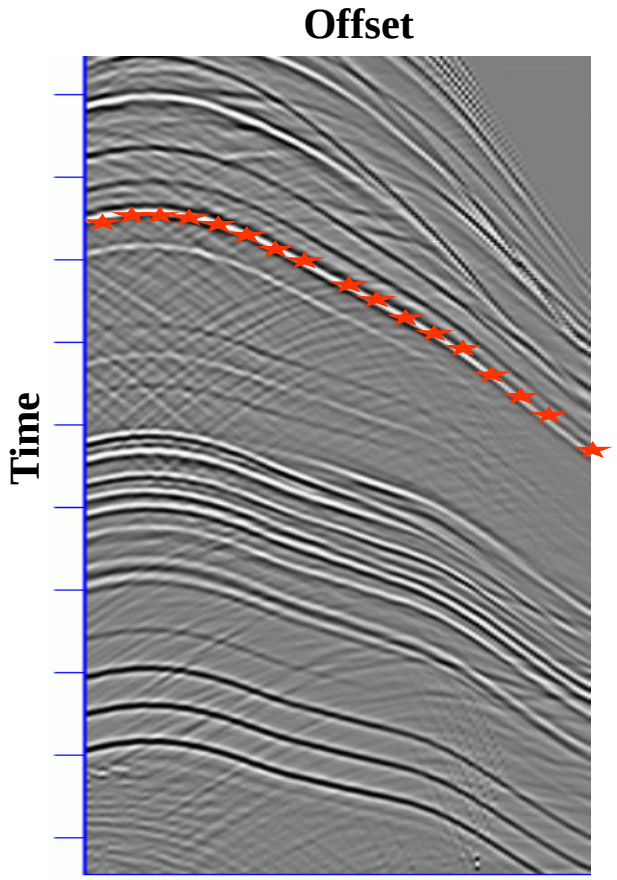

Moveout correction

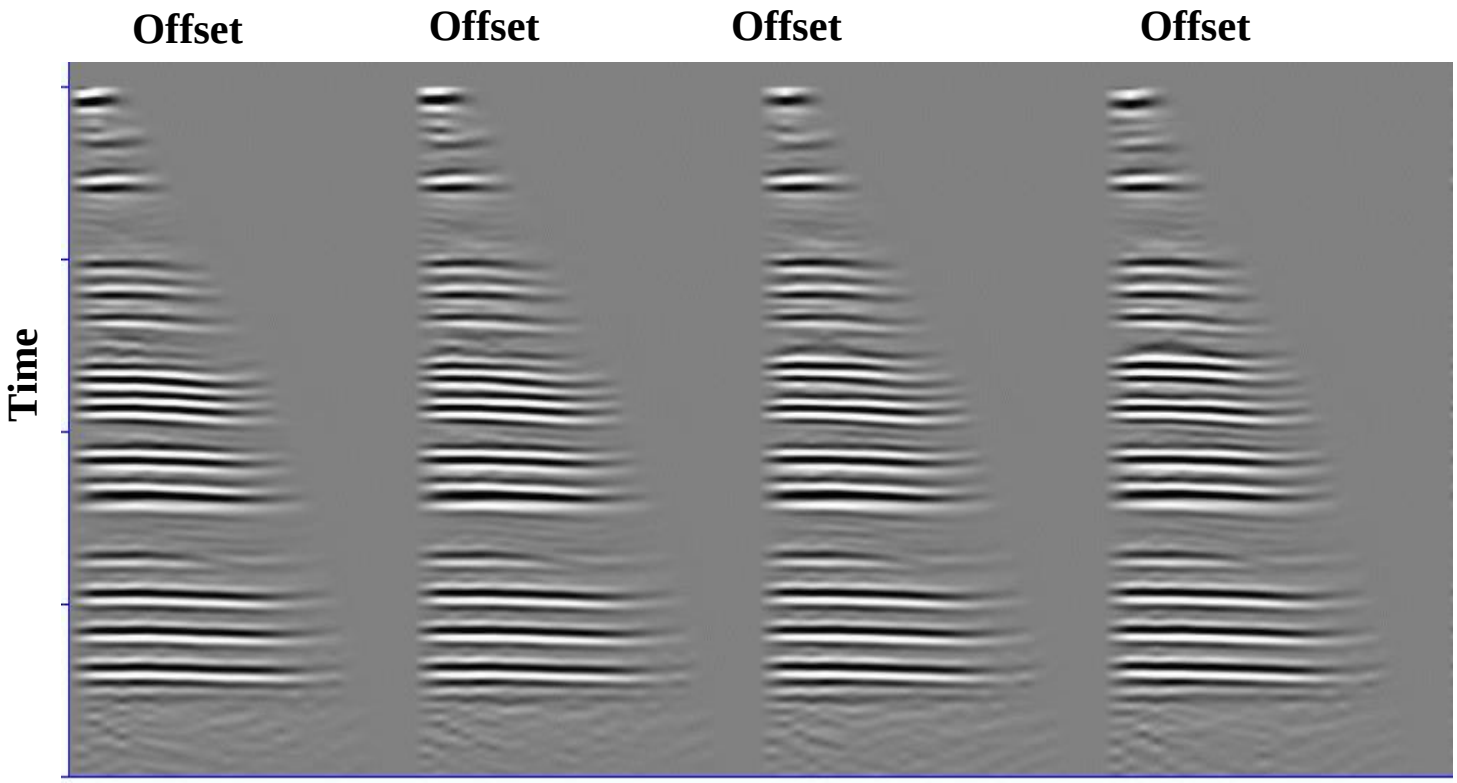

Stack

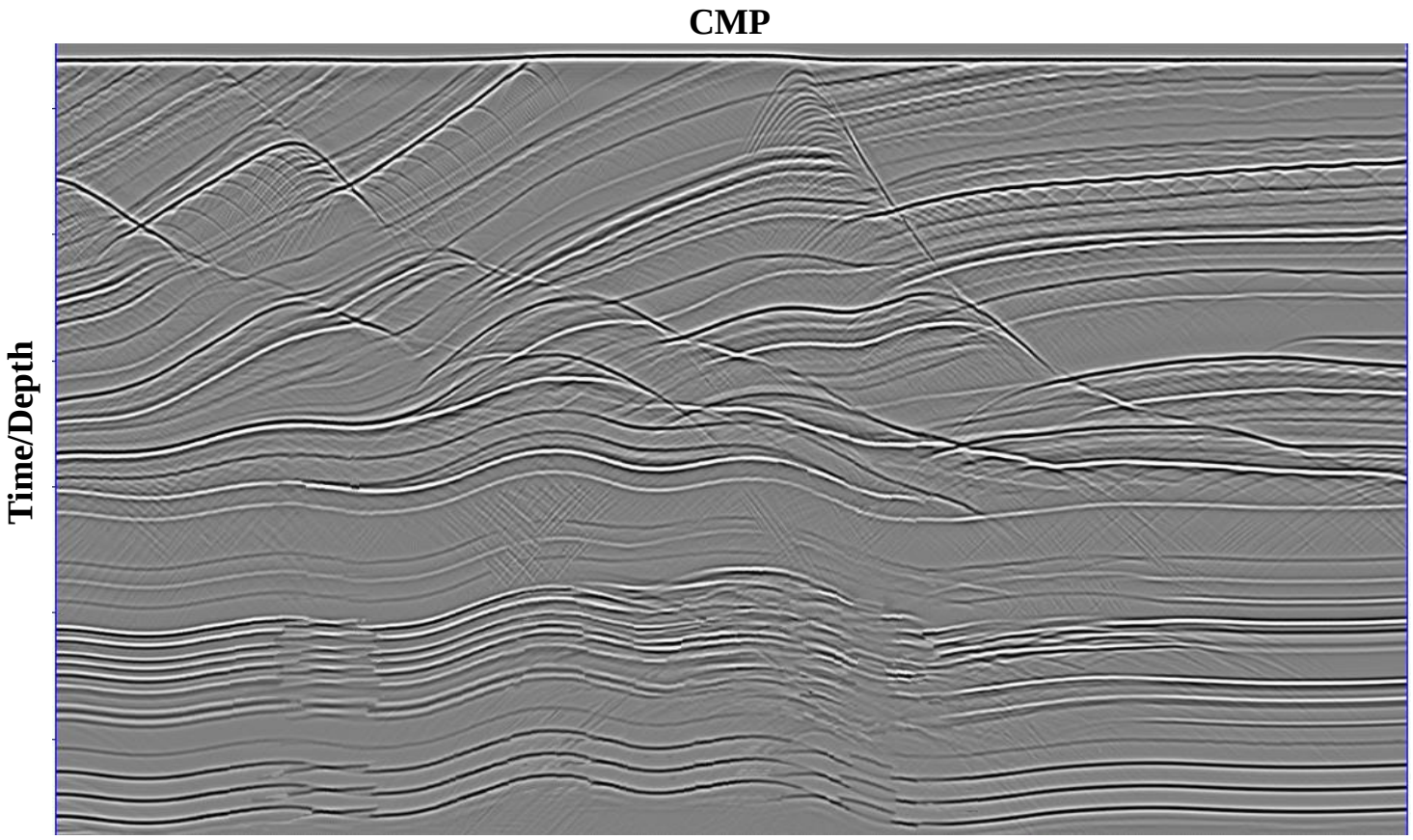

Time field

"Each seismic operator is a function of two pairs parameters"
G. Gamburtsev

The most important characteristic of seismic wavefield is arrival times of different type of waves

$$T(\vec{s},\vec{r})$$

The time field (time surface) contains an important information about the subsurface. A section of the time field is named **"traveltime curve"**.

For example, CMP time field can be define in this case as:

$$T(m,h)$$

$$m=(s+r)/2 \quad h=(s-r)/2$$

What is the main physical meaning of this coordinate transform?

- In models with a moderate complexity, lateral velocity variations (including reflector geometry) of the subsurface appear mostly in sections *h=constant* of the function $T(m,h)$, while velocity in the overburden including vertical velocity variations appear mostly in sections *m=constant.*

- Function $T(m,h)$ is even with respect to variable *h* . It means that section $T_m(h)$ (traveltime curve) is a symmetric function:

$$T(m,h) = T(m,-h)$$

Approximation of the CMP traveltime:

$$T(m,h) = \sqrt{(t_0^2(m) + a_1(m)h^2 + a_2(m)h^4 + \ldots}$$

$$a_1 = 4\cos^2\psi / V_{\text{int}}^2$$

Introduction of the time field important because it has features which does not have the "classical" traveltime curve $T_s(r)$

Time field is directly connected to solutions of forward and inverse kinematic problems.
Estimation of the time field from the observed data is a crucial issue in solving problems of velocity model building and seismic imaging.
The simplest statistical model of a trace is:

$$u(t,s,r) = f((t-\tau(s,r)) + \xi(t,s,r)$$

To estimate the time field is possible by:

$$F[\sum_{s,r\in\sigma} u(t+\tau(s,r,\vec{c}))] \to \max_{\vec{c}}$$

C is a parameter vector describing the time field

We distinguish between local parameters $\vec{c}^{\,i}$ and global $\langle \vec{c}^{\,j} \rangle$.

Global estimate of the time field $\widehat{\alpha}$ is taken as a collection of local estimates

$$\langle u^j \rangle \to \langle c^j \rangle = \widehat{\alpha}$$

Velocity model $\vec{\theta}$ can be computed as

$$\langle u^j \rangle \to \langle c^j \rangle \to \widehat{\alpha} \to \vec{\theta}$$

$$\langle u^j \rangle \to \langle \vec{\theta}^{\,j} \rangle \to \vec{\theta} \quad \text{or even} \quad \langle u^j \rangle \to \vec{\theta}$$

Time Imaging

Time correction equation is a key to successful time imaging.

This equation should satisfy two conditions:

1. **It should be valid for arbitrary media** (be model independent);
2. **It should be valid for arbitrary observation geometry**

Why CMP method *works* ?

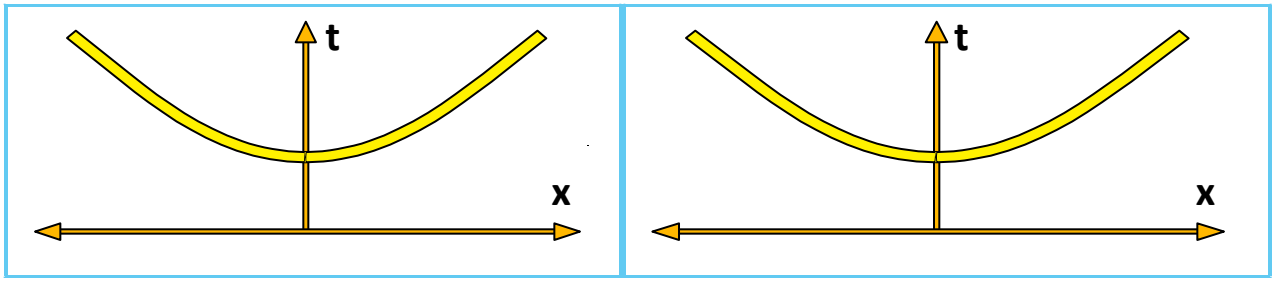

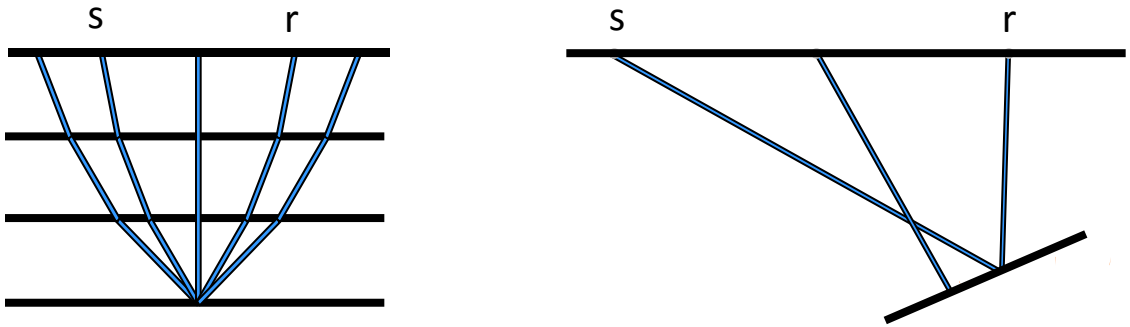

$$t(m) = \sqrt{t_0^2(m) + \frac{4h^2}{V_{st}^2}}$$

Stacking chart

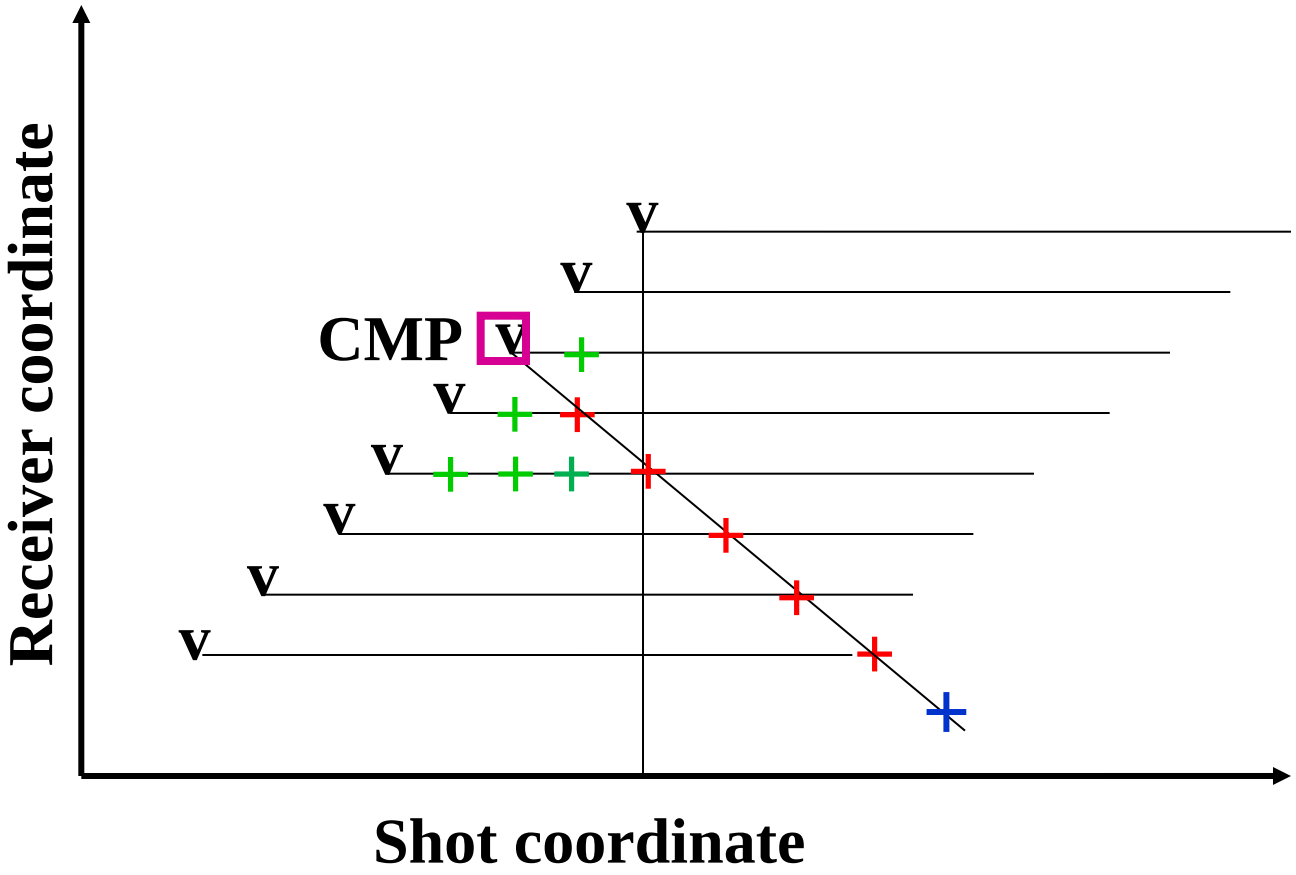

Convex interface

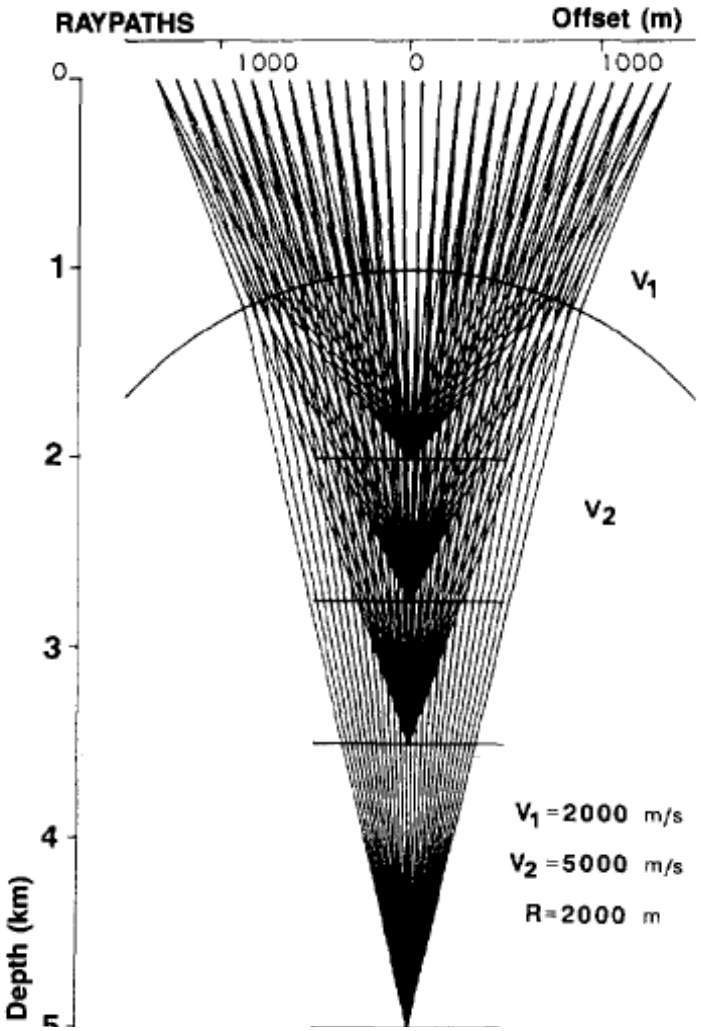

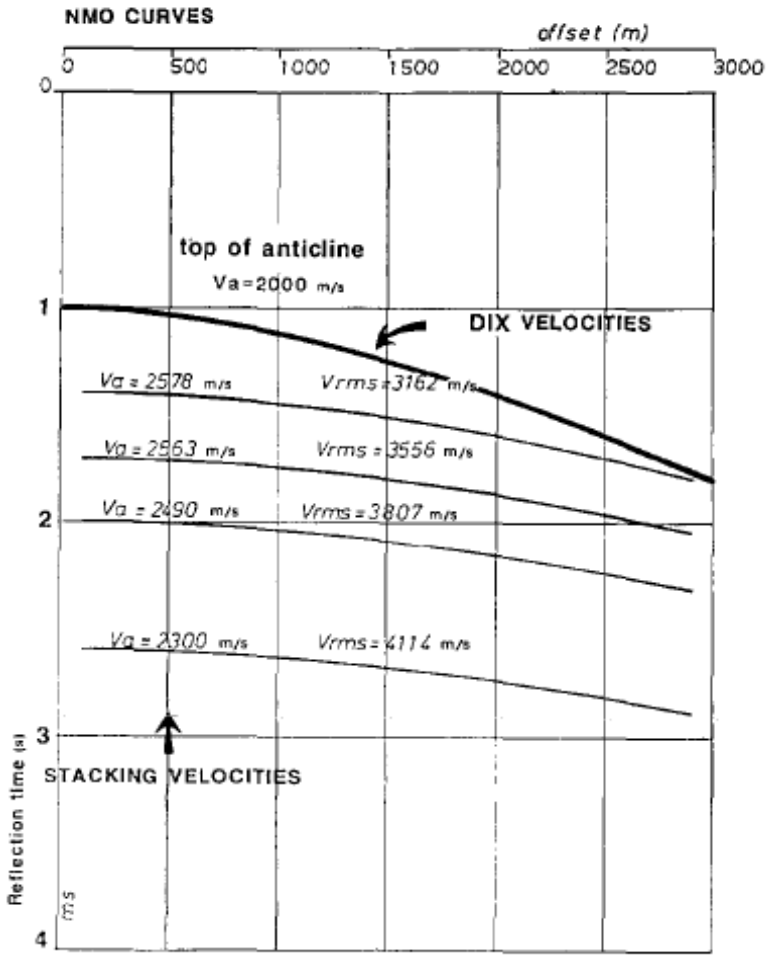

After de Bazelaire, 1988

RMS velocities are computed and stacking velocities are estimated using a velocity analysis. Interval velocities computed by Dix formula are completely wrong

Concave interface

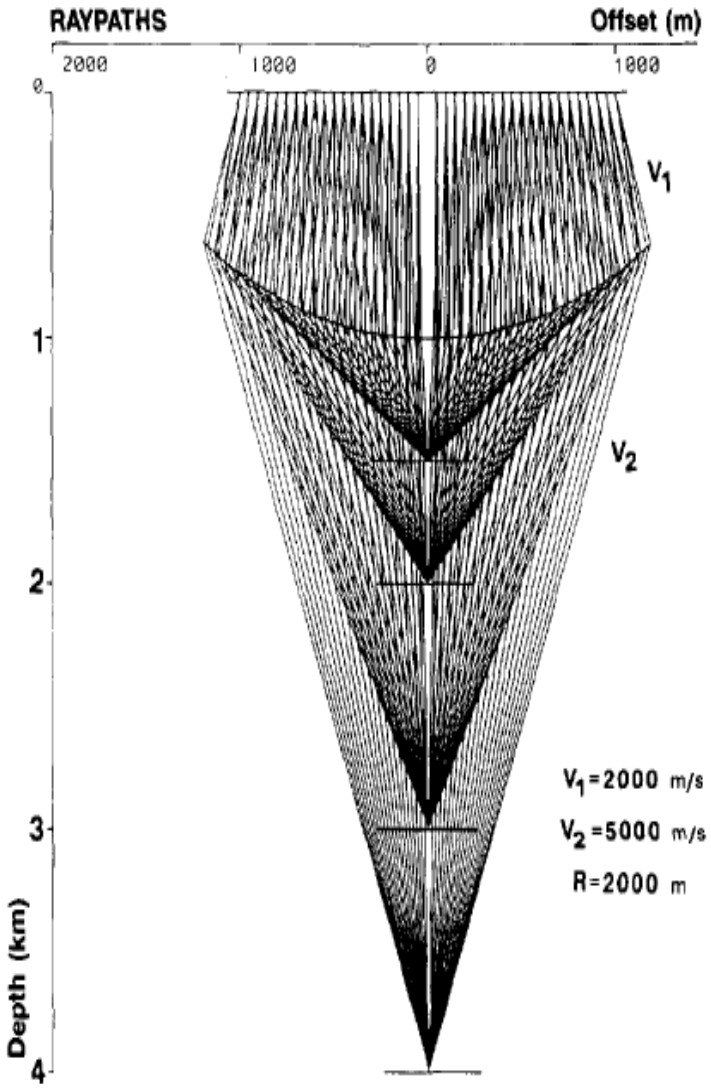

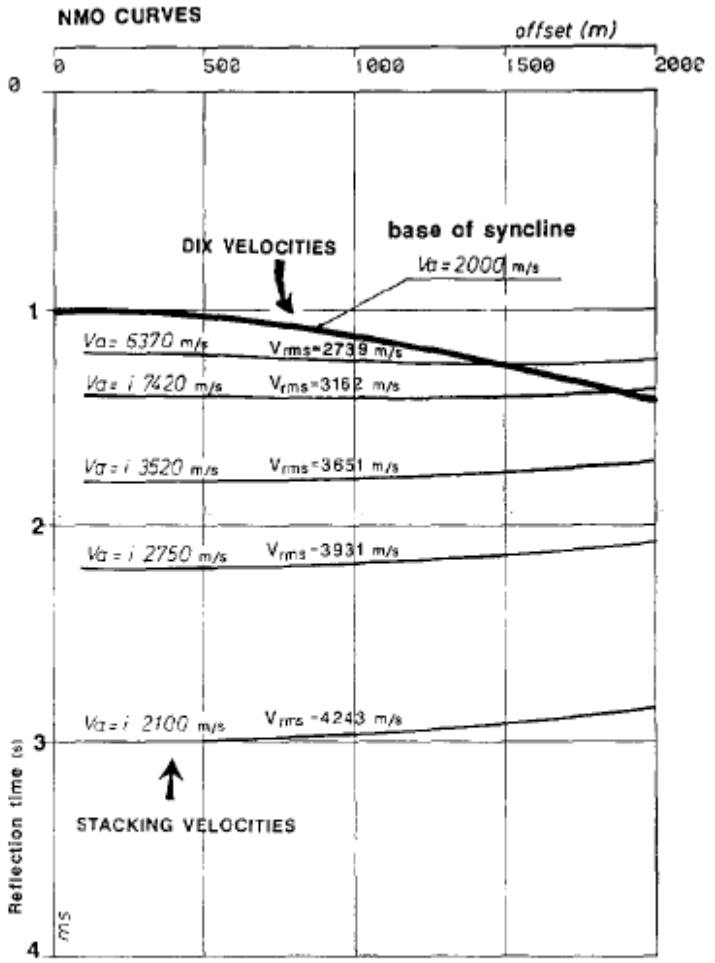

After de Bazelaire, 1988

All the NMO curves have inverse curvature. Stacking velocities are imaginary.

These CMP records show that upward curvatures can actually be observed.
The corresponding stacking velocities are imaginary.

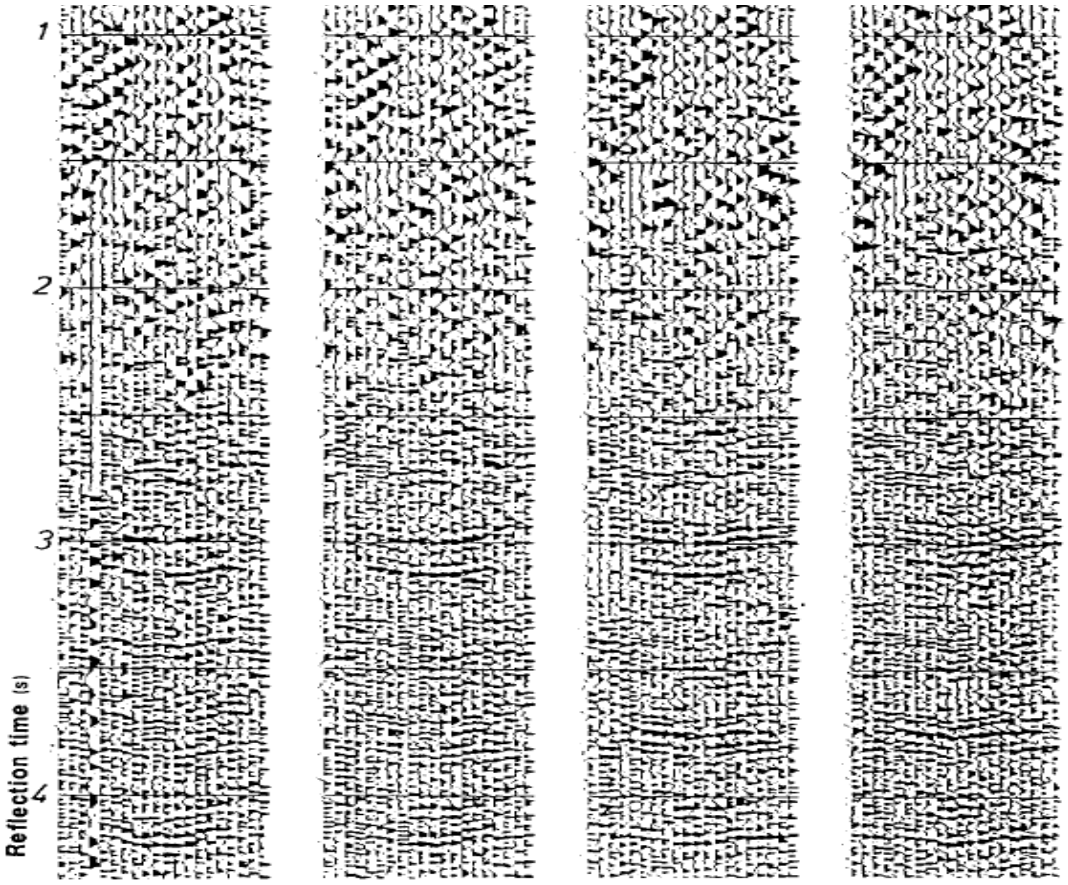

After de Bazelaire, 1988

Shifted hyperbola

The ‘delayed ’ or ‘ shifted ’ hyperbola (de Bazelaire 1988) is not symmetrical about the x-axis. It includes two parameters, the reflection time t_0 and the focusing time t_r , and is given by

$$(t+t_r)^2 = (t_0+t_r)^2 + x^2/V_a^2$$

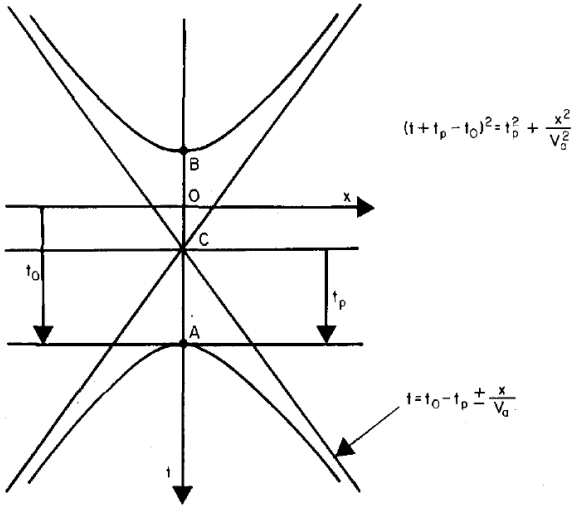

V_a , average velocity

$t_r = AM'/V_1 - AM/V_2$ *is the difference between the actual and vertical traveltime*

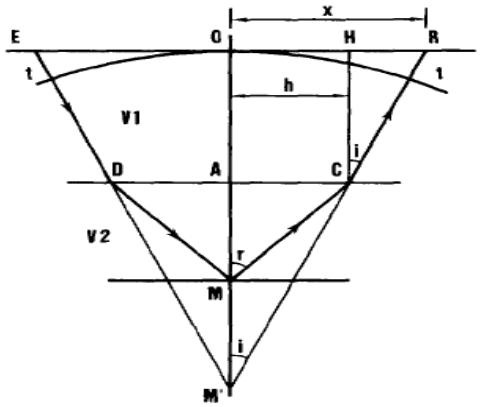

The centers of these hyperbolas do not coincide with the center of coordinates, but are shifted along the time axis.

Actual ray path TMR and equivalent ray path $TM'R$ for two media, plane and parallel layers, with small apertures.

De Bazelaire, E., 1988, Normal moveout revised – Ingomogeneous media and curved interfaces: *Geophysics*, 53, 143-157

Shifted hyperbola

Making the variable change $t_p = t_0 - t_r$ and after some algebraic transformation, we obtain a shifted hyperbola moveout correction:

$$t = t_0 - t_p + \sqrt{t_p^2 + 4h^2 / V^2}$$

For small offsets the parameter *V* may be replaced by the near surface velocity, resulting in a robust single-parameter correlation procedure. For a given t_p, the correction is a function of a trace distance to the source only. Whatever the time t_0, all the seismic events which can be stacked into focus at this time are corrected simultaneously.

Shifted hyperbola

All the events that assume the shape of a hyperbola receive equal treatment. However the multiples have very different velocities. Clear where the reflections stop and where the diffractions start.

Shifted hyperbola stack

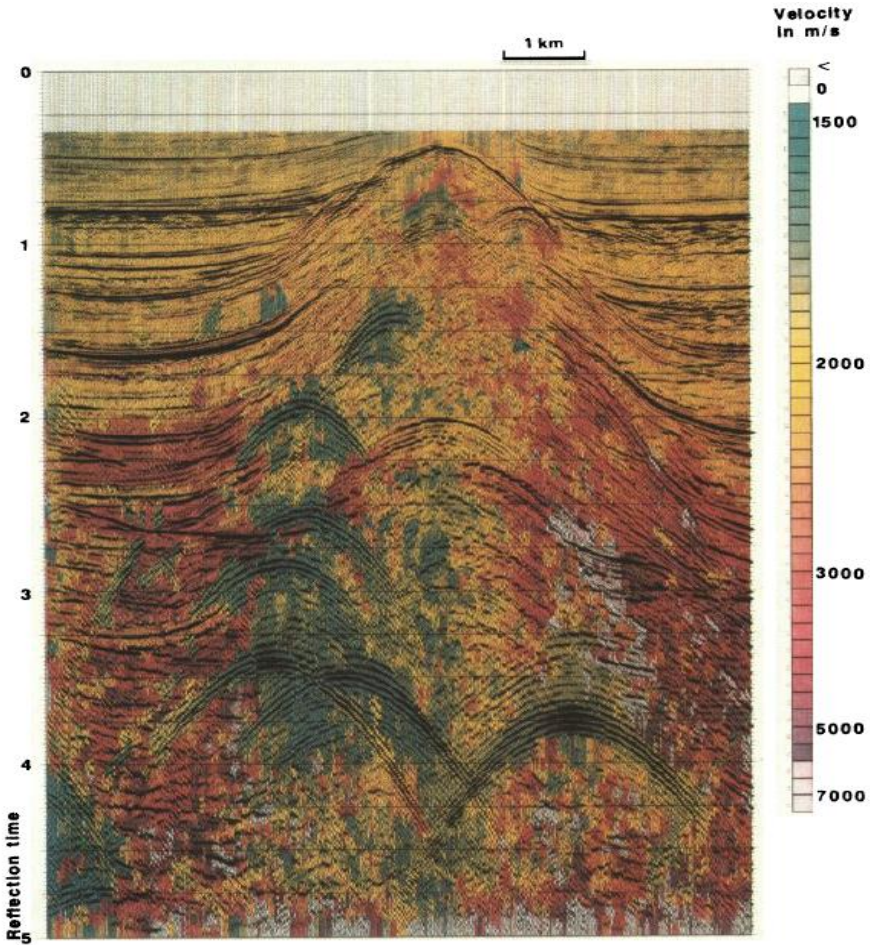

Conventional stack

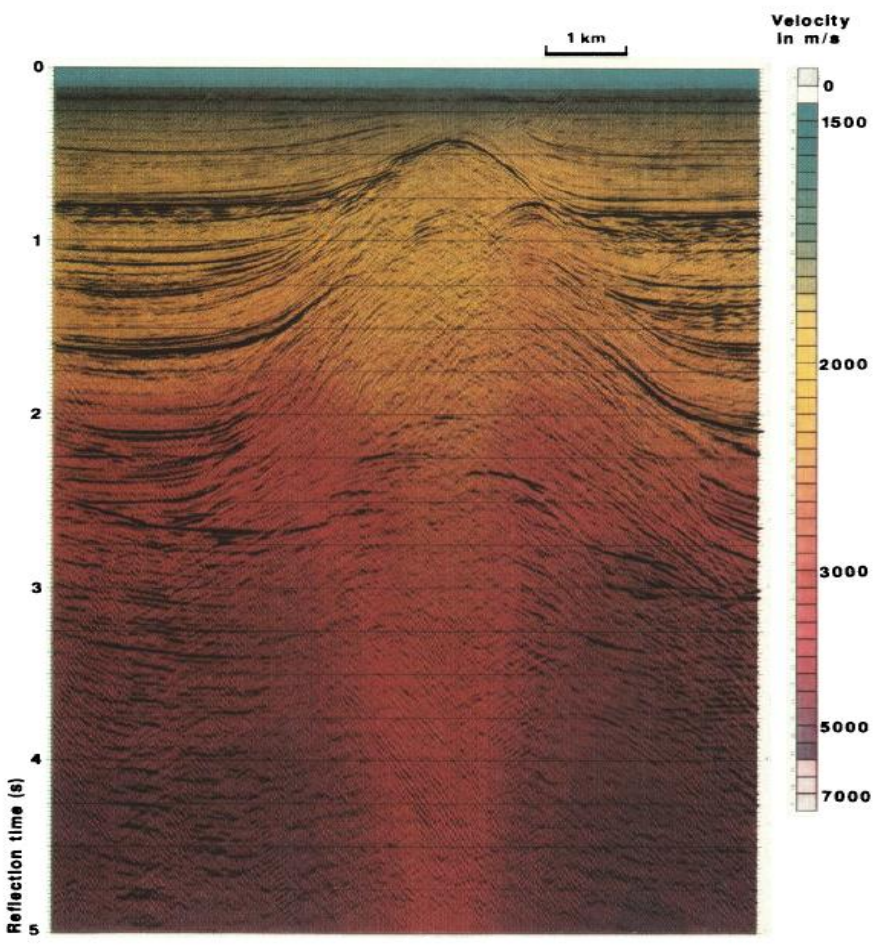

After de Bazelaire, 1988

Non-hyperbolic (anisotrophic) moveout

$$t^2(x) = t_0^2 + A_2 x^2 + \frac{A_4 x^4}{1 + Ax^2}$$

$$A_2 = \frac{1}{\alpha_0^2 (1 + 2\delta)},$$

$$A_4 = -\frac{2(\varepsilon - \delta)[1 + 2\delta(1 - \frac{\beta_0^2}{\alpha_0^2}]^{-1}}{t_0^2 \alpha_0^2 (1 + 2\delta)^4}$$

$$A = \frac{A_4}{v_h^{-2} - A_2}$$

where ε *and* δ represent the Thomsen anisotropic parameters,
α_0 *and* β_0 are the vertical P and S velocities and

$v_h = \sqrt{\alpha_0 (1 + \varepsilon)}$ is the horizontal velocity

Offset dependent NMO velocity model

Non-hyperbolic behaviors can be modeled using the horizontal velocity acceleration model

$$t(x) = \sqrt{t_0 + x^2 / V^2(x)} \qquad V(x) = V_0 + ax^2$$

where V_0 is the velocity at zero offset, and *a* is a *horizontal velocity acceleration parameter*. Both parameters can be estimated from the data

For horizontally stratified model:

$$V_0 = \frac{\sum_{j=1}^{N} x_j^4 \sum_{j=1}^{N} V(x_j) - \sum_{j=1}^{N} x_j^2 \sum_{j=1}^{N} x_j^2 V(x_j)}{N \sum_{j=1}^{N} x_j^4 - \left(\sum_{j=1}^{N} x_j^2 \right)^2}$$

$$a = \frac{N \sum_{j=1}^{N} x_j^2 V(x_j) - \sum_{j=1}^{N} x_j^2 \sum_{j=1}^{N} V(x_j)}{N \sum_{j=1}^{N} x_j^4 - \left(\sum_{j=1}^{N} x_j^2 \right)^2}$$

Taner, T., S. Treitel, M. Al-Chalabi, and S. Fomel, 2007, An offset dependent NMO velocity model, EAGE meeting.

Comparison of different CMP approximations

The Taylor series of the standard hyperbola, Alkalifa & Tsvankin, Taner's and de Bazelair's. Each formula is expanded up to the 4th order:

$$T_4(x)_{stand} = t_0 + \frac{1}{2v_{st}^2 t_0} x^2 - \frac{1}{8v_{st}^4 t_0^3} x^4$$

$$T_4(x)_{Alk} = t_0 + \frac{1}{2v_{st}^2 t_0} x^2 - (\frac{\eta}{v_{st}^4 t_0^3} + \frac{1}{8v_{st}^4 t_0^4}) x^4$$

$$T_4(x)_{Taner} = t_0 + \frac{1}{2v_{st}^2 t_0} x^2 - (\frac{\alpha}{v_{st}^4 t_0^3} + \frac{1}{8v_{st}^4 t_0^4}) x^4$$

$$T_4(x)_{shift} = t_0 + \frac{1}{2v_a^2 t_p} x^2 - \frac{1}{8v_a^4 t_p^4} x^4$$

Standard, Alkalifa's and Taner contain the same second-order coefficients. Shifted hyperbola depends on v_a *and* t_p. Relationship between v_{st}, v_a, t_0 *and* t_p:

$$v_a^2 t_p = v_{st}^2 t_0$$

After Sabrina Ernst, 2006

Comparison of different CMP approximations

Synthetic model

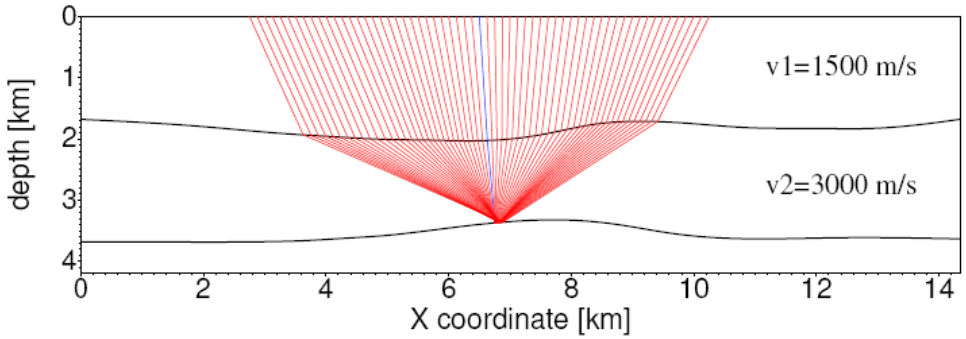

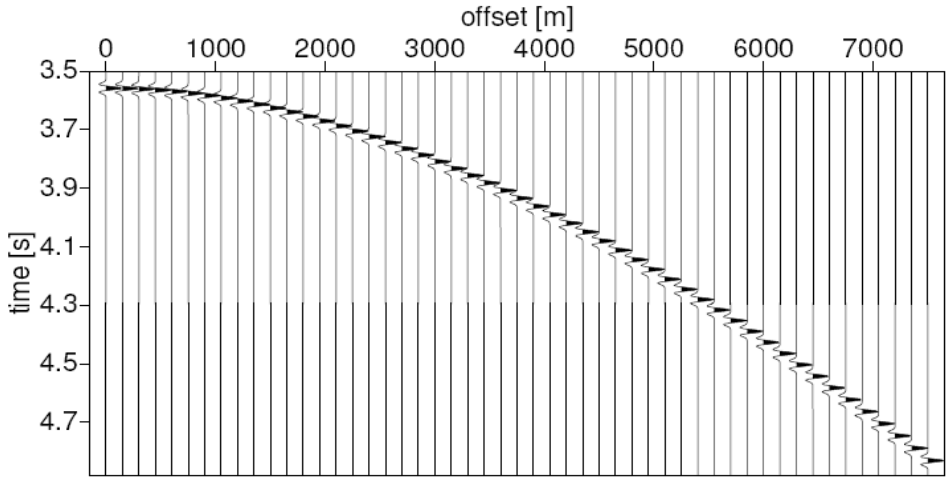

After Sabrina Ernst, 2006

Comparison of different CMP approximations

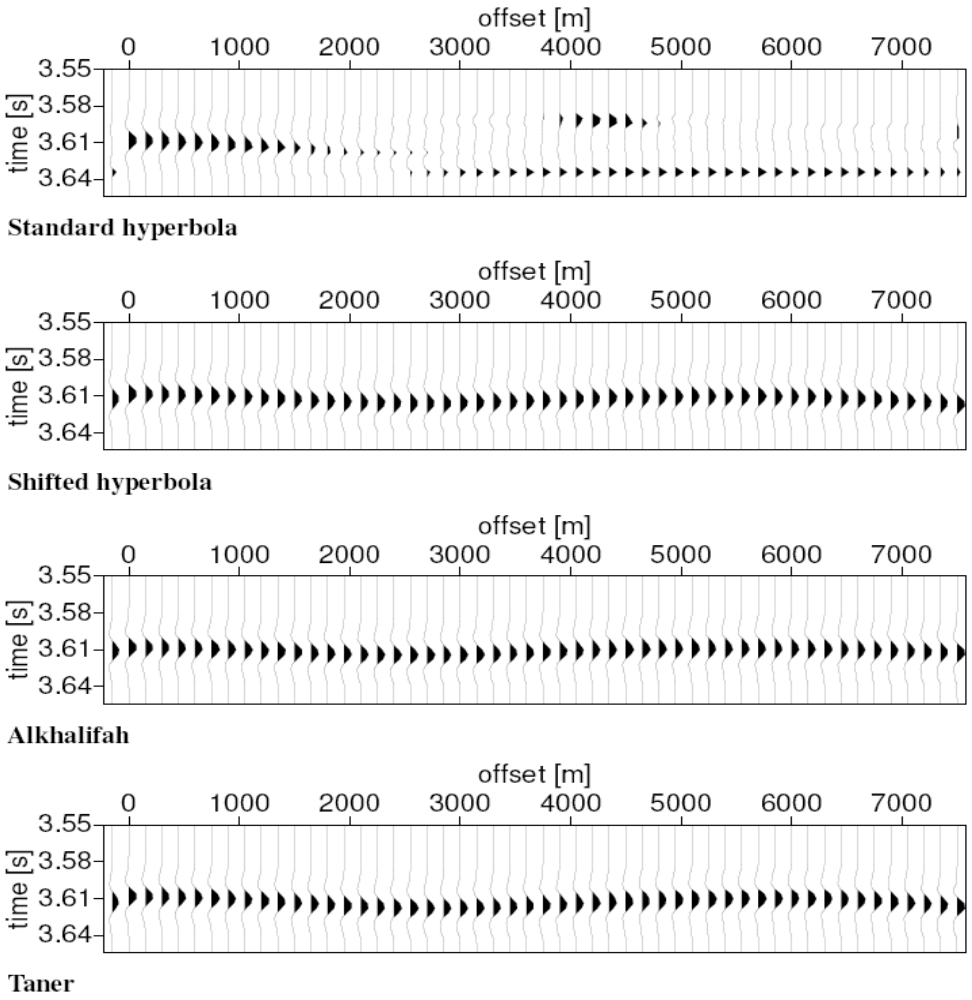

Traveltime could be adequately described by two-parameter equation

After Sabrina Ernst, 2006

Comparison of different CMP approximations

Synthetic model

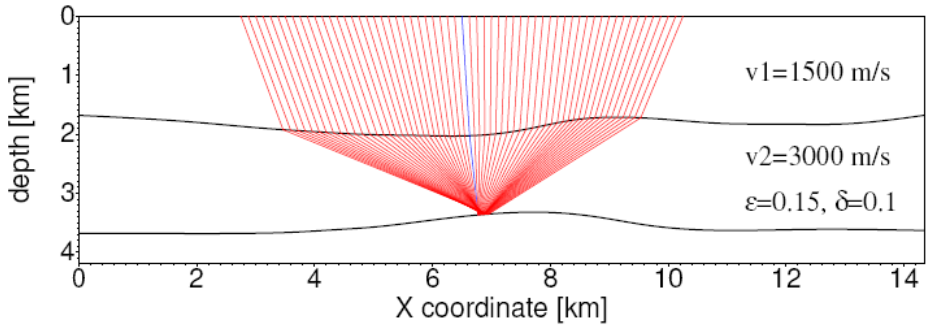

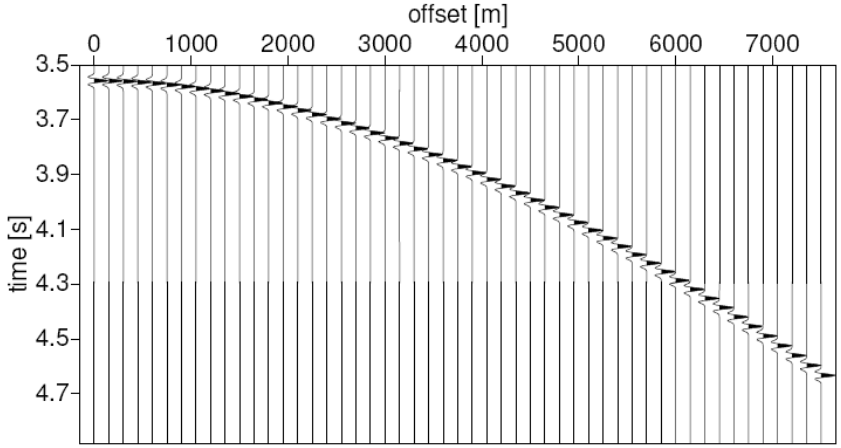

After Sabrina Ernst, 2006

Comparison of different CMP approximations

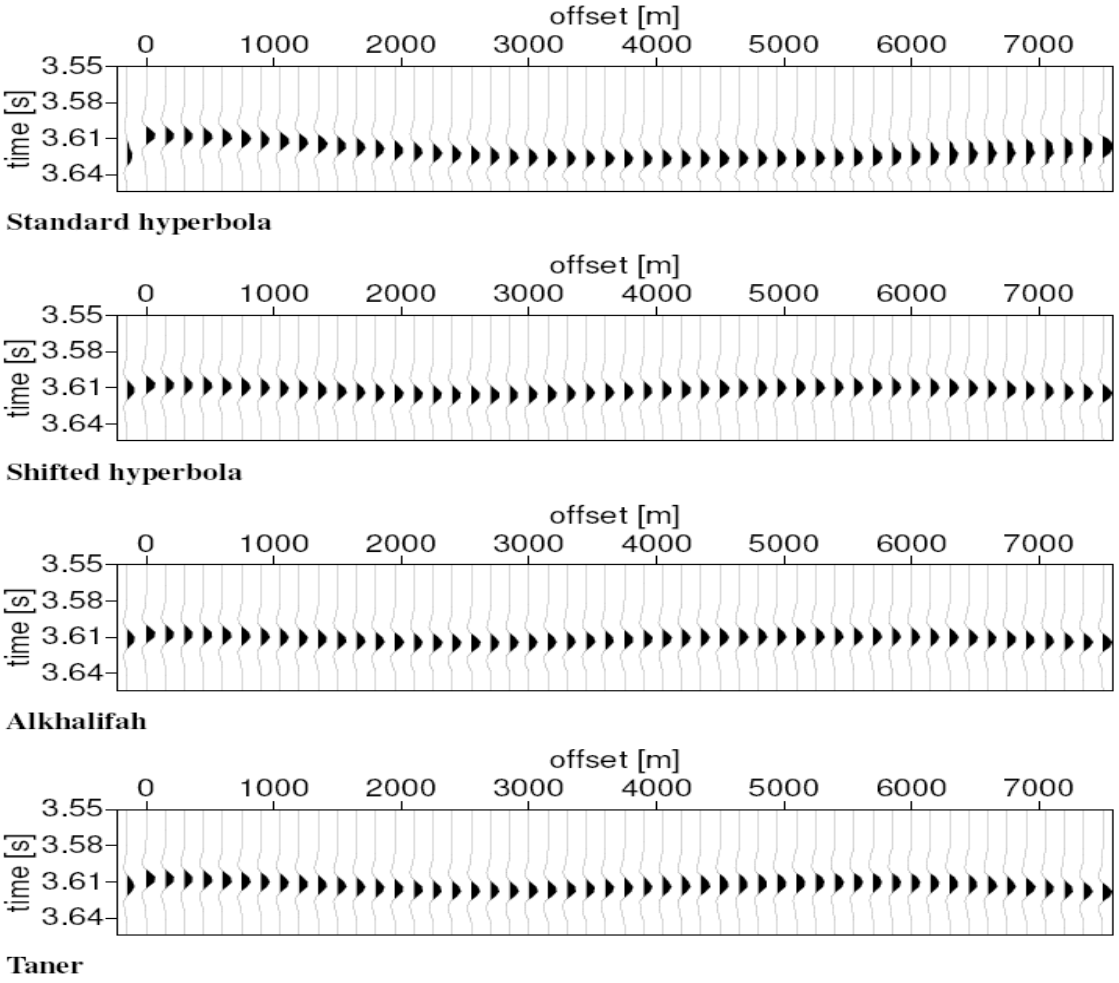

Anisotropy can ***reduce*** the deviation of the reflection event from a standard hyperbola. Compared to the standard hyperbola the two-parameter equations slightly improve the moveout correction

After Sabrina Ernst, 2006

Comparison of different CMP approximations

Synthetic model

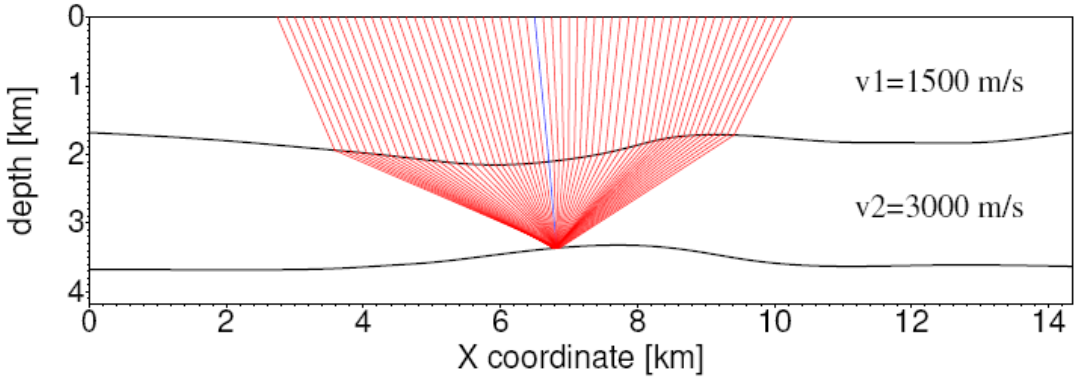

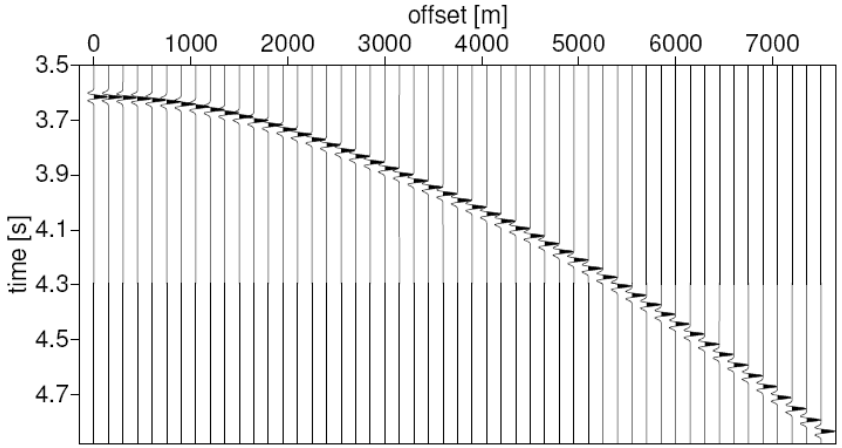

After Sabrina Ernst, 2006

Comparison of different CMP approximations

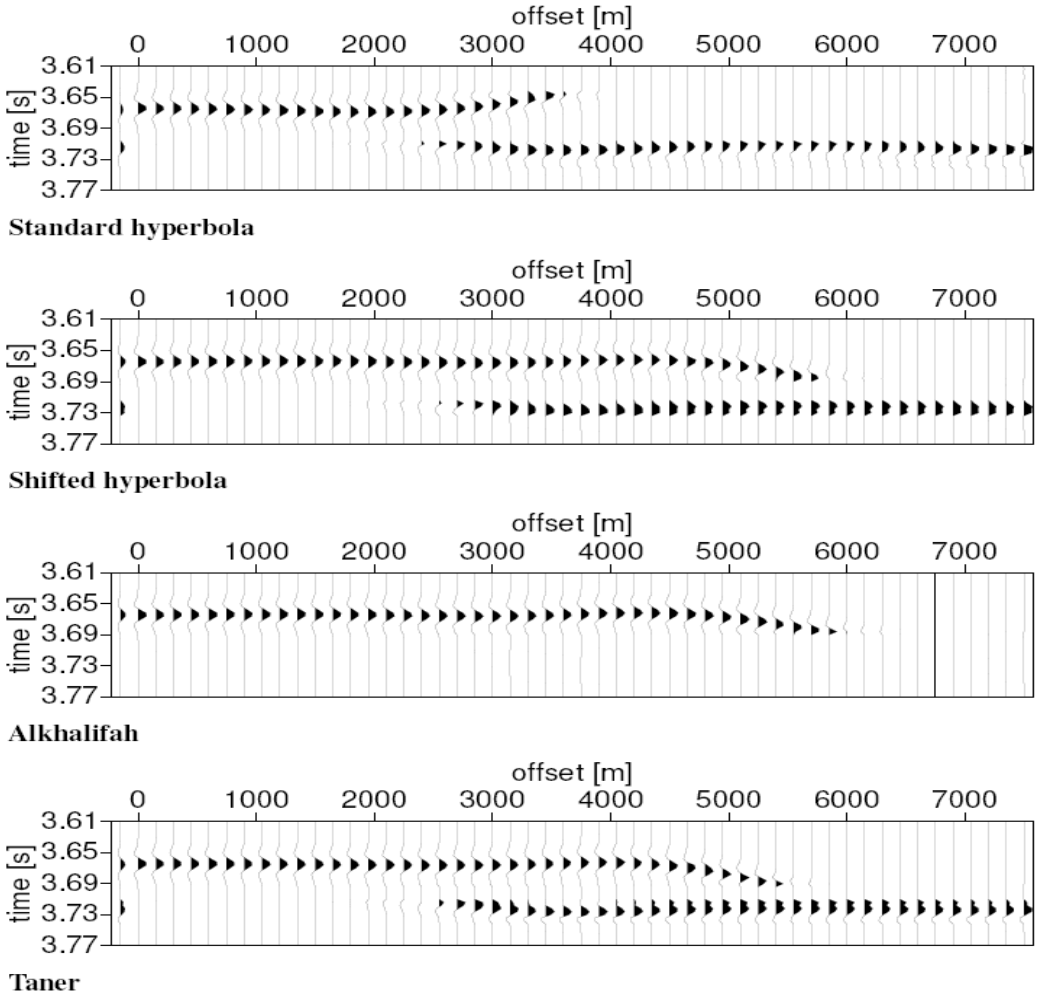

Reflection events can split into two parts due to the complexity of the model

After Sabrina Ernst, 2006

And the conclusion of comparison of different CMP-based approximations is…

2 > 1

Why CMP-based methods fail ?

1. **Short offset approximation**
2. **Non-hyperbolicity**
3. **Low signal to noise ratio**
4. **Stretch**

Non-CMP based methods

Local time correction equation is a key to successful time imaging. Good time correction should satisfy two conditions:

1. ***It should be valid for arbitrary media***
2. ***It should be valid for arbitrary observation geometry***

In practice it implies that:

a) the time correction formula should be model independent

b) the formula is valid for arbitrary distribution of source-receiver pairs

Non-CMP based seismic data analysis, processing and imaging

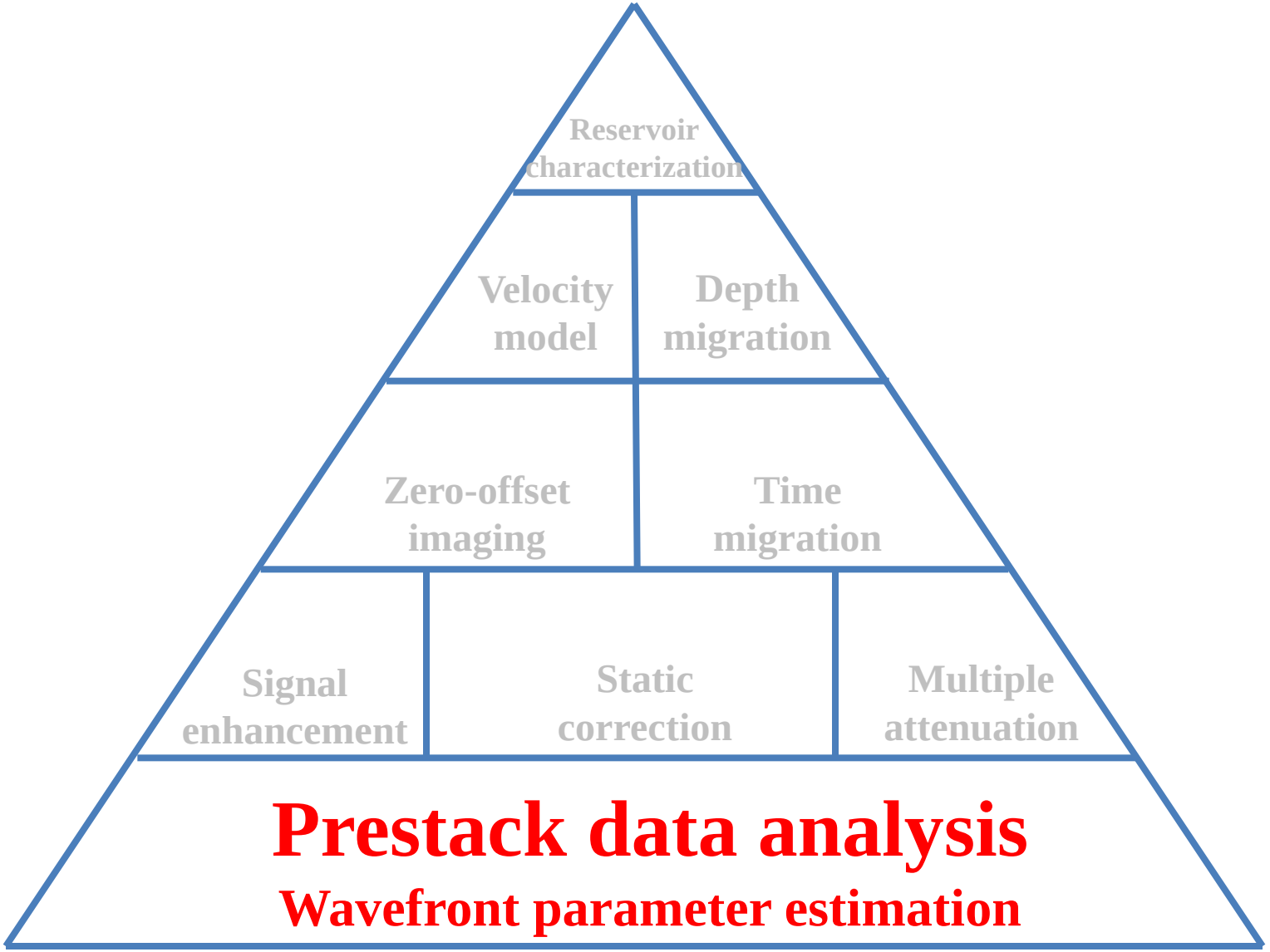

Non-CMP based seismic data analysis, processing and imaging

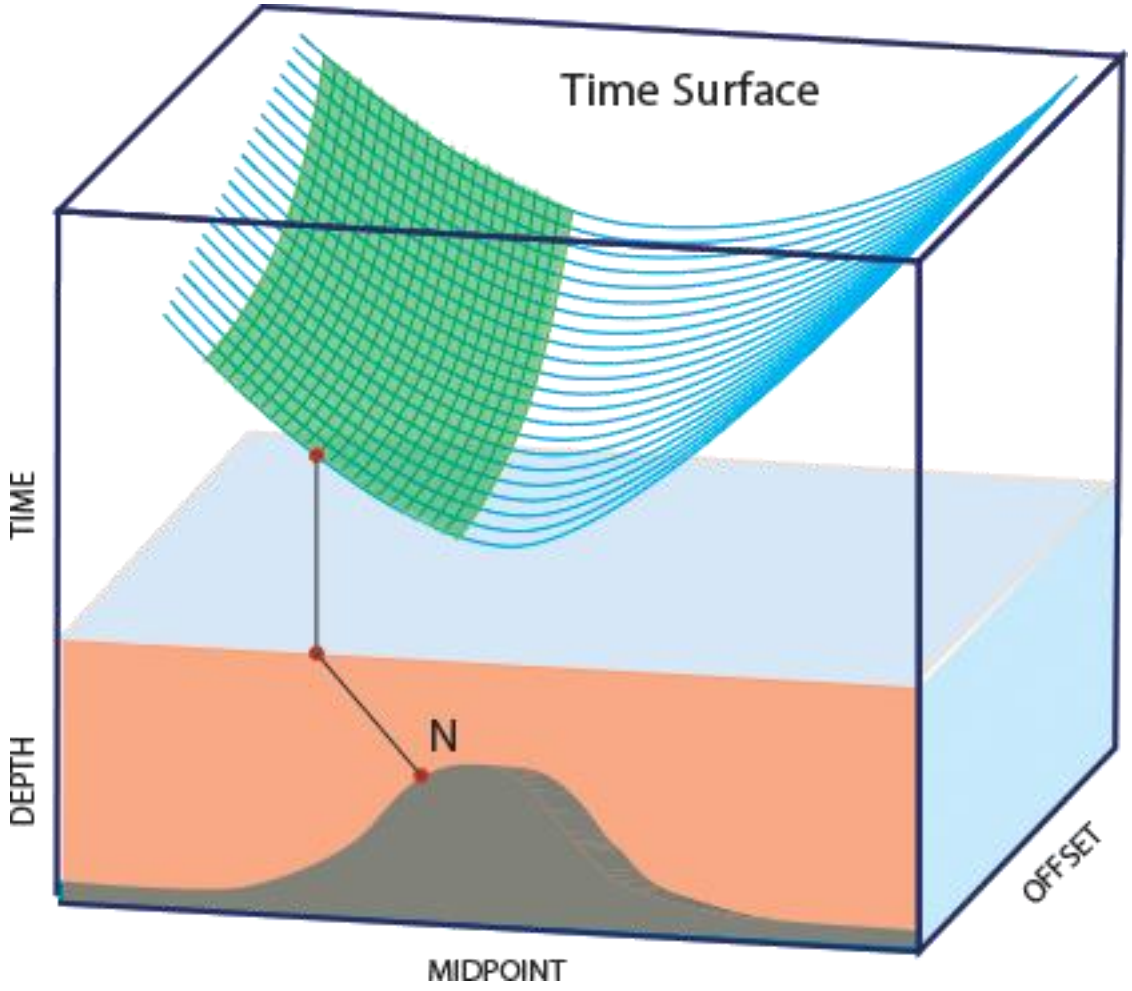

Actual traveltime surface is shown in blue. MF surface is shown in green.

Non-CMP based seismic data analysis, processing and imaging

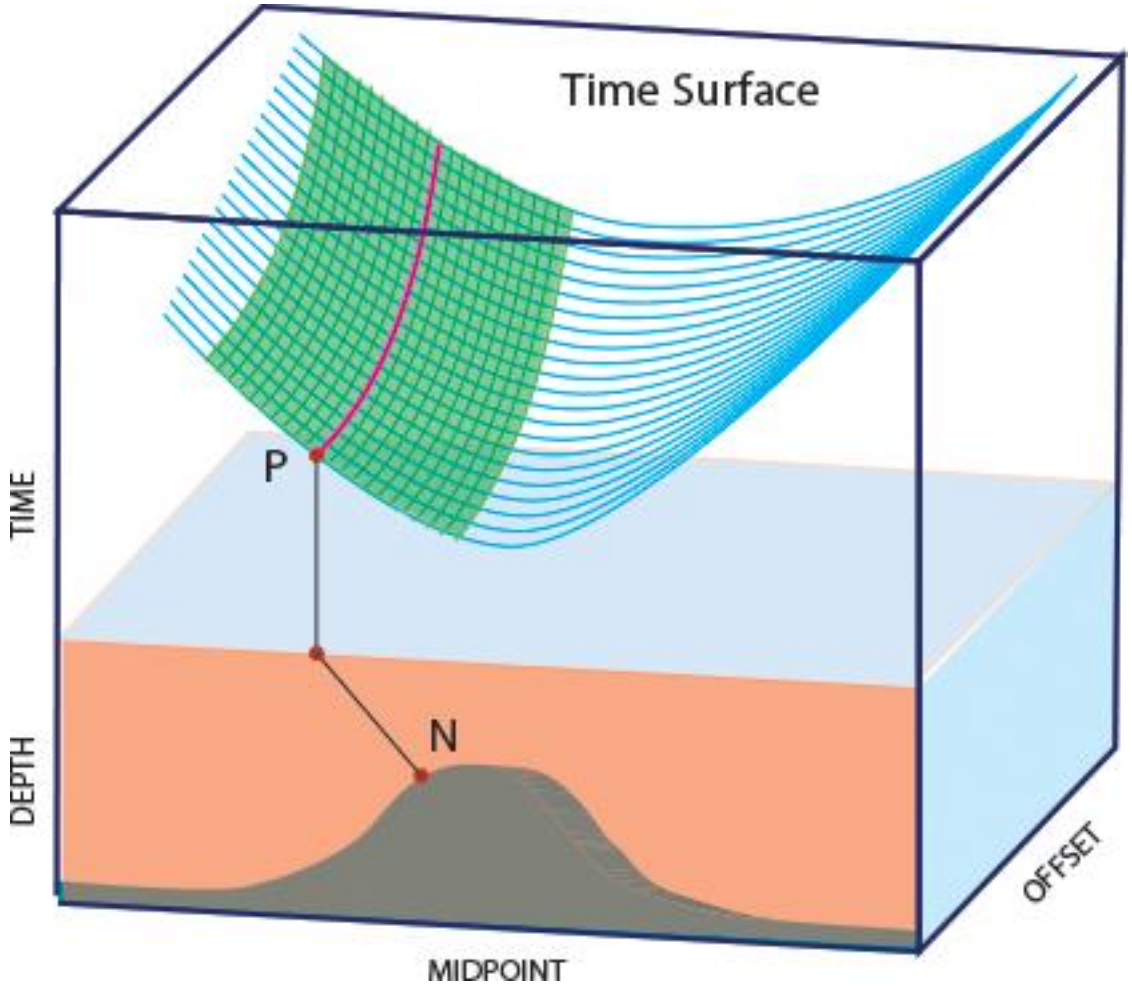

Actual traveltime surface is shown in blue. MF surface is shown in green. The purple line shows CMP trajectory for point P.

Multifocusing: Ray scheme zero-offset case

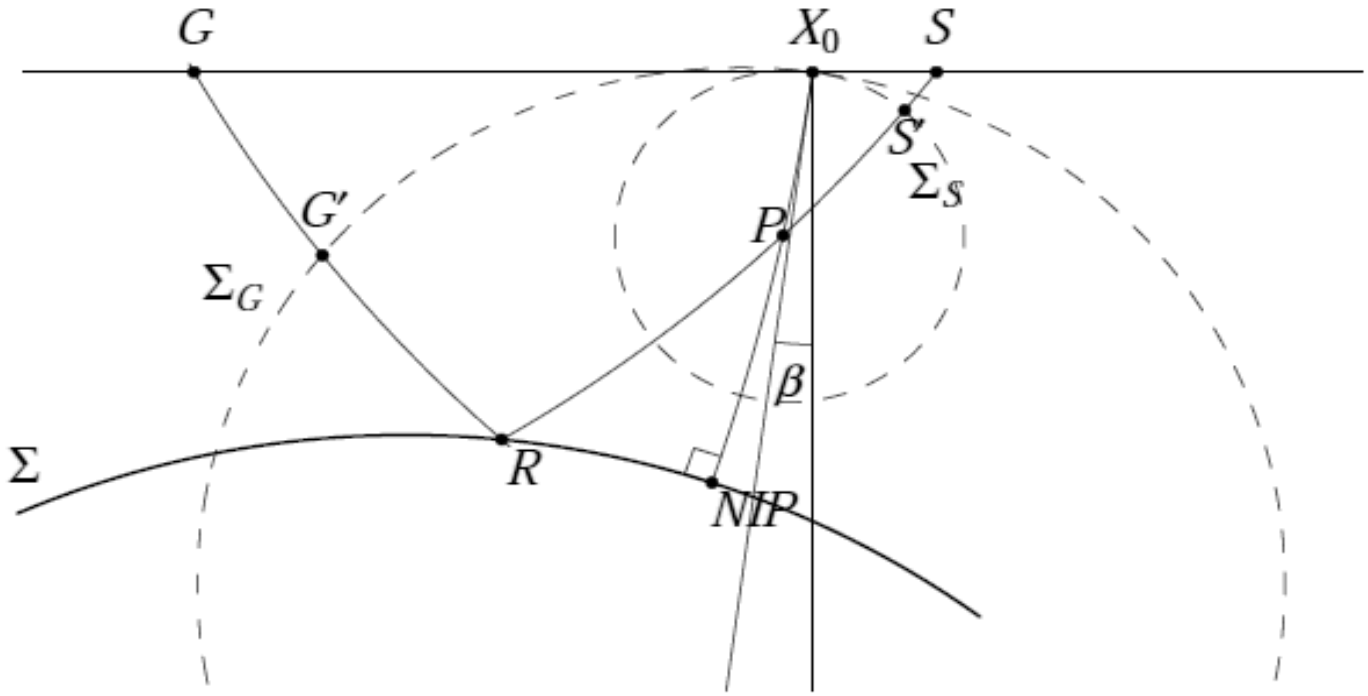

A central (normal) ray starts at the central point *X*0 at an angle β with the vertical, hits the reflector Σ at the normal-incidence point *NIP* and turns back to *X*0. Its reflection traveltime is denoted by *T*0. A neighboring (paraxial) ray from the source point *S*, reflecting at *R* and emerging at the receiver *G*. The purpose of multifocusing is to express the traveltime *S*-*R*-*G* in terms of *T*0 and two corrections at *S* and *G*. This is done by considering a fictitious wave, which initially has the wavefront Σ_s, then implodes and focuses at the intersection point *P* of the normal and paraxial ray and emerges at *X*0 as the wavefront Σ_G .

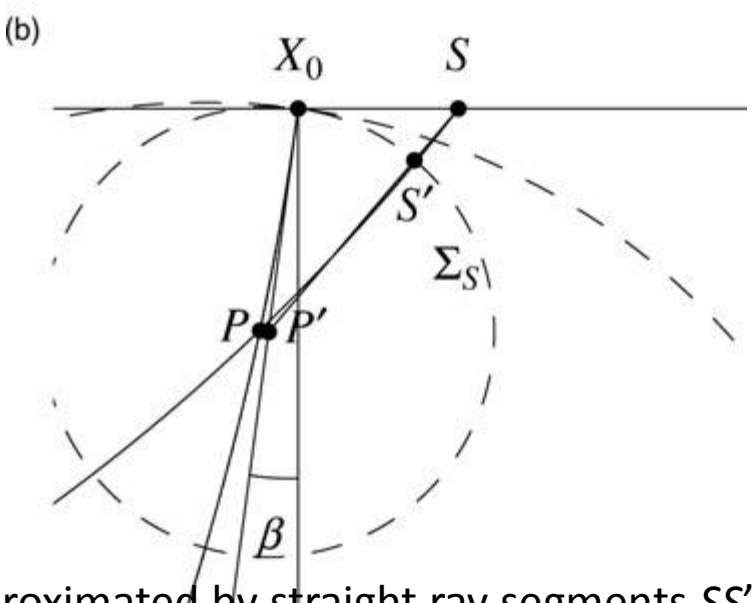

The corrections can be approximated by straight ray segments *SS*’ and *GG*’. The normal ray is rectified along its tangent at *X*0 and the point P' is chosen so that $X_0P = X_0P'$. Then in the triangle *P* − *X*0 − *S* we apply the law of cosines and obtain the correction for the traveltime along SS'. The result for both *S* and *G* is a double-square root equation for the traveltime, which is expressed as follows:

$$\Delta t = \frac{\sqrt{(R^+)^2 + 2\sin\beta_0 R^+ \Delta X^+ + (\Delta X^+)^2} - R^+}{V_0} + \frac{\sqrt{(R^-)^2 - 2\sin\beta_0 R^- \Delta X^- + (\Delta X^-)^2} - R^-}{V_0}.$$

R^+ and R^- are the radii of curvature of the fictitious wave fronts Σ_s and Σ_G, respectively. By moving the source and receiver point along the surface, the focusing point *P* is moved up and down along the normal ray – hence the name multifocusing. Based on dynamic ray theory, it is possible to show that the radii R^+ and R^- are related to the radii of curvature of the two fundamental wave fronts corresponding to the normal (N) and NIP wave

$$R^{\pm} = \frac{1 \pm \sigma}{\frac{1}{R_N} \pm \frac{\sigma}{R_{NIP}}}$$

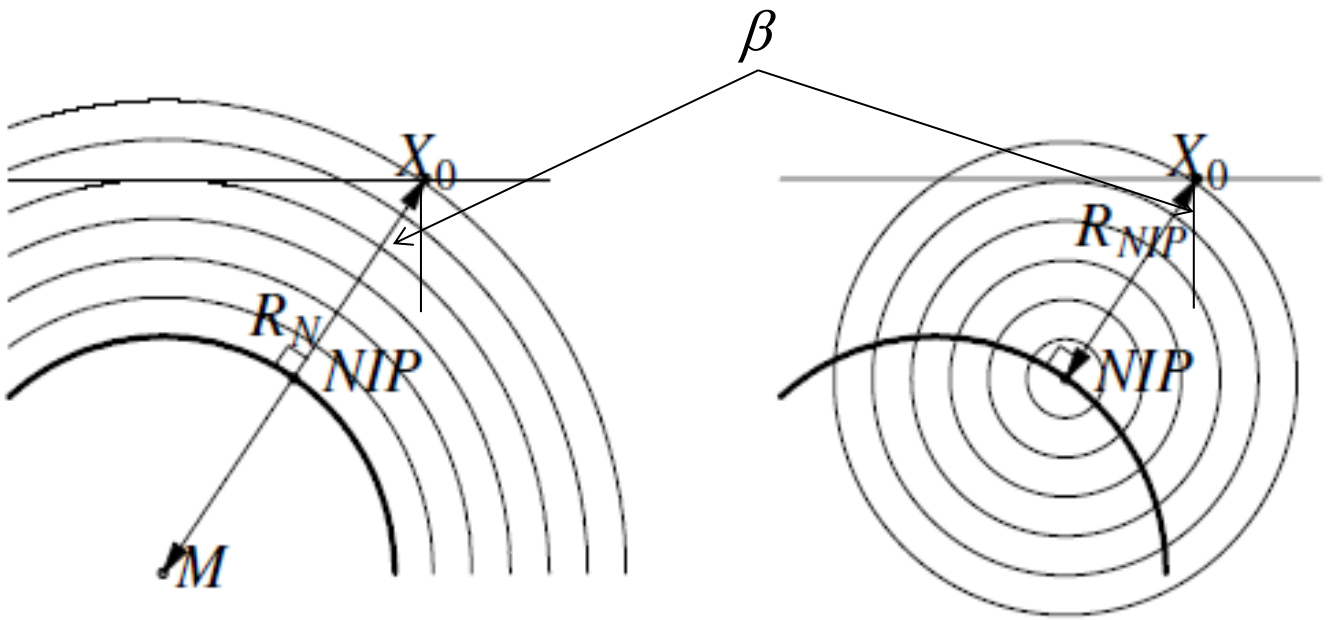

Geometrical meaning of R_N and R_{NIP} -waves.

The N-wave radius of curvature is related to reflector curvature, the NIP-wave radius of curvature to its depth.

Focusing quantity σ for plane reflector

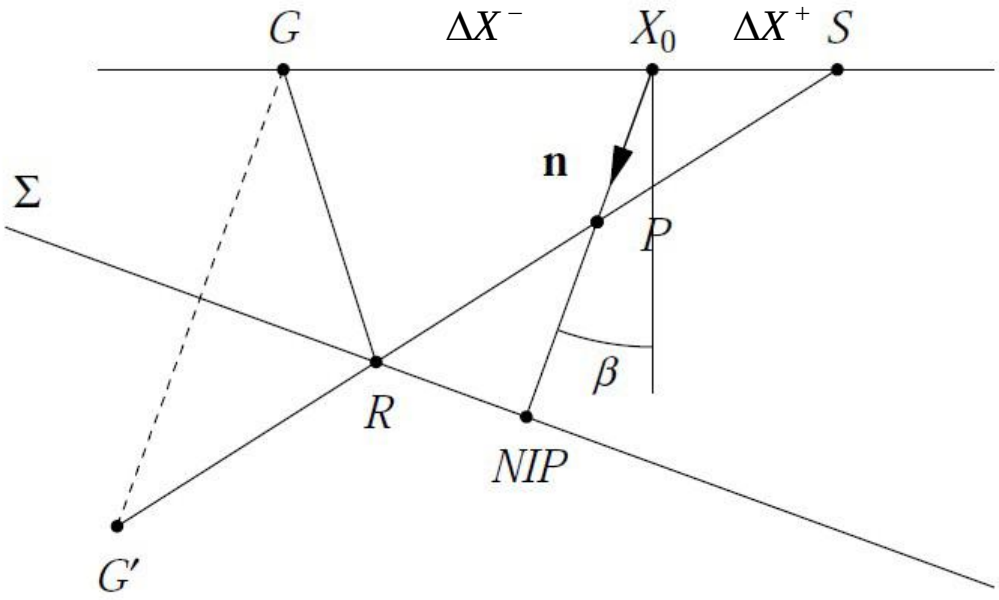

$$\sigma = \frac{\Delta X^+ - \Delta X^-}{\Delta X^+ + \Delta X^- + 2\dfrac{\Delta X^+ \Delta X^-}{R_{NIP}} \sin\beta}$$

- **Defines the location of the focusing point *P along the* central ray**
- **Is used to classify subsets of super-gather, e.g., common-shot, common-receiver, common-midpoint**
- **The quantity σ is *not a fixed parameter, but depends on* source and receiver location**
- **A σ function can be designed for every reflector geometry, such that the MF moveout is *exact***

σ -is the *focusing parameter*, which defines the position of the focusing point P on the normal ray

σ = 0 means that $R^+ = R^- = R_N$ which implies that point P coincides with the centre of curvature of the normal wave and corresponds to the case of coinciding source and receiver (zero-offset configuration).

σ = 1 or –1 imply $R^+ = 0$ *or* $R^- = 0$ and correspond to the common shot or common receiver configuration

σ = ∞ leads to $R^+ = R^- = R_{NIP}$ and corresponds to the situation where the focusing point P coincides with NIP. CRP configuration

Spherical Multifocusing

Reflection travel time and *σ on* spherical reflector

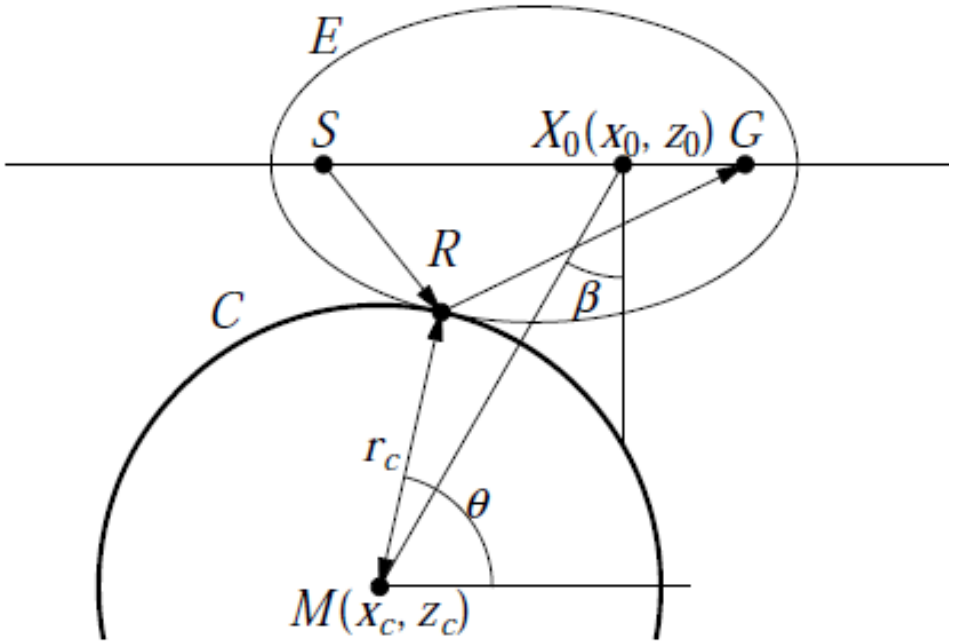

$$R_N = [(x_0 - x_c)^2 + (z_0 - z_c)^2]^{1/2} \ , \quad R_{NIP} = R_N - r_c \ ,$$

$$\sin\beta = (x_c - x_0)/R_N$$

exact for curved reflectors of all curvatures!

Spherical Multifocusing in 3D

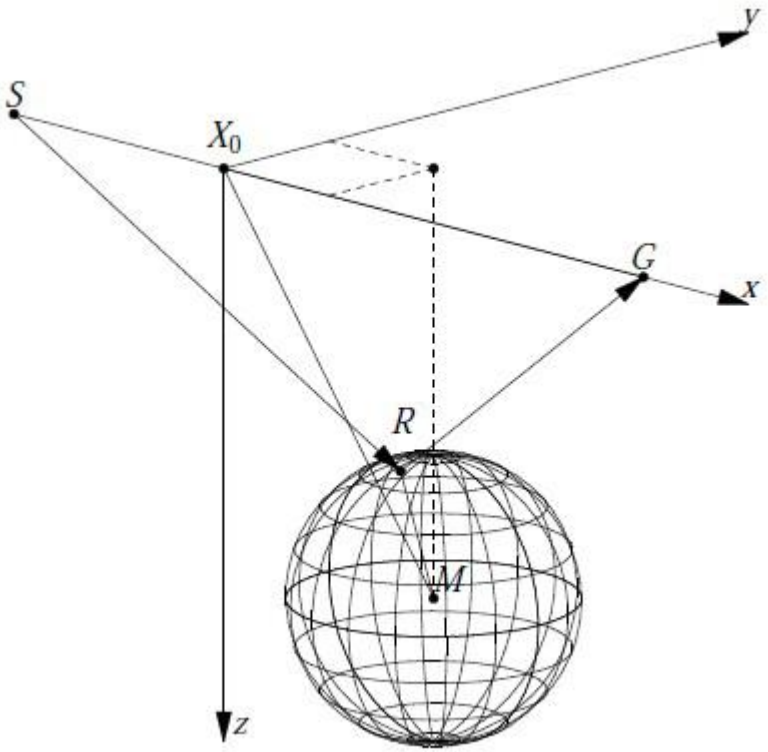

Four MF attributes: β, Rnip , Rn **and inclination** ***φ***

COMMON REFLECTION SURFACE STACK (CRS)

Taylor expansion of the squared traveltime moveout $T_2(x_m, h)$ as a function of the common midpoint (CMP) location $x_m = (x_s + x_g)/2$ and half-offset $h = (x_s - x_g)/2$ around a central CMP location x_0 .

$$T^2(x_m, h) = (T_0 + A(x_m - x_0))^2 + B(x_m - x_0)^2 + Ch^2 + O((x_m - x_0)^3, h^4).$$

$$A = \frac{2\sin\beta}{v_0}, B = \frac{2T_0\cos^2\beta}{v_0 R_N}, C = \frac{2T_0\cos^2\beta}{v_0 R_{NIP}}.$$

MF versus CRS

Multifocusing method: single CMP

$$\Delta\tau_{CMP}^{MF} = \frac{\sqrt{\left(R^{+}\right)^2 + 2R^{+}h\sin\beta + h^2} - R^{+}}{V_0} + \frac{\sqrt{\left(R^{-}\right)^2 - 2R^{-}h\sin\beta + h^2} - R^{-}}{V_0}$$

$$R^{\pm} = \frac{1 \pm \sigma}{\frac{1}{R_N} \pm \frac{\sigma}{R_{NIP}}}$$

$$\sigma = -\frac{R_{NIP}}{h\sin\beta}$$

$R_N = \infty$ (plane reflector)

$$t_{MF} = t_0 - t_p + \sqrt{t_p^2 + \frac{h^2\cos^2\beta}{V_0^2}}$$

Shifted hyperbola of de Bazelaire, $t_p = 2R_{NIP}/V_0$

CRS method: single CMP

$$t_{CMP}^{CRS} = \sqrt{t_0^2 + \frac{h^2}{V_{st}^{\ 2}}}$$

MF versus CRS

Circular reflector - one CMP

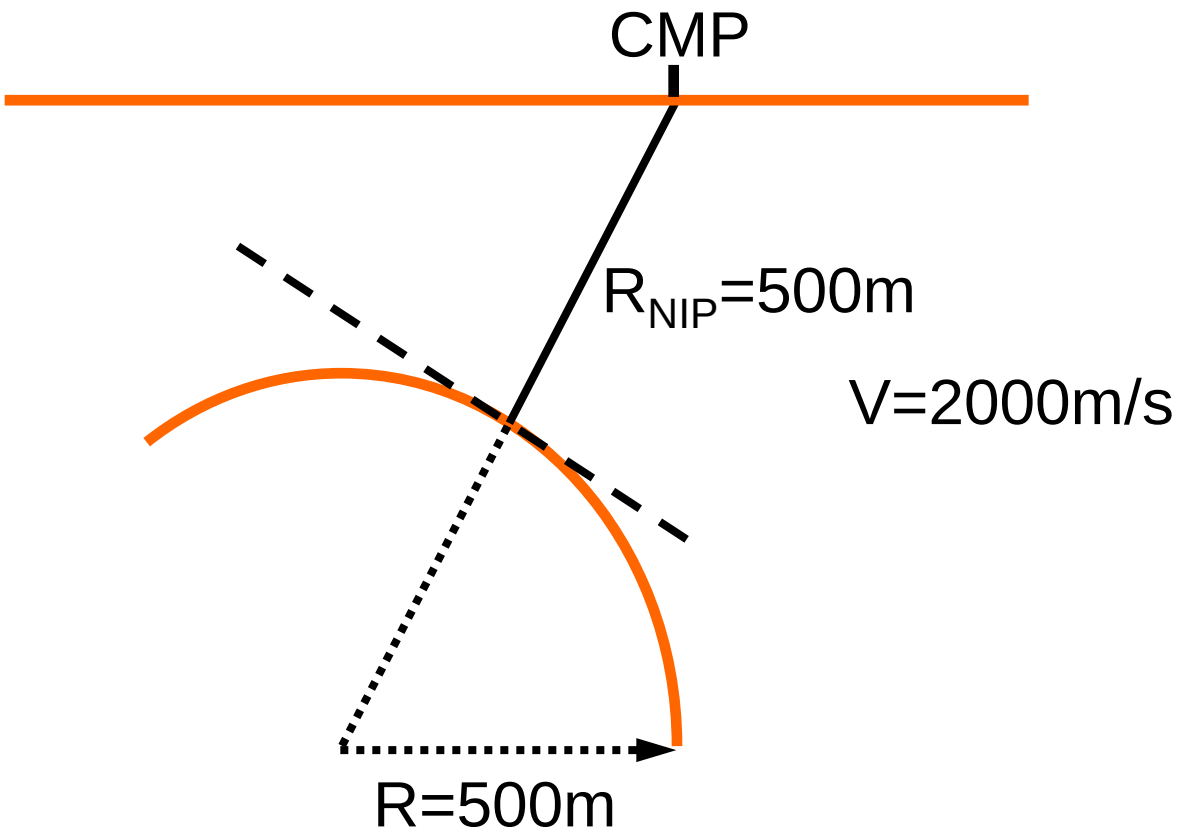

MF versus CRS

Circular reflector - one CMP

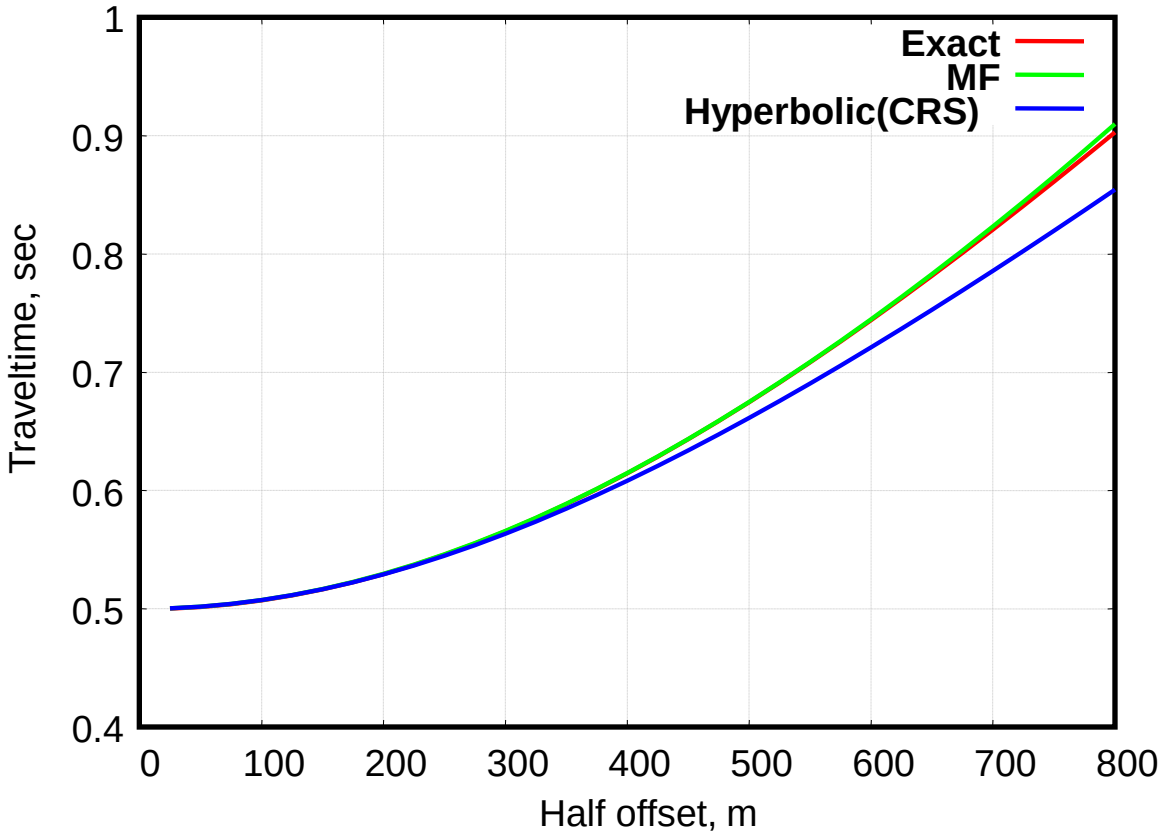

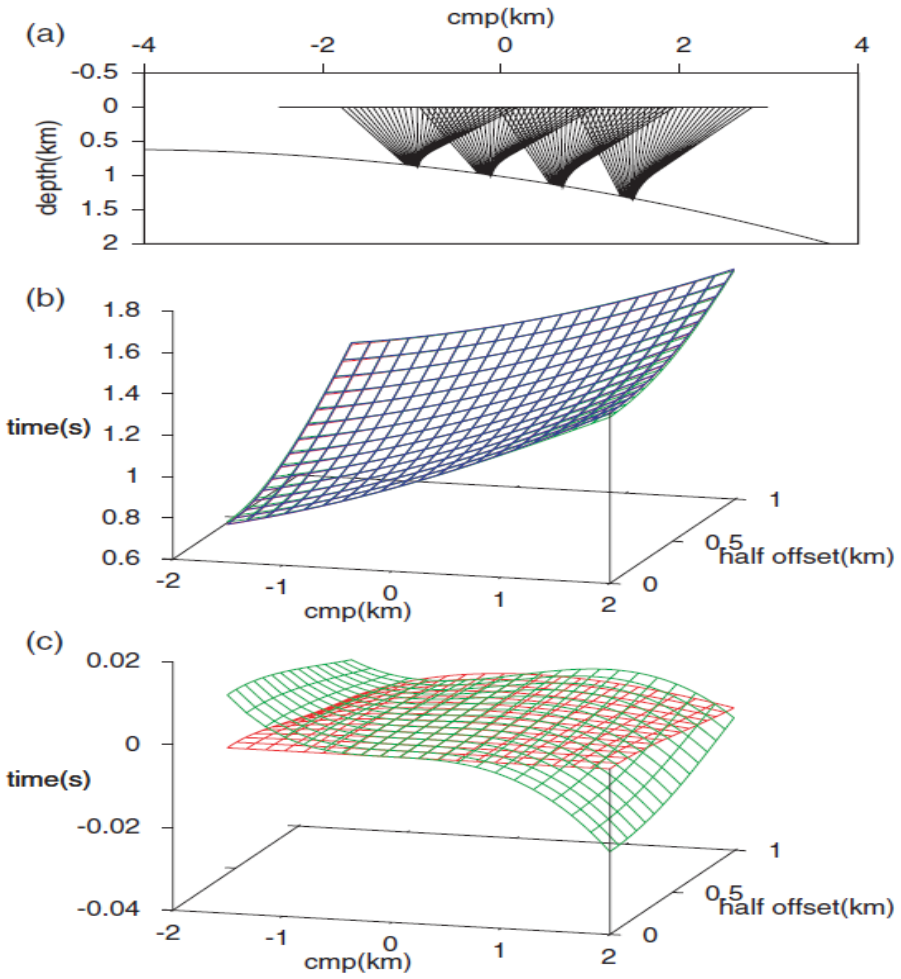

Gently curved reflector. a) Ray geometry. b)Moveout surfaces: common-reflection surface CRS (green), planar multifocusing (red), spherical multifocusing (blue). The spherical multifocusing expression is exact for this case. Note that the planar multifocusing moveout coincides almost completely with the spherical multifocusing move-out. c) Moveout errors: CRS (green), planar multifocusing (red).

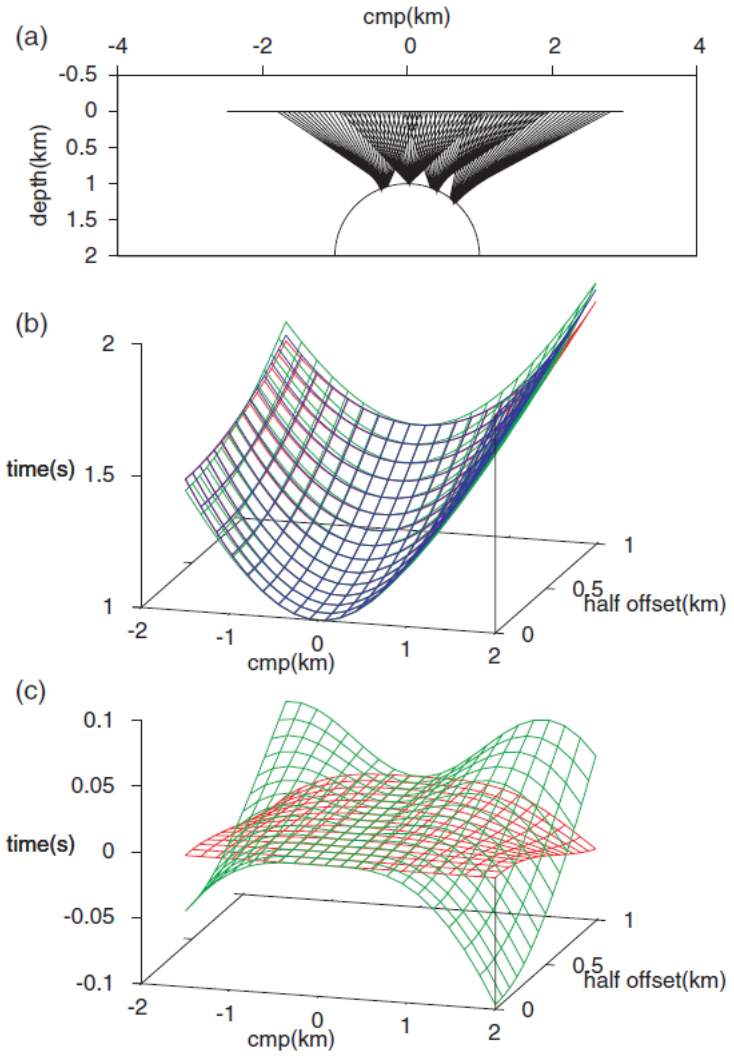

Strongly curved reflector. a) Ray geometry. b)Moveout surfaces: common-reflection surface CRS (green), planar multifocusing (red), spherical multifocusing (blue). The spherical multifocusing expression is exact for this case. c)Moveout errors: CRS (green), planar multifocusing (red).

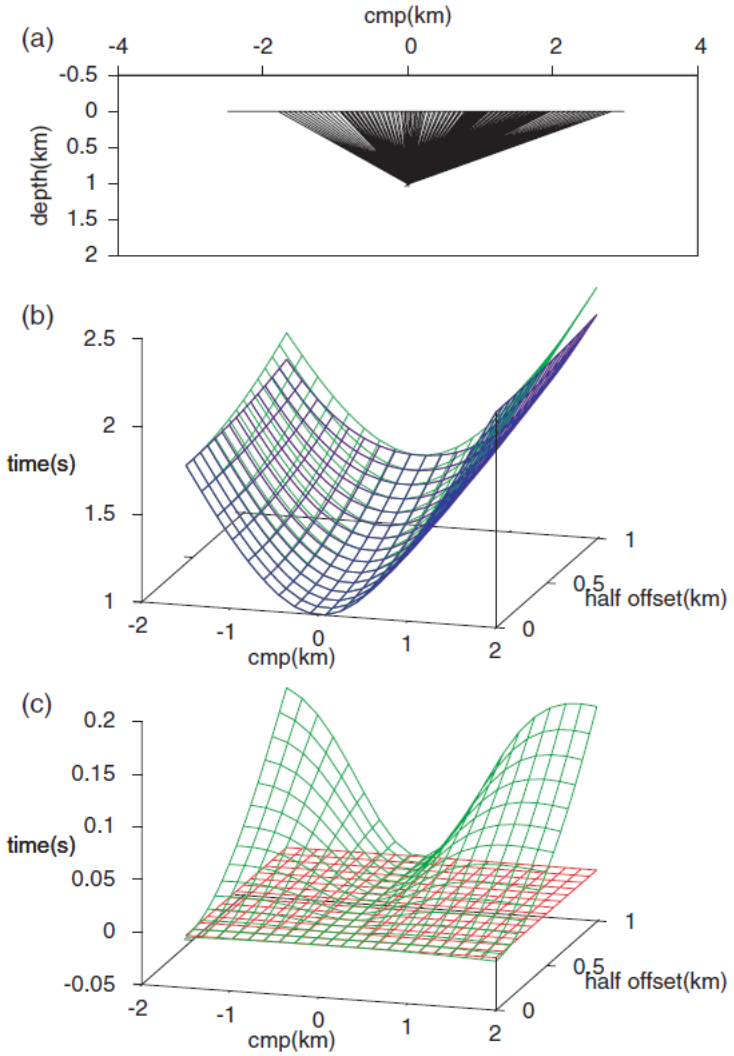

Limit to point diffractor. a) Ray geometry. b)Moveout surfaces: common-reflection surface CRS (green), planar multifocusing (red), spherical multifocusing (blue). The spherical multifocusing expression is exact for this case. c)Moveout errors: CRS (green), planar multifocusing (red).

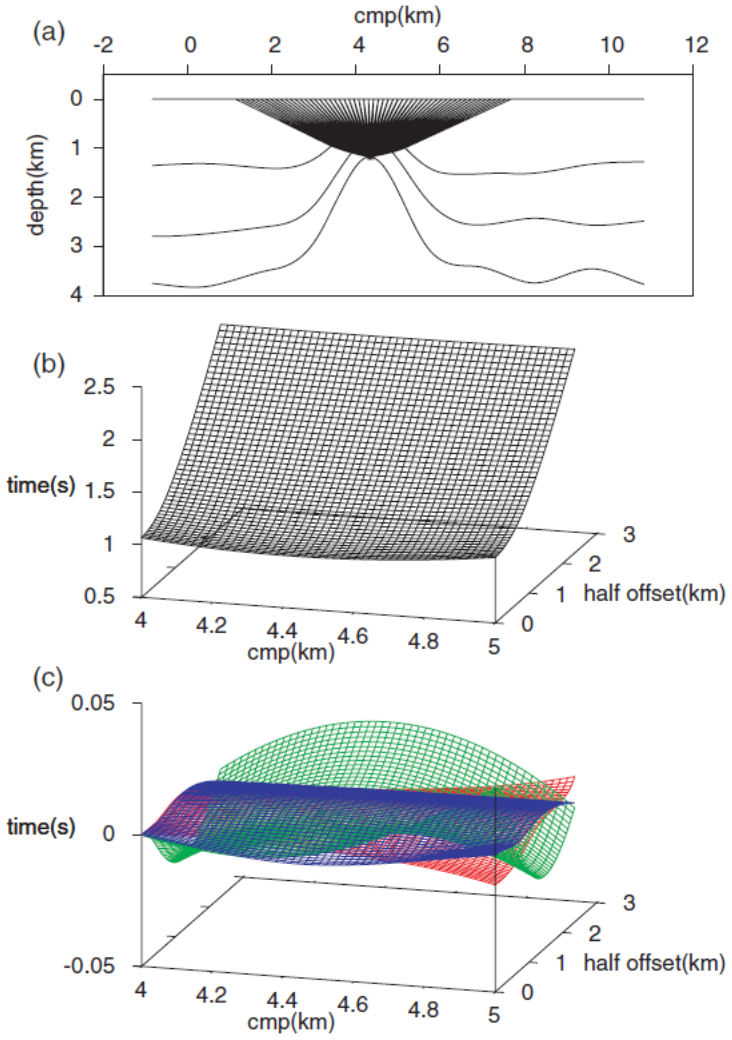

Multilayered model. a) Ray geometry. b) Moveout surface from raytracing. c) Moveout errors: CRS (green), planar multifocusing (red), spherical multifocusing (blue).

Non-CMP based seismic data analysis, processing and imaging: *3D case*

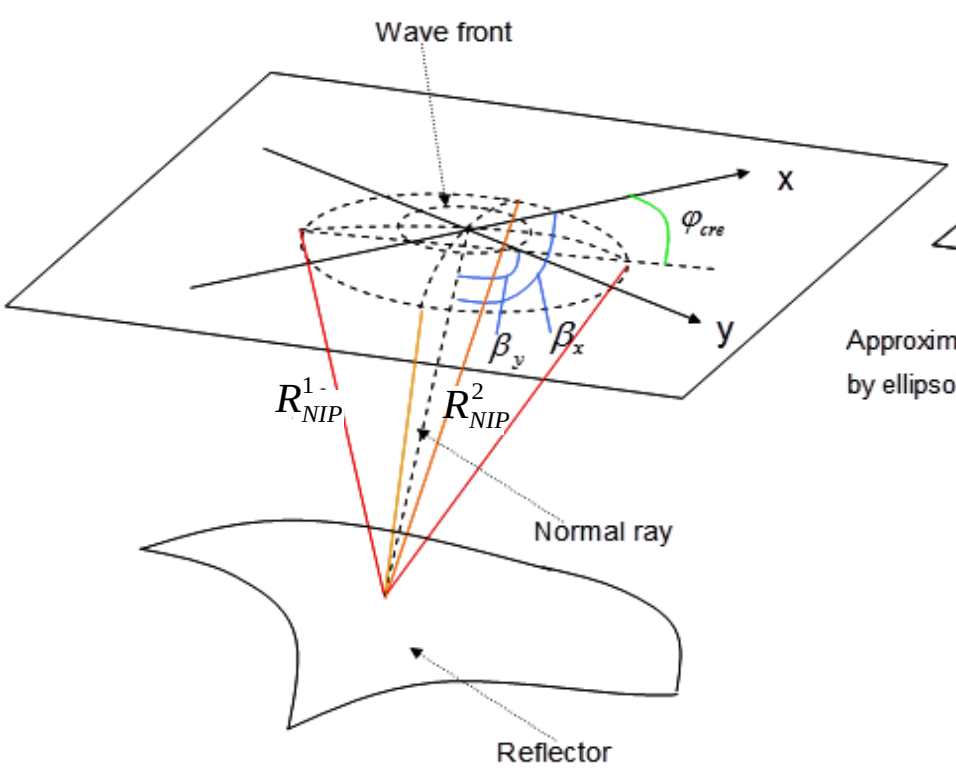

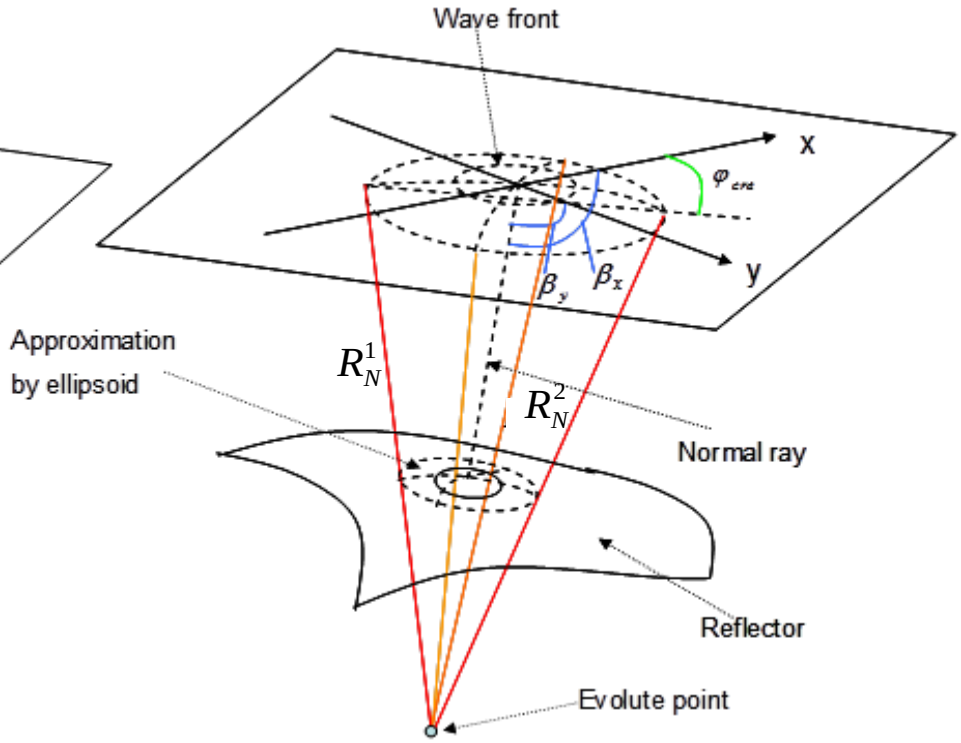

$$T(\vec{x}_0, \vec{x}_s, \vec{x}_r) = F(\vec{x}_s, \vec{x}_r, \vec{c}) = F(\Delta\vec{x}_s, \Delta\vec{x}_r, \vec{\beta}, \vec{R}_{NIP}, \vec{R}_N, V_0)$$

$$\vec{c} = \max_{\vec{c}}[F[\sum_{\vec{s},\vec{r}\in\sigma} u(t + \tau(\vec{s}, \vec{r}, \vec{c}))]]$$

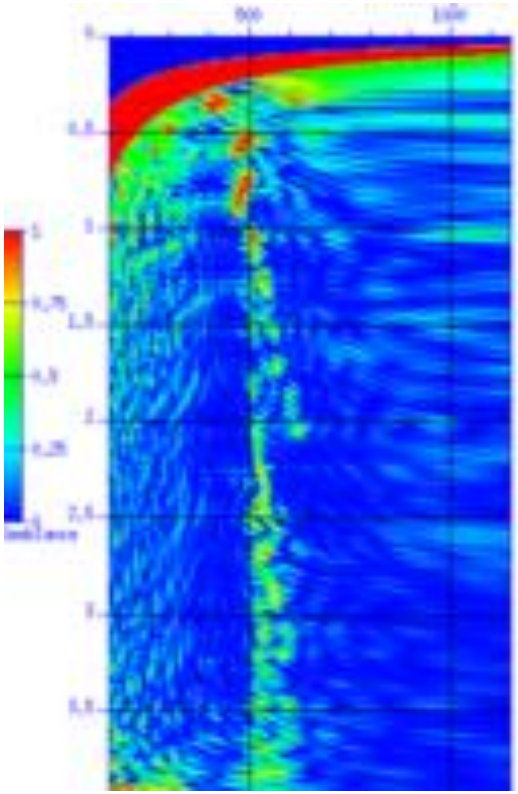

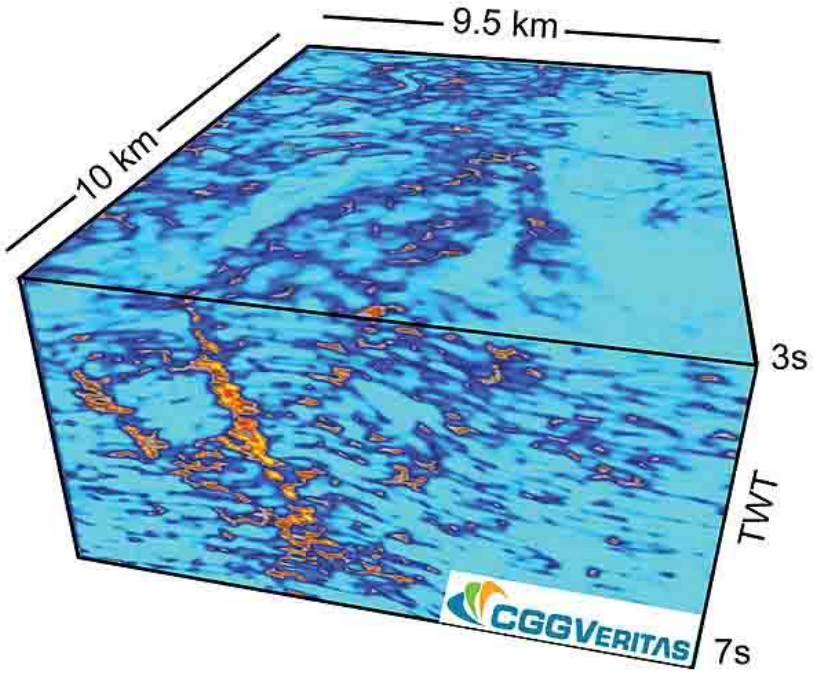

Non-CMP based seismic data analysis, processing and imaging

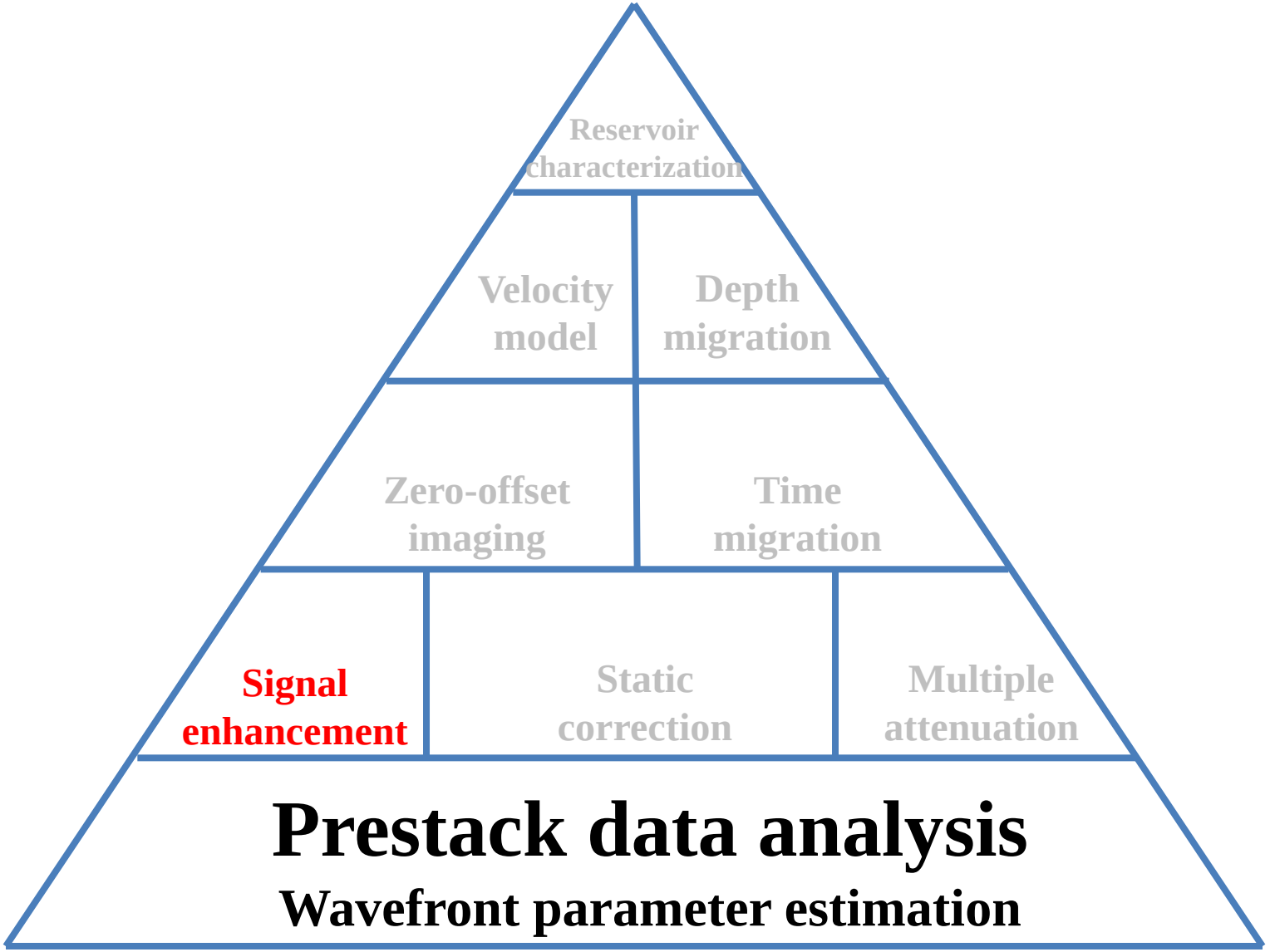

Non-CMP based seismic data analysis, processing and imaging

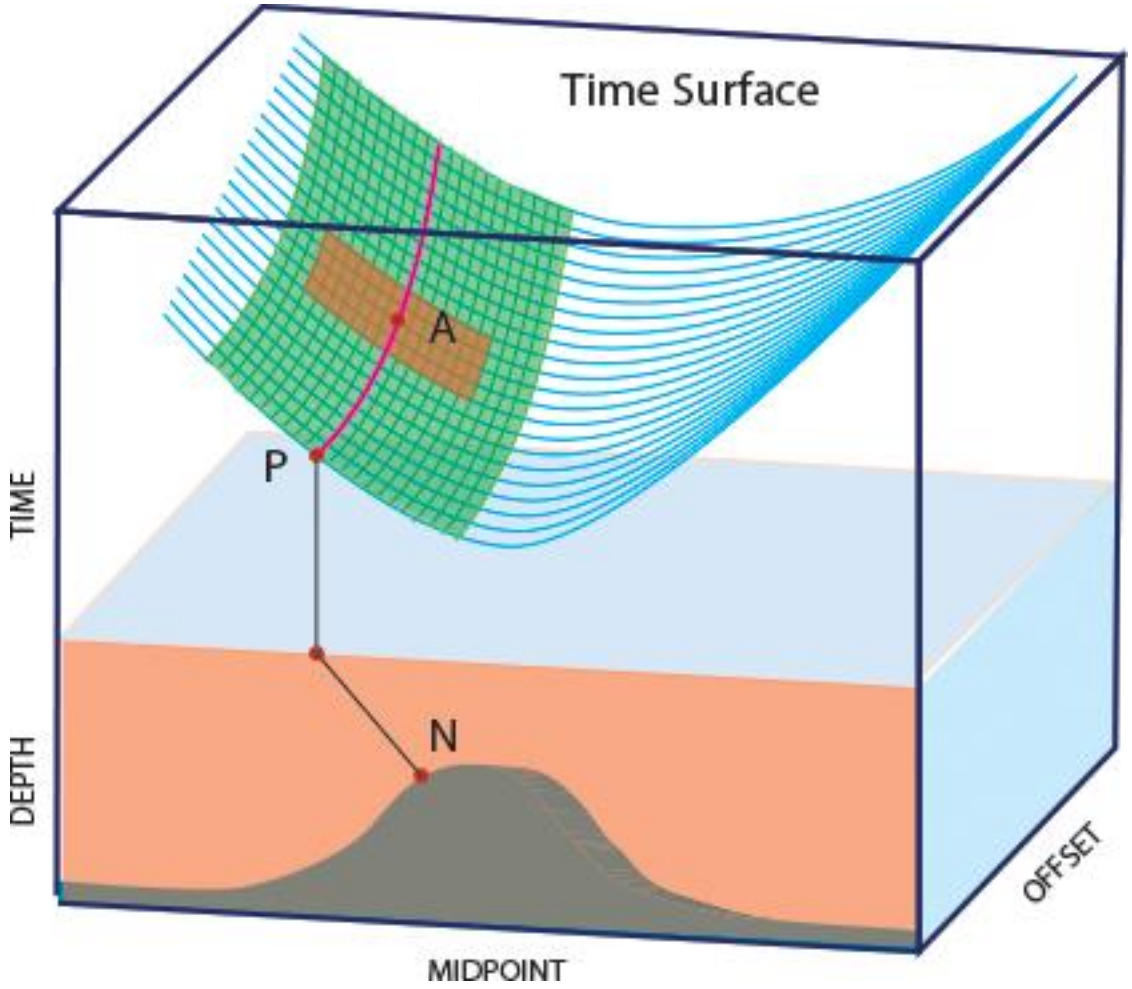

Time surface is shown in green. The purple line shows CMP trajectory for point P. Local time surface is shown in red around point A.

CO Multifocusing: ray scheme

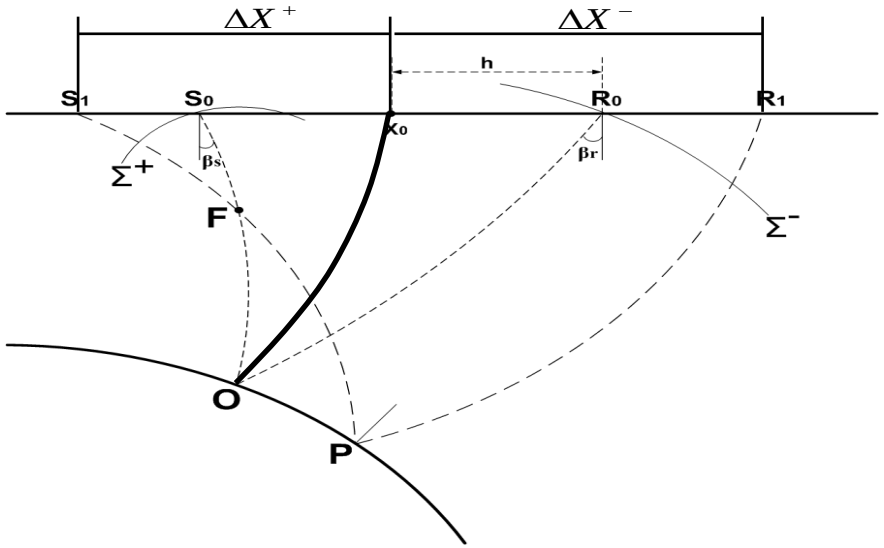

$$\Delta t = \frac{\sqrt{(R^+)^2 + 2\sin\beta_s R^+ \Delta X^+ + (\Delta X^+)^2} - R^+}{V_0} + \frac{\sqrt{(R^-)^2 - 2\sin\beta_r R^- \Delta X^- + (\Delta X^-)^2} - R^-}{V_0}.$$

$$R^{\pm} = \frac{1+\sigma}{\frac{1}{R_1^{\pm}} + \frac{\sigma}{R_2^{\pm}}}, \qquad \frac{1}{R_{1,2}^{\pm}} = \pm\frac{1}{2L} + \frac{1}{R_{s,r}},$$

$$\Delta X^+ = \frac{(1+\sigma)}{\cos\beta_s} Y + \frac{\sin\beta_s}{\cos^2\beta_s}(1+\sigma)\left(\frac{1}{R_1^+} + \frac{\sigma}{R_2^+}\right)^2 Y^2$$

$$\Delta X^- = \frac{(1-\sigma)}{\cos\beta_r} Y + \frac{\sin\beta^-}{\cos^2\beta_r}(1-\sigma)\left(\frac{1}{R_1^-} - \frac{\sigma}{R_2^-}\right)^2 Y^2$$

- Local wavefront parameters estimated for each *X,Y* position and for each time sample allow to perform local coherent summation around each time-space sample

- It overcomes hyperbolic assumption for traveltime approximation

Original Gather

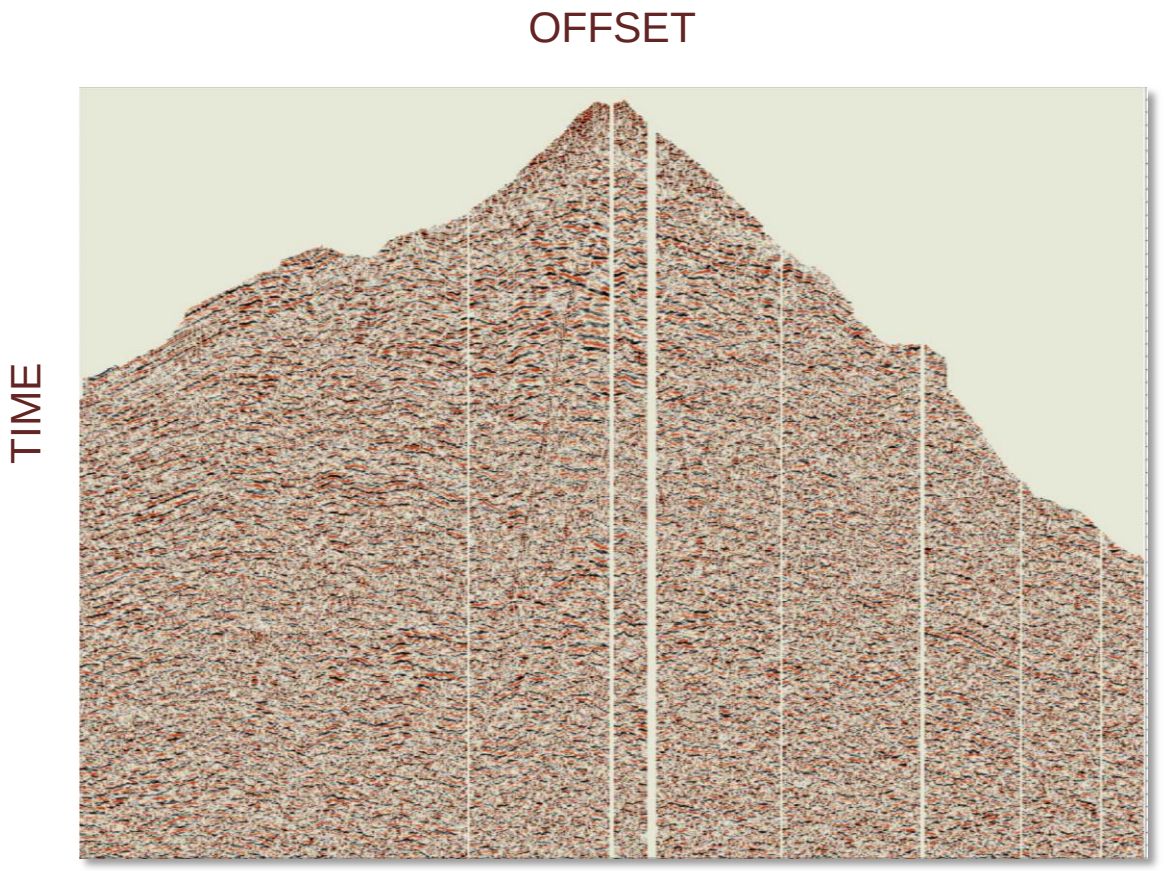

MF

Enhanced Pre-Stack Gather

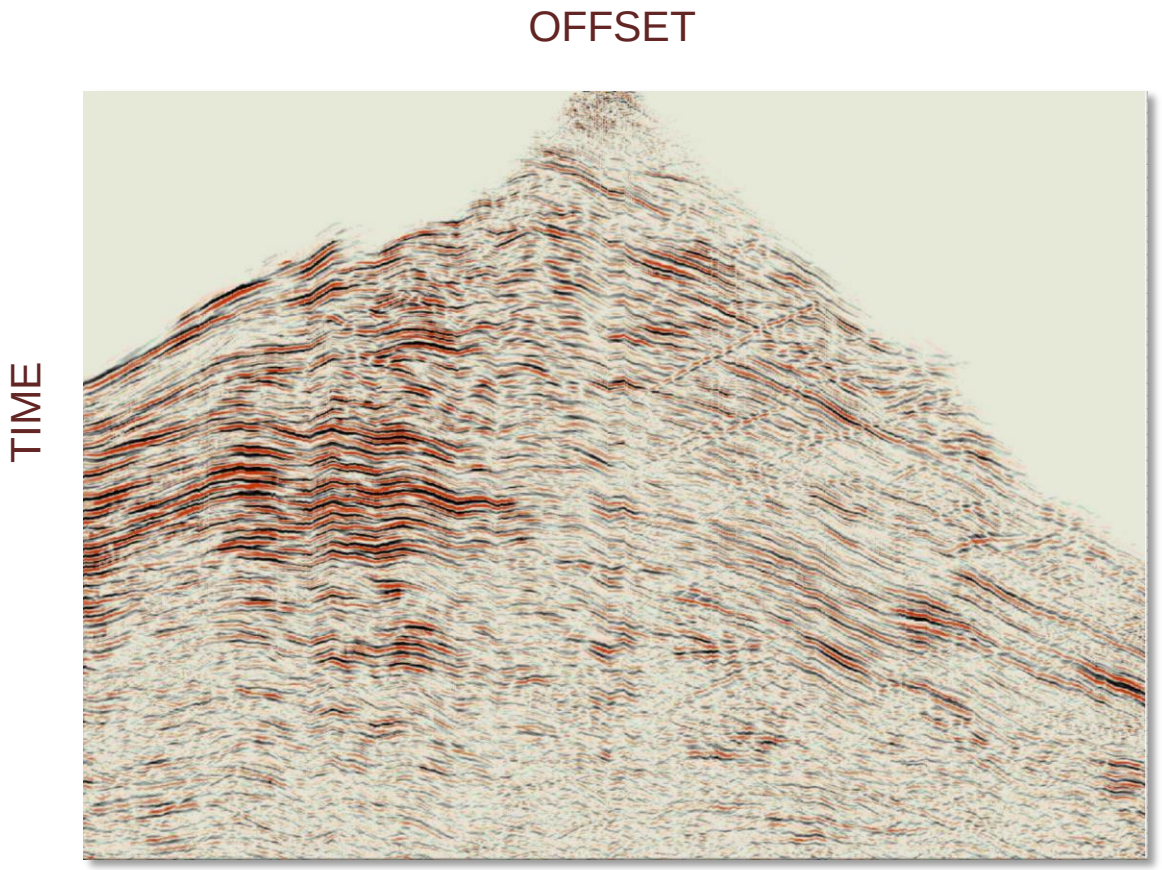

Original

Gathers

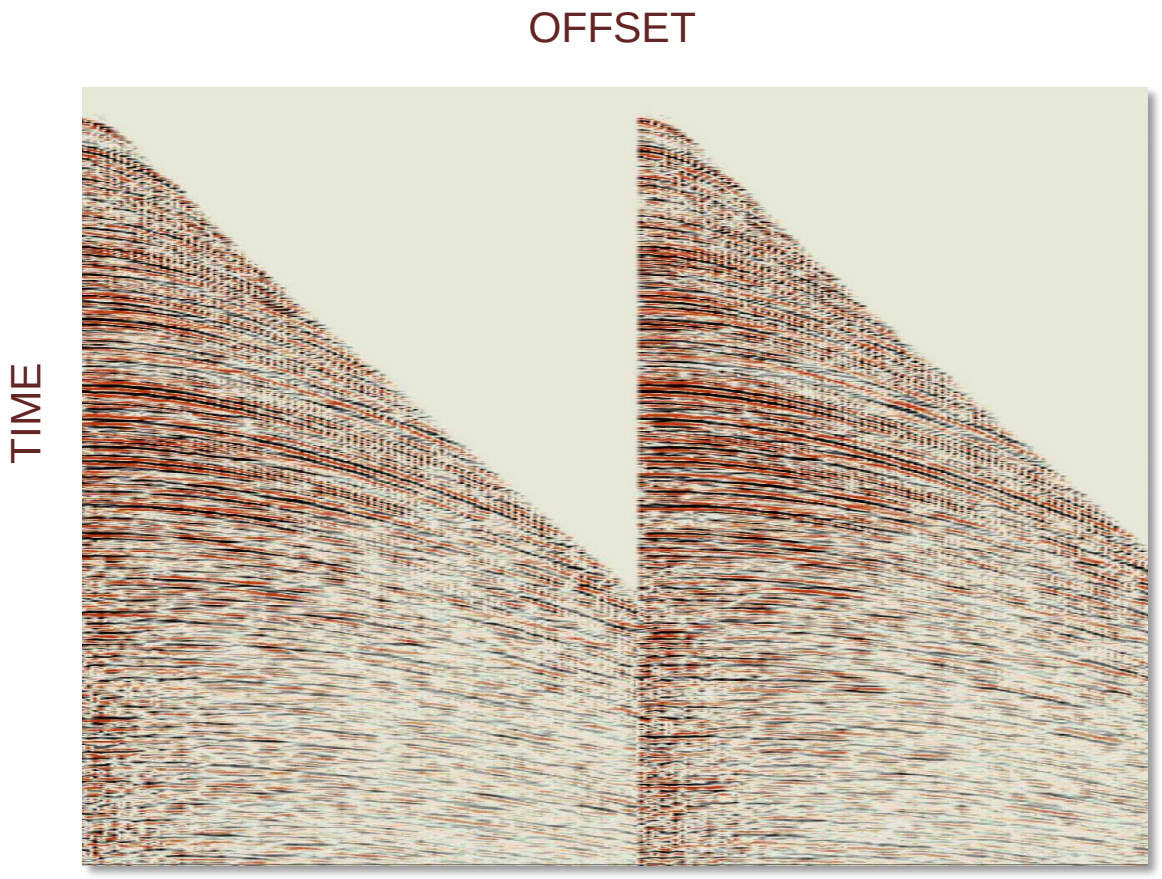

MF

Enhanced Pre-Stack Gather

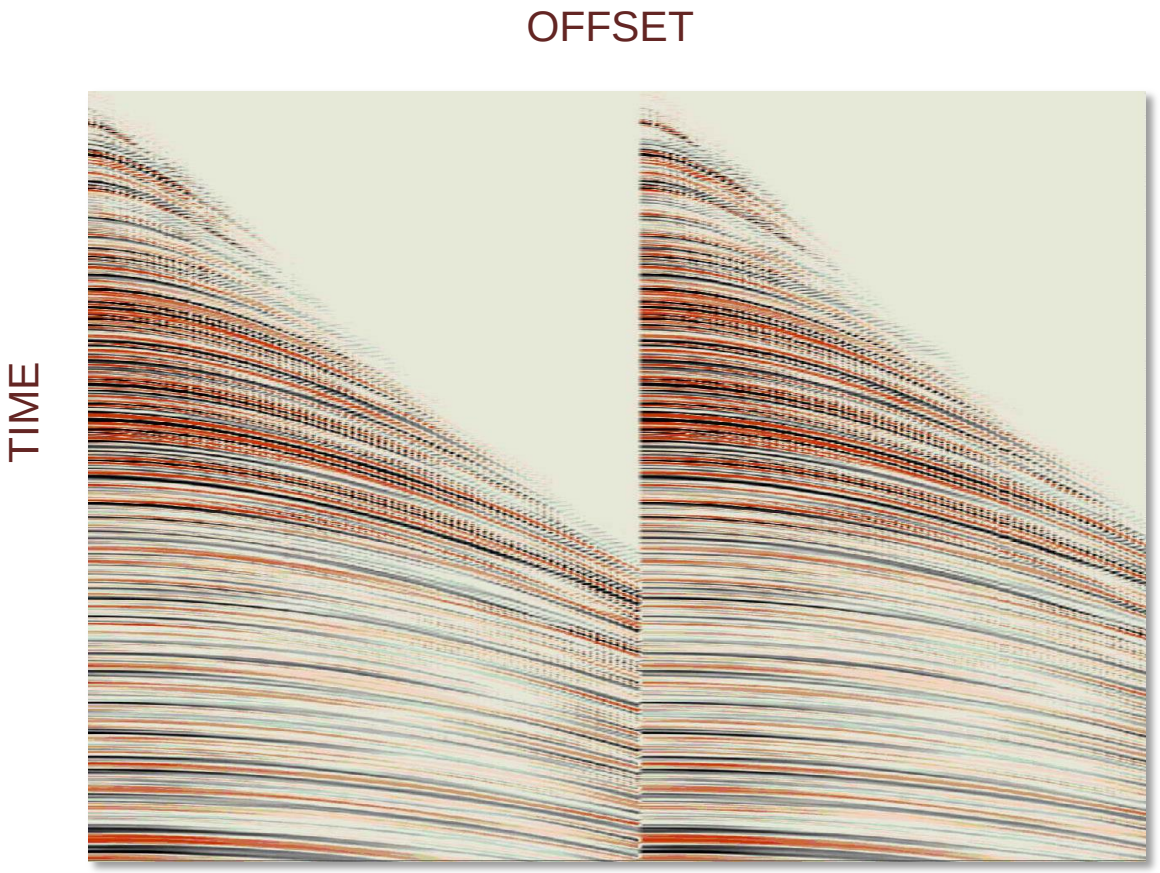

Original

Gathers

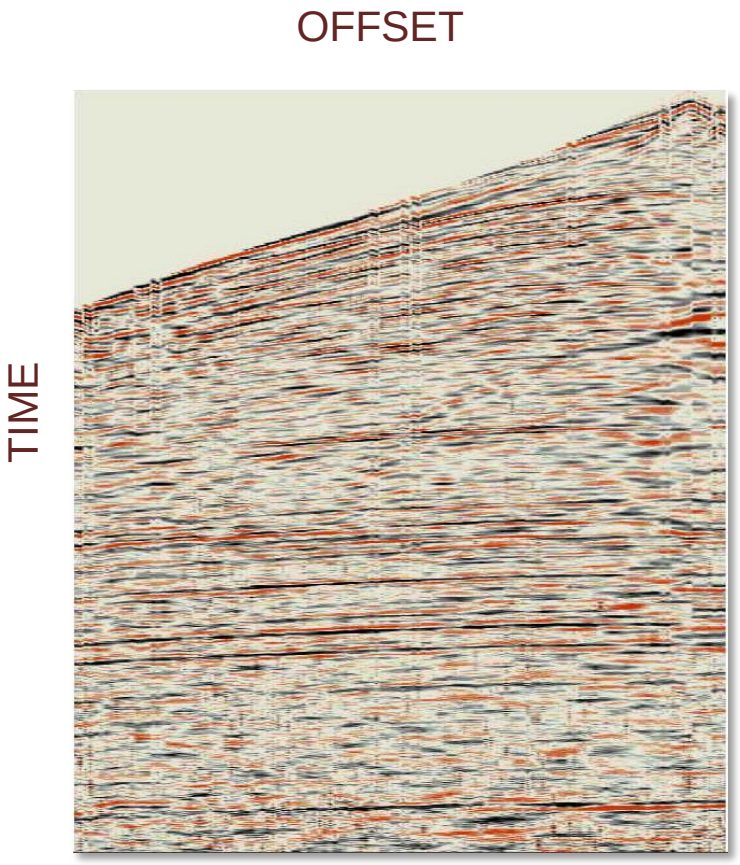

MF

Enhanced Pre-Stack Gather

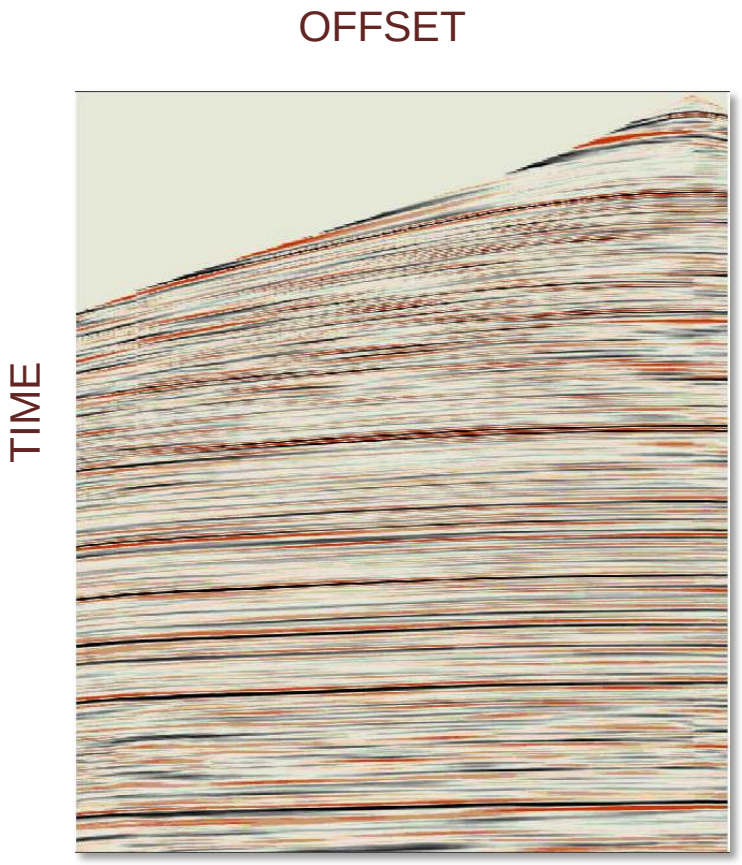

Original

Gathers

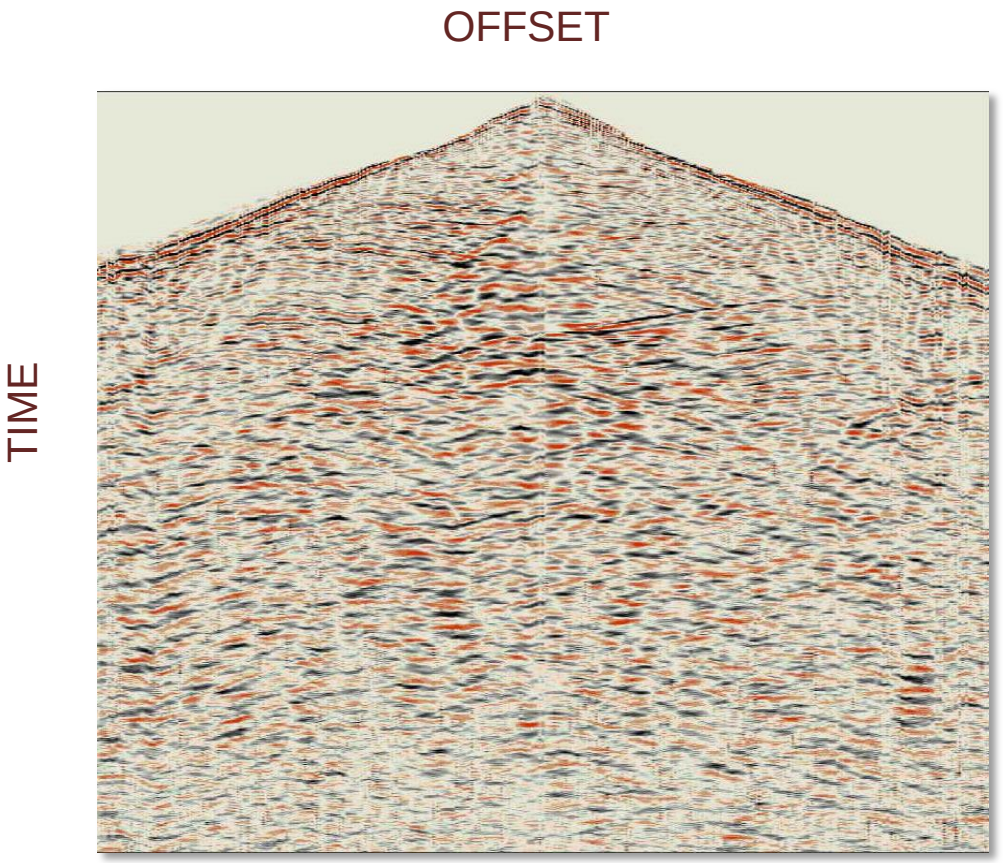

MF

Enhanced Pre-Stack Gather

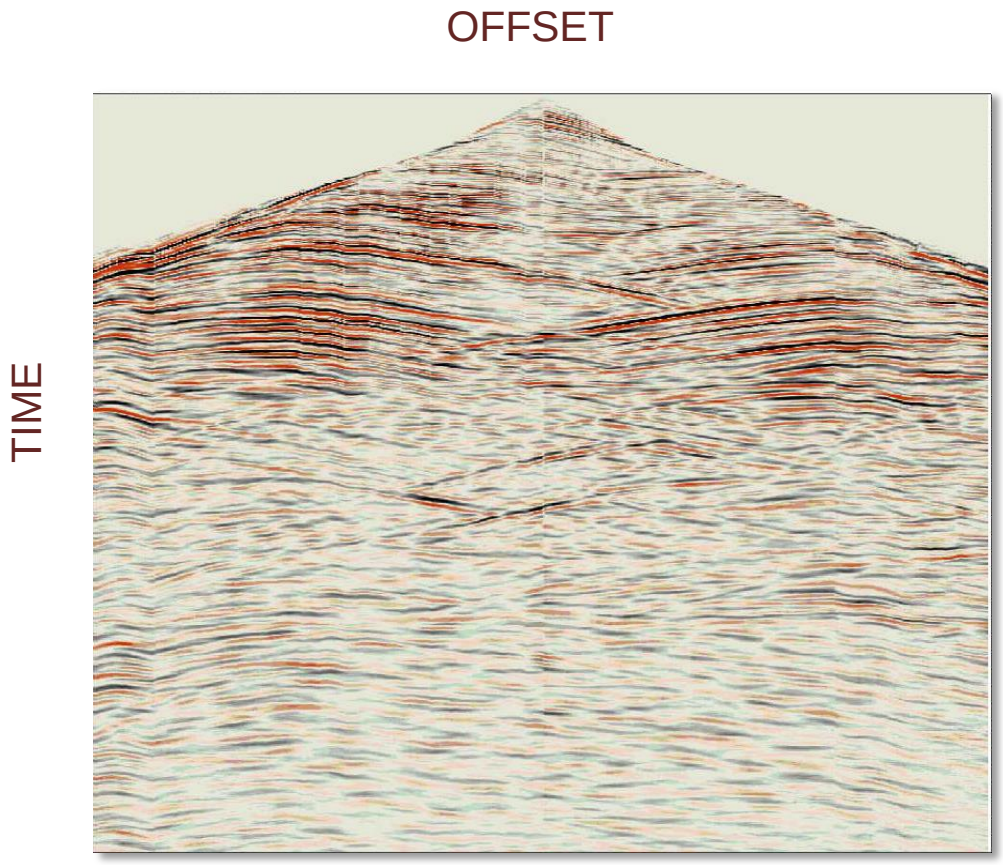

Operator oriented CO CRS-based signal enhancement

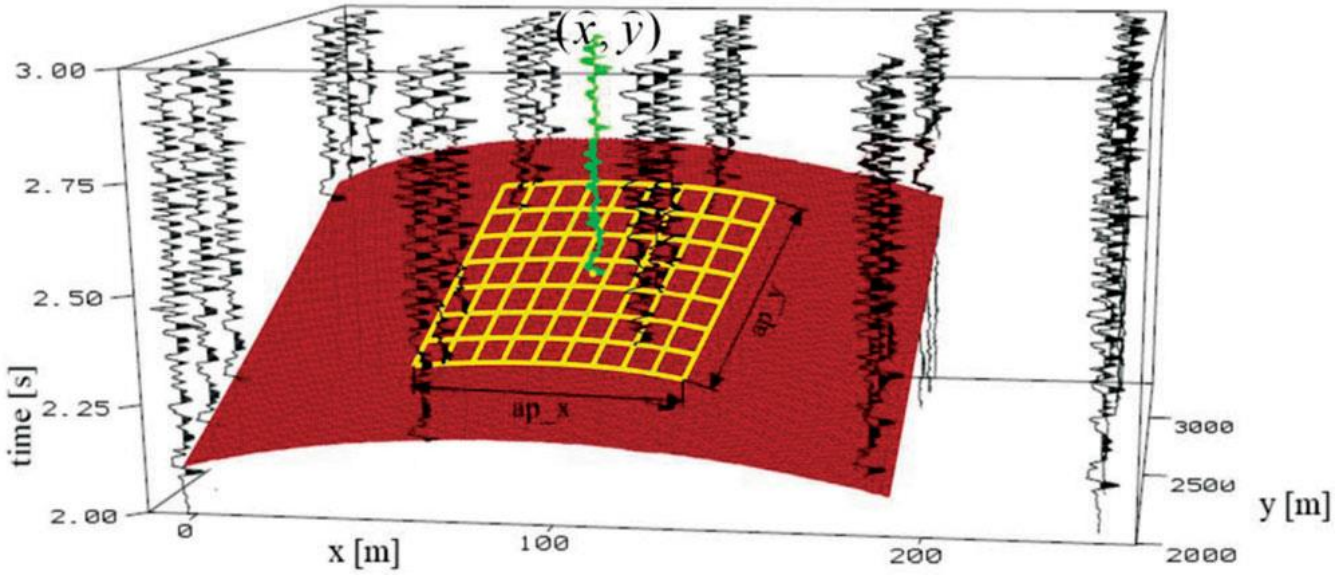

Signal enhancement in 3D data space: the observed traces are shown in black; the target trace is shown in green; the stacking operator for one sample is shown in brown. The summation aperture is shown in yellow

$$\Delta t = t(\Delta x, \Delta y) - \hat{t} = b_0 \Delta x + b_1 \Delta y + a_{00} \Delta x^2 + a_{01} \Delta x \Delta y + a_{11} \Delta y^2$$

where, the time-shift *t* is the moveout of a reflection event relative to the investigated sample $\hat{t}$ of the target trace and $\Delta x = x - \hat{x}$ and $\Delta y = y - \hat{y}$ are the positions of the data traces relative to the target trace location. The unknown parameters b_0, b_1 are the first-order special traveltime derivatives and a_{00}, a_{01}, a_{11} the second-order ones.

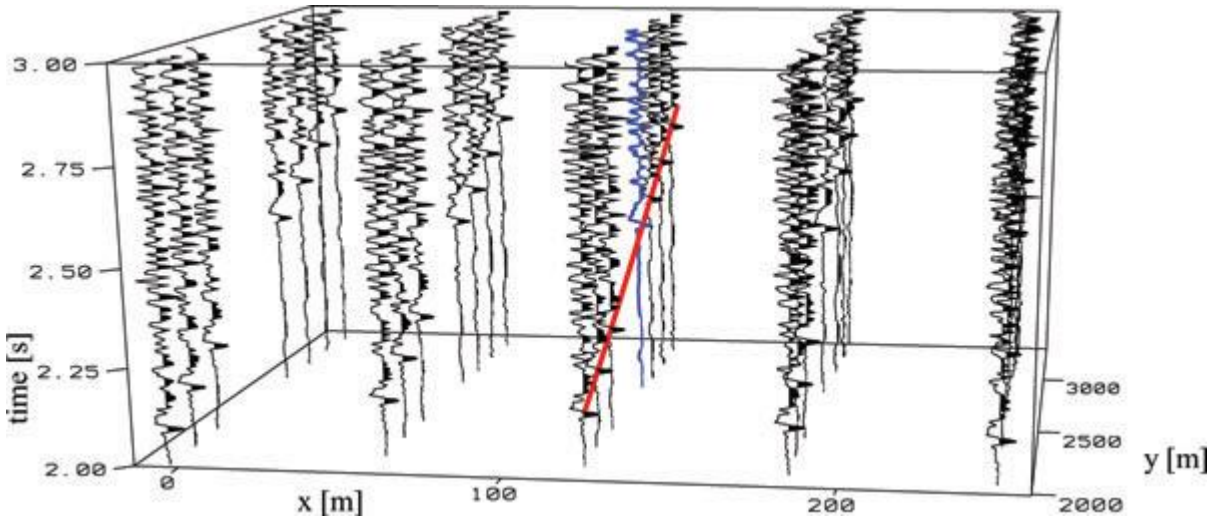

Estimation of the parameters $b1$ and $a11$ for a sample of a parameter trace (blue) within a bin in x-direction. The estimated operator is shown in red.

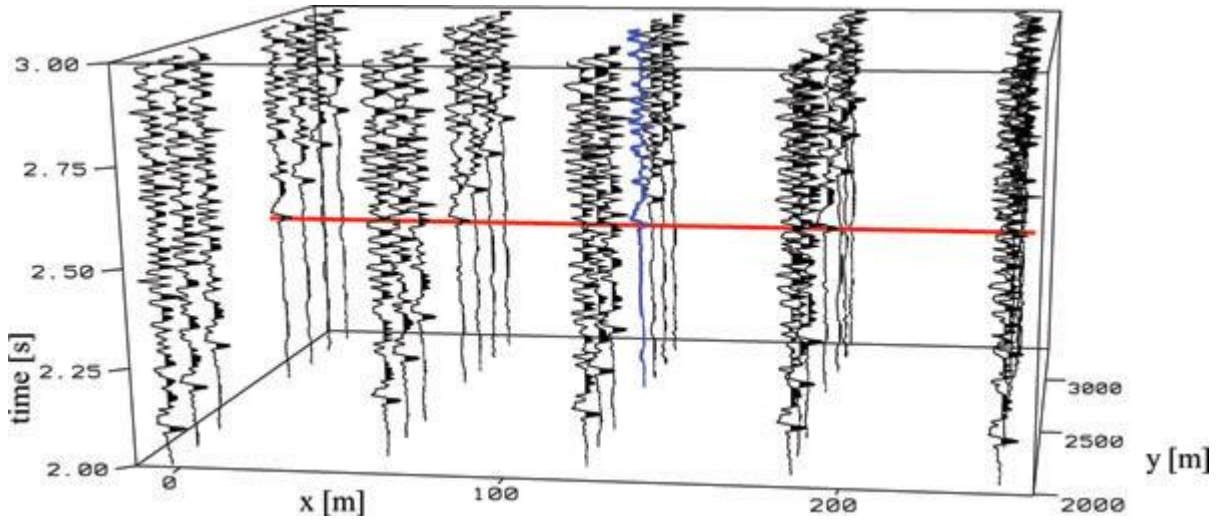

Estimation of the parameters *b*0 and *a*00 for a sample of a parameter trace (blue) within a bin in *y*-direction. The estimated operator is shown in red.

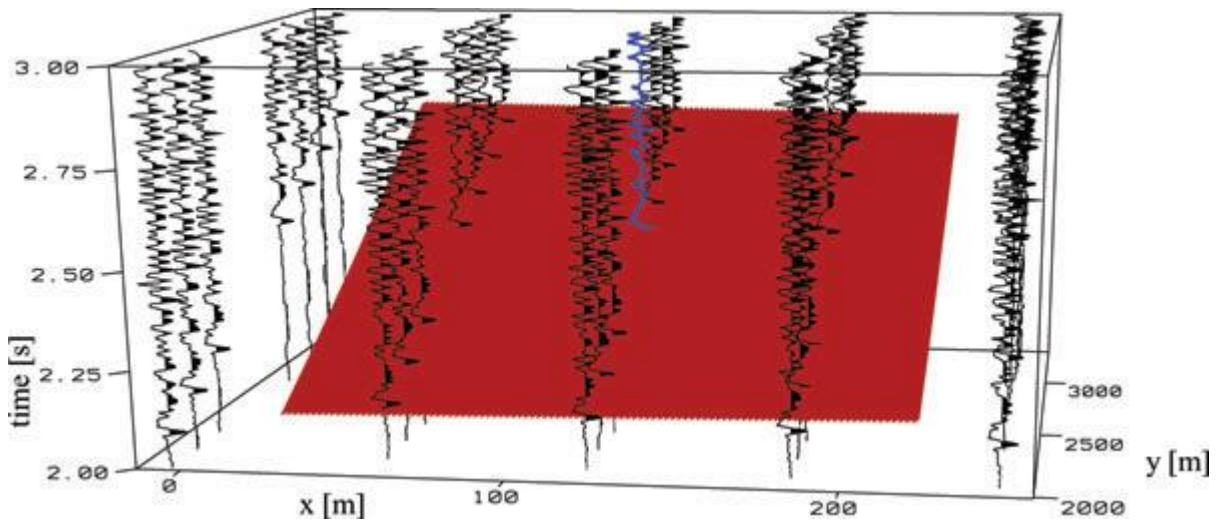

Estimation of the parameter *a*01 for a sample of a parameter trace (blue) within the data volume. The final operator is shown in red.

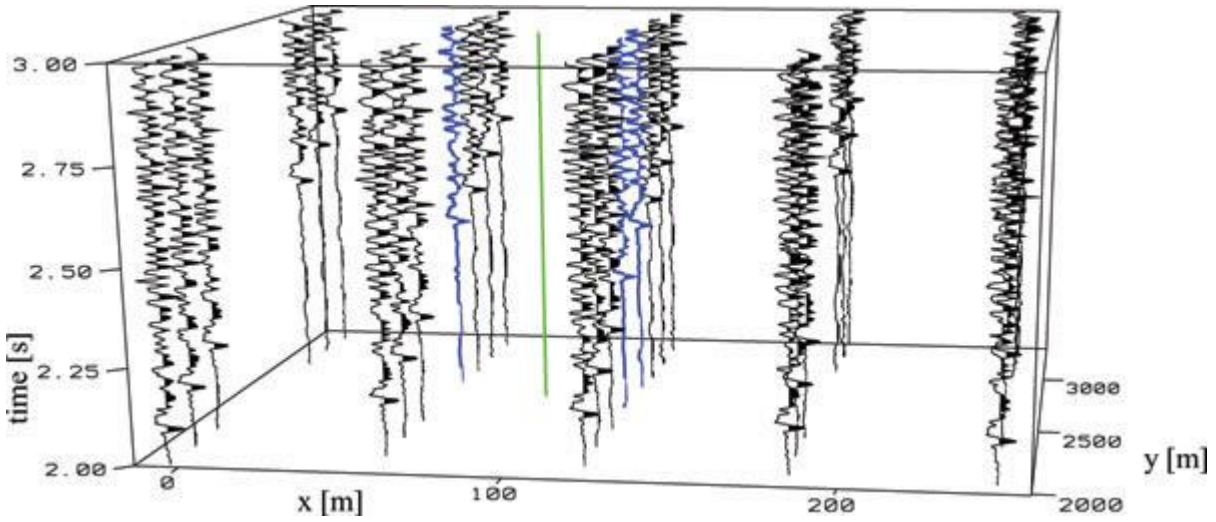

Position of a target trace (green) and three enclosing parameter traces (blue). The parameters allow to construct the operators at the parameter traces but these are required at the target trace.

Scheme of Data Enhancement

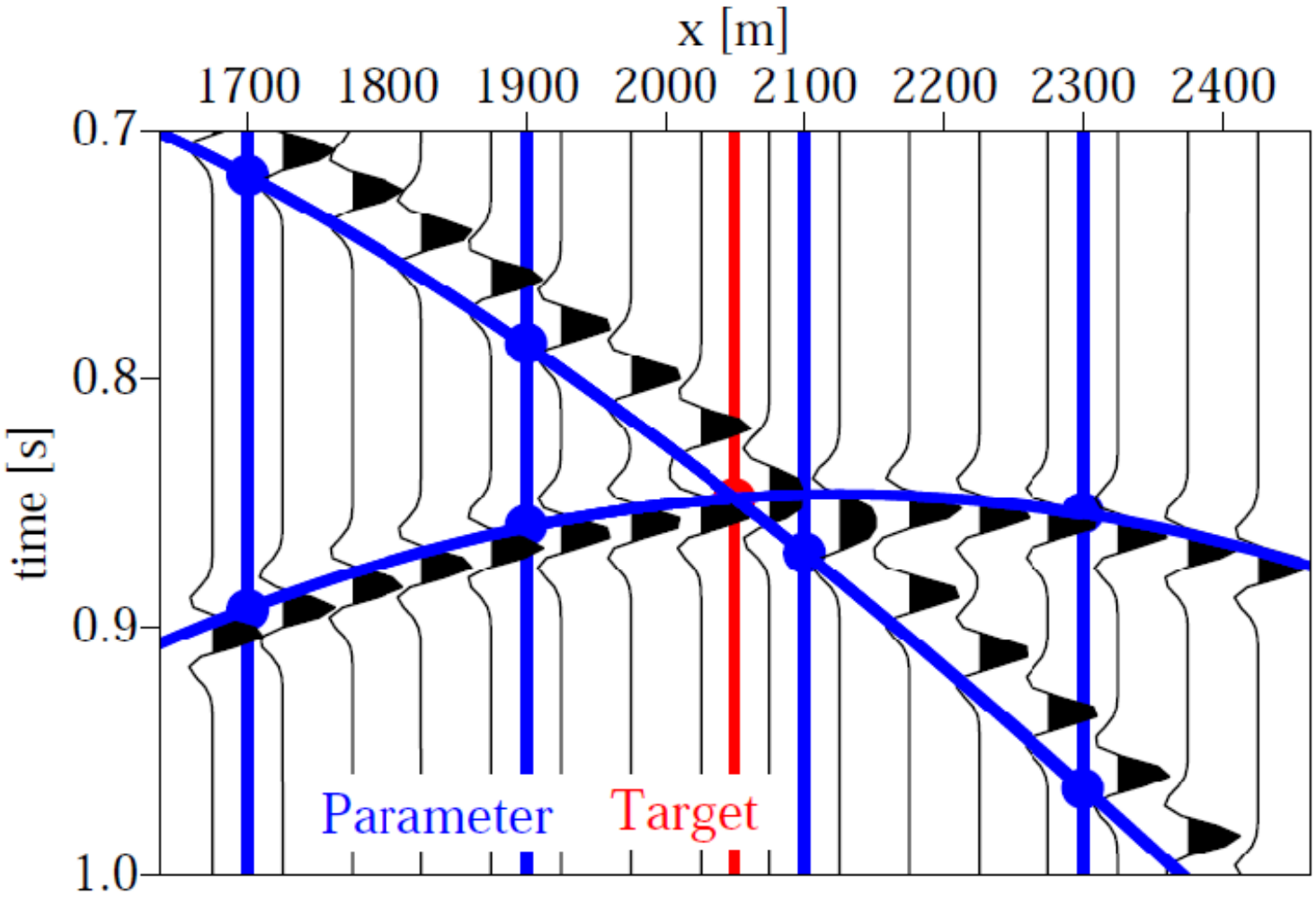

Scheme of Data Enhancement

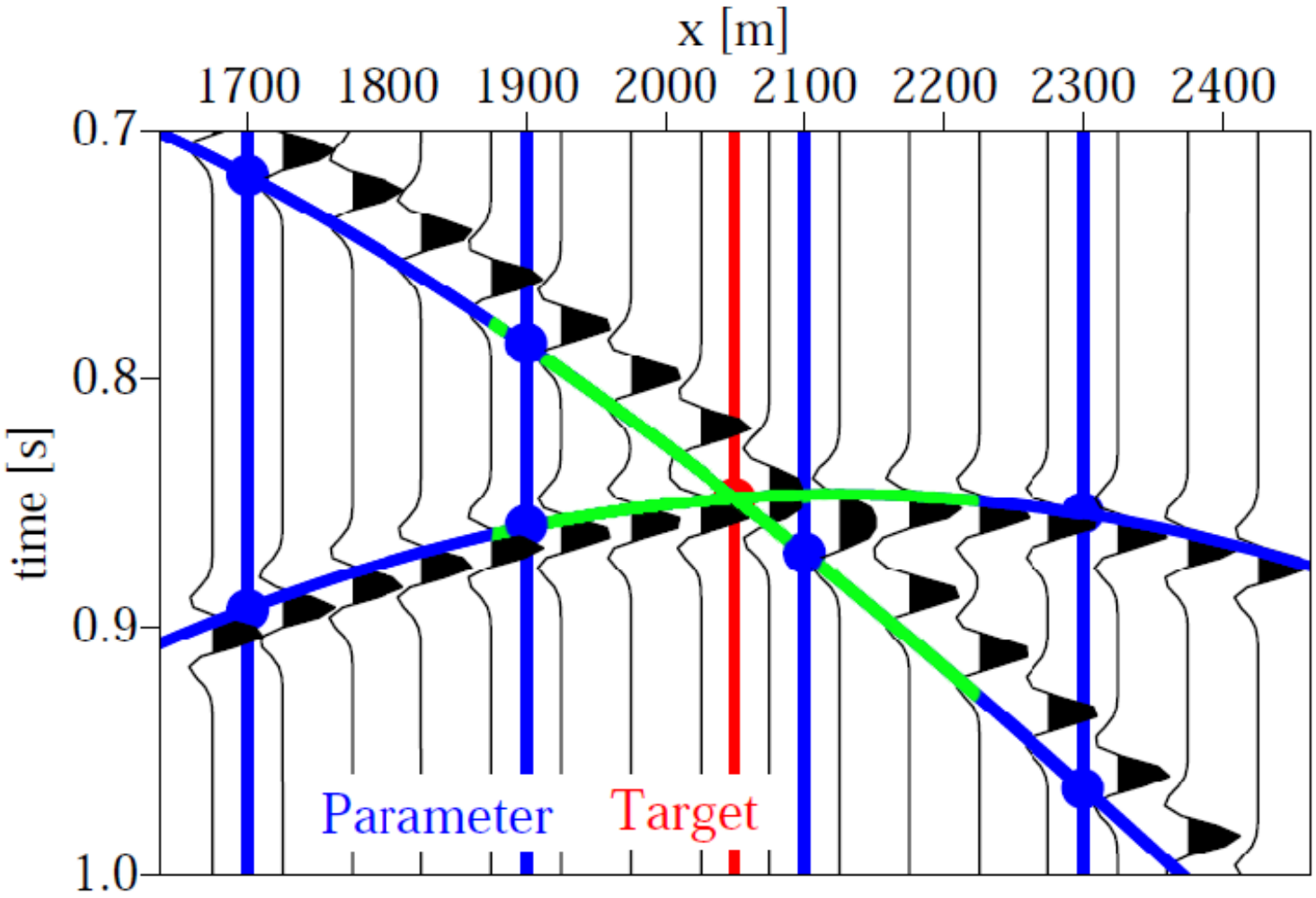

Input data

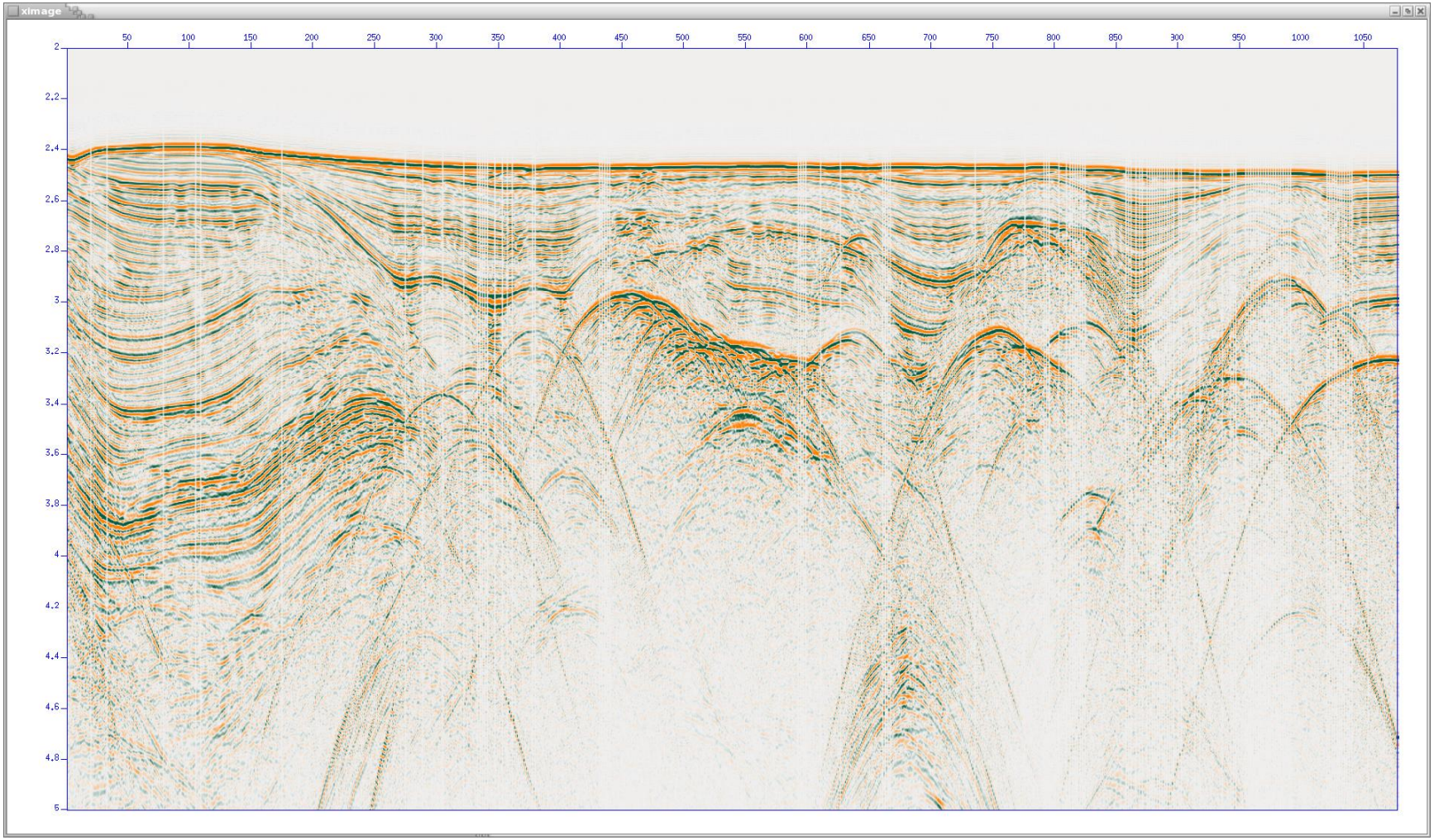
ximage
50 100 150 200 250 300 350 400 450 500 550 600 650 700 750 800 850 900 950 1000 1050
2 2.2 2.4 2.6 2.8 3 3.2 3.4 3.6 3.8 4 4.2 4.4 4.6 4.8 5

Interpolated and enhanced data

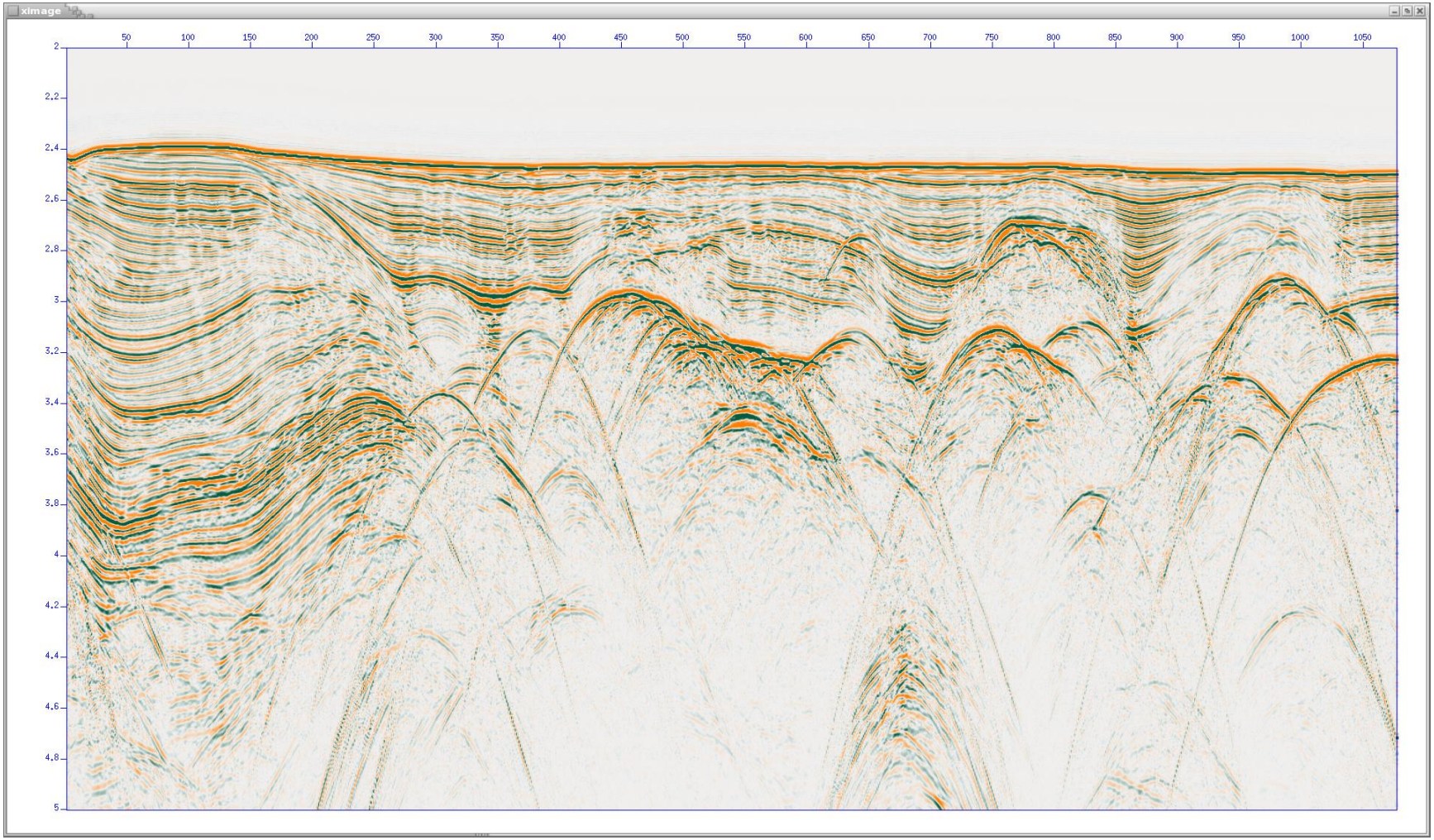

Interpolated and enhanced data

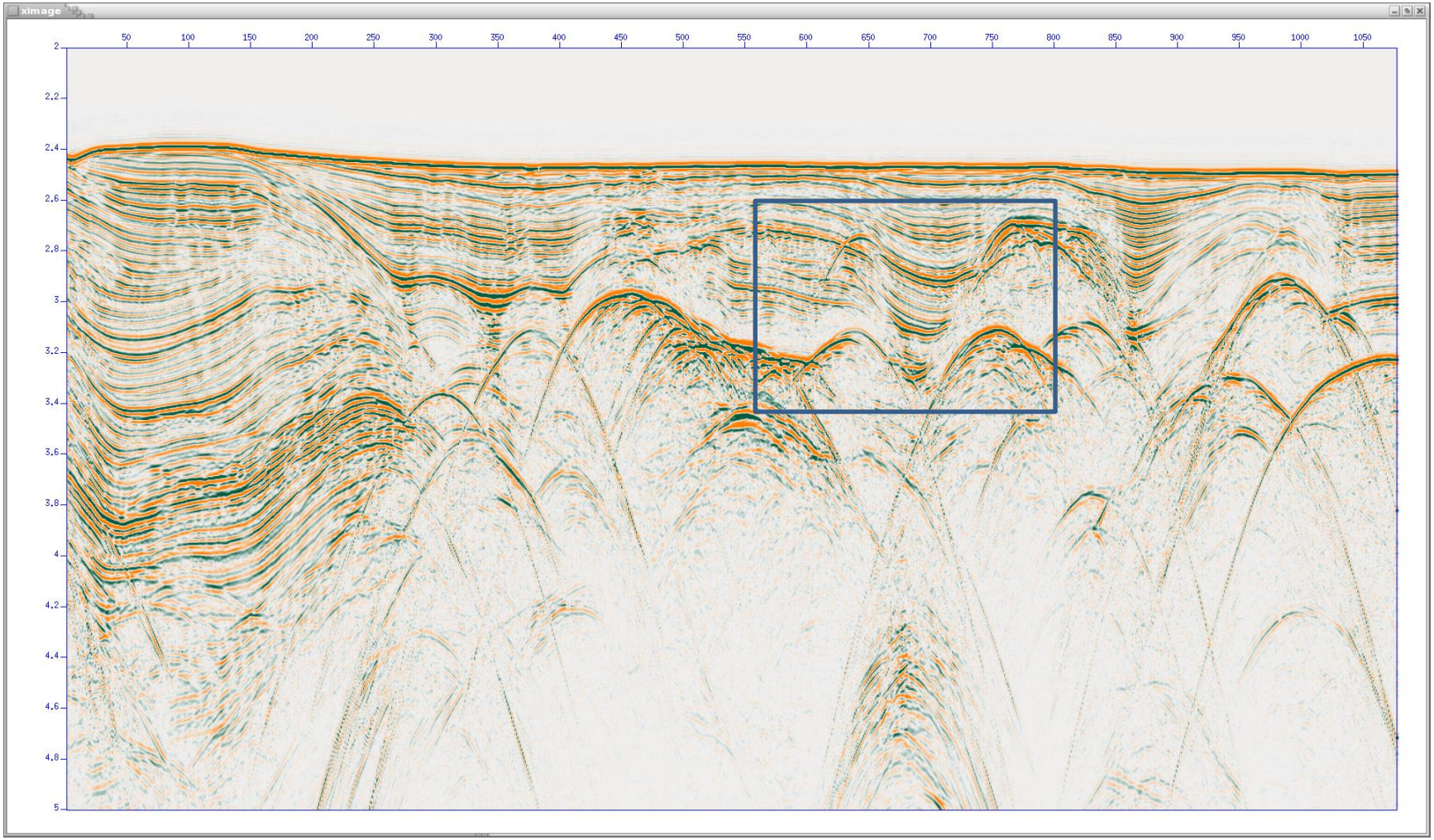

Input dataset:

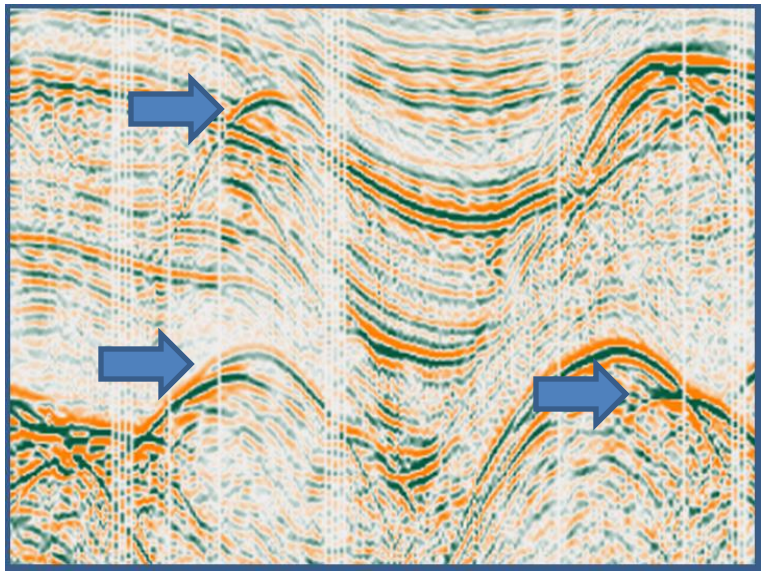

Enhanced dataset:

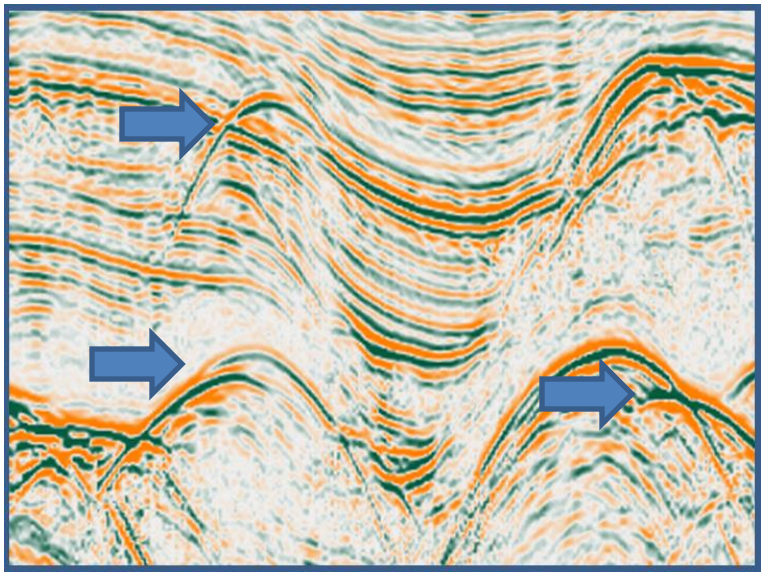

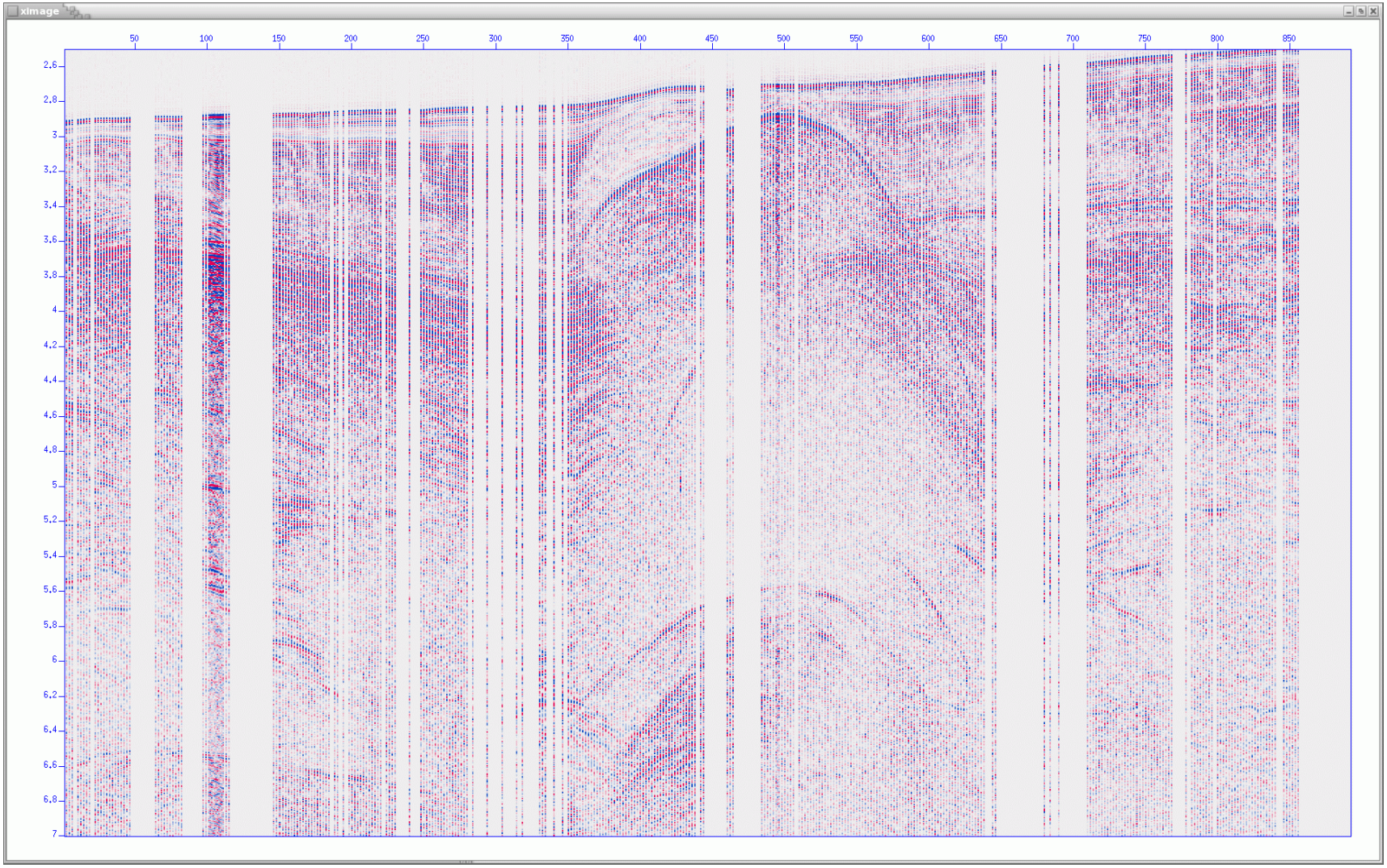

Input: CO Class=500m

Interpolated and enhanced data

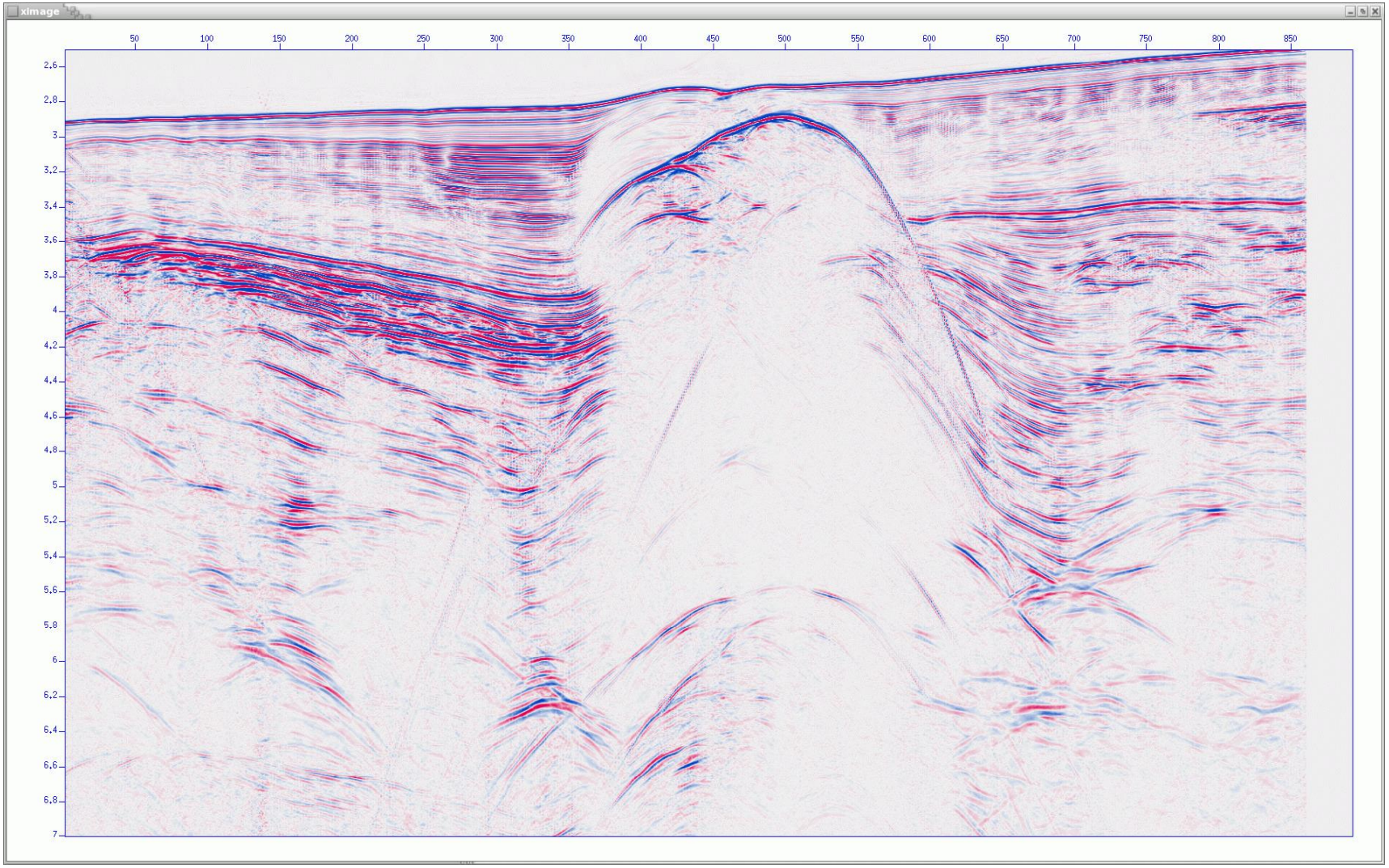

Output: CO Class=500m

Input data

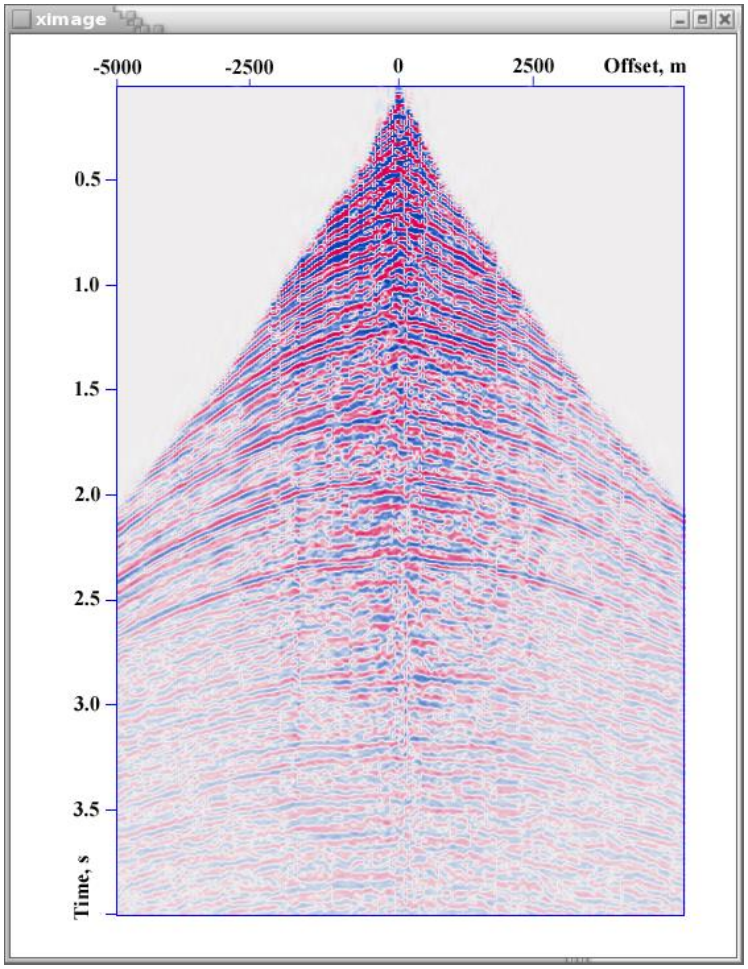

Enhanced data

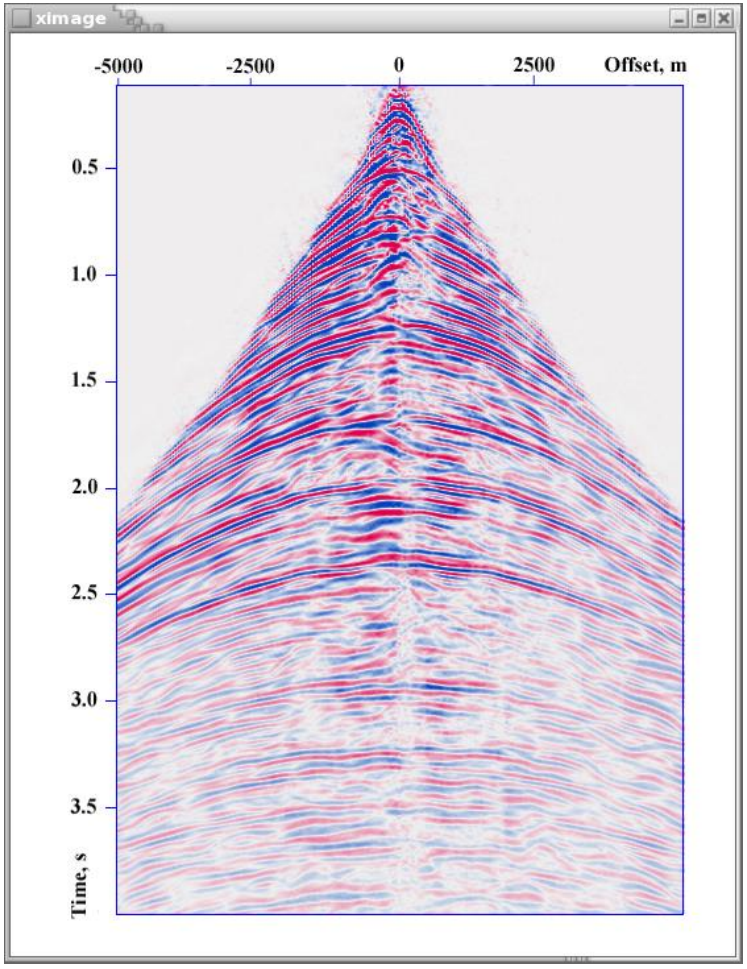

original CMP 505 enhanced

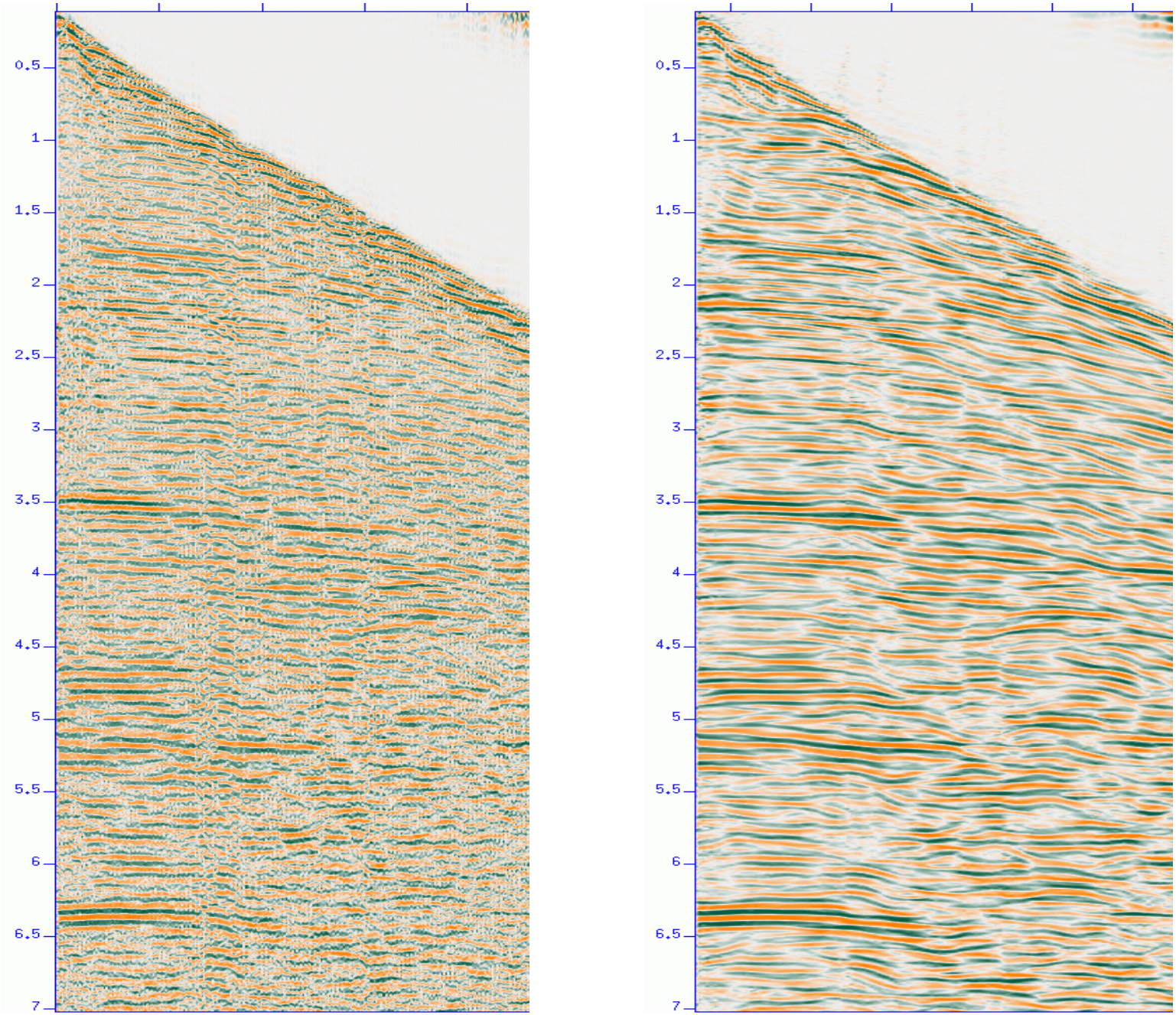

original CMP 2505 enhanced

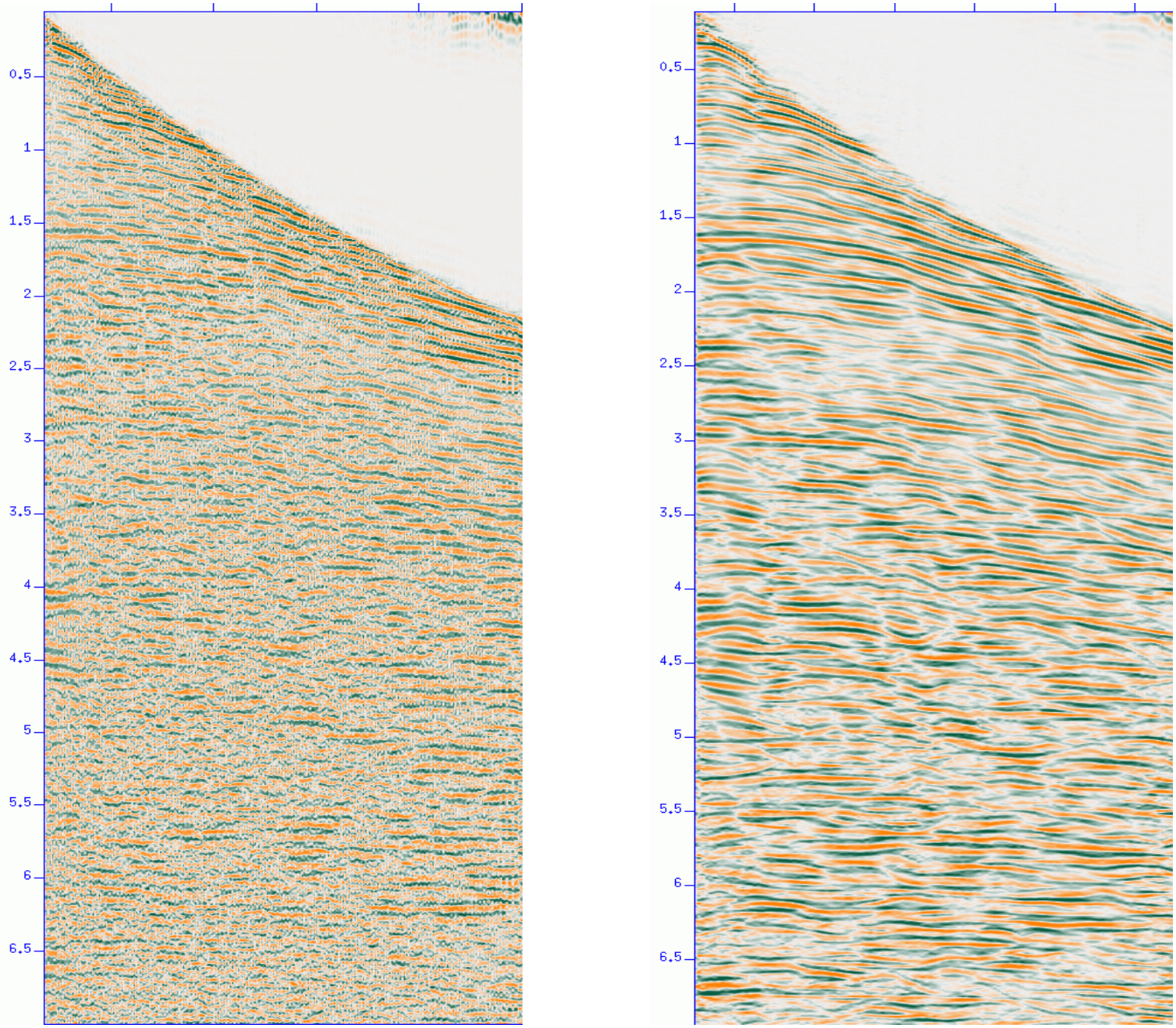

original CMP 3400 enhanced

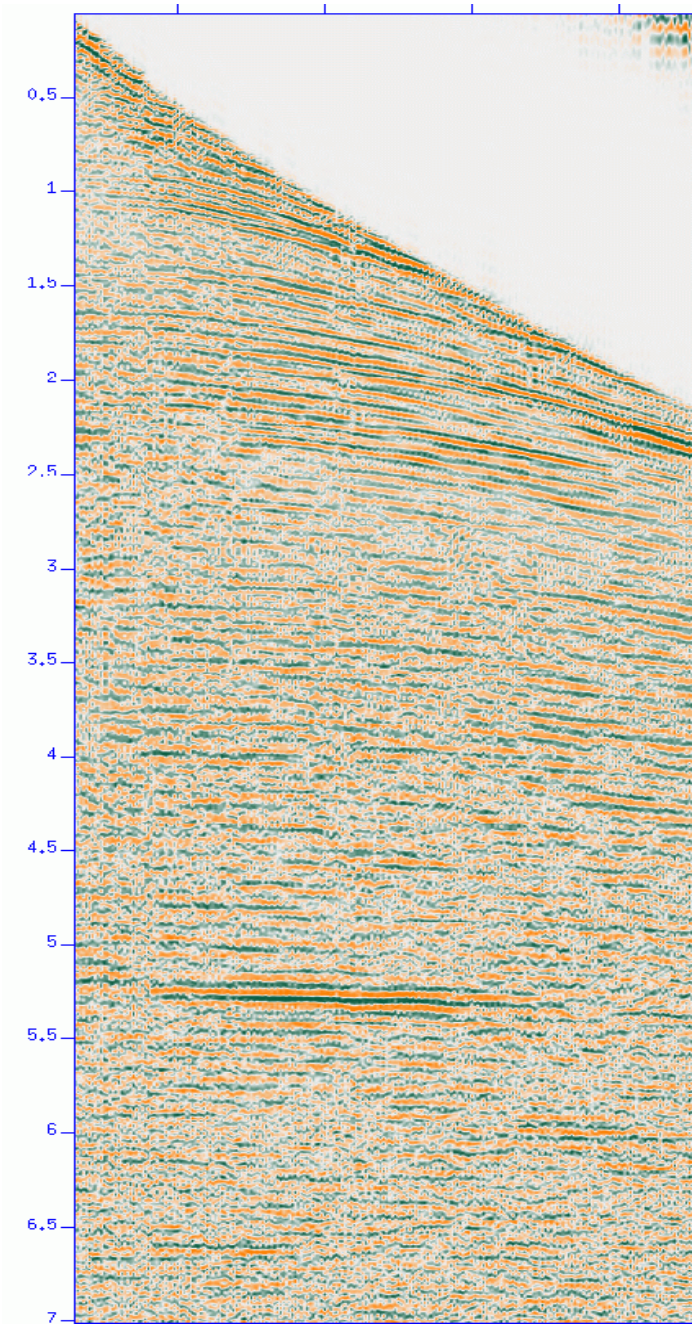

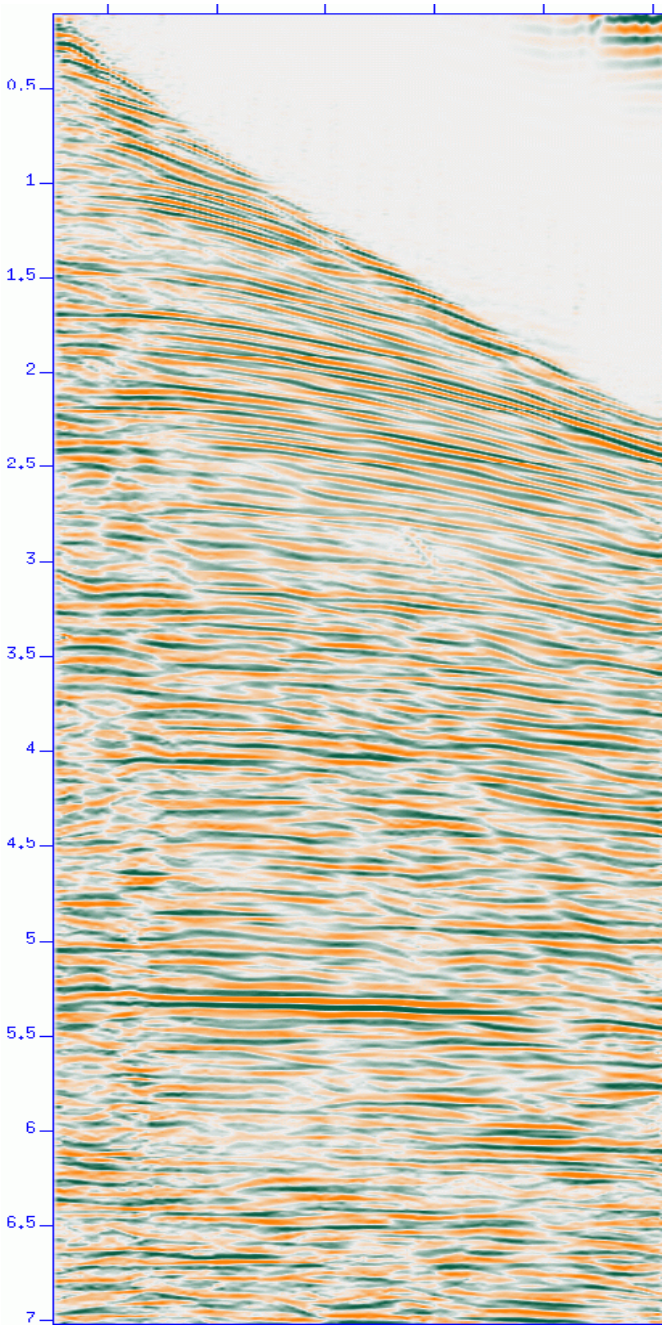

Original stacked cube

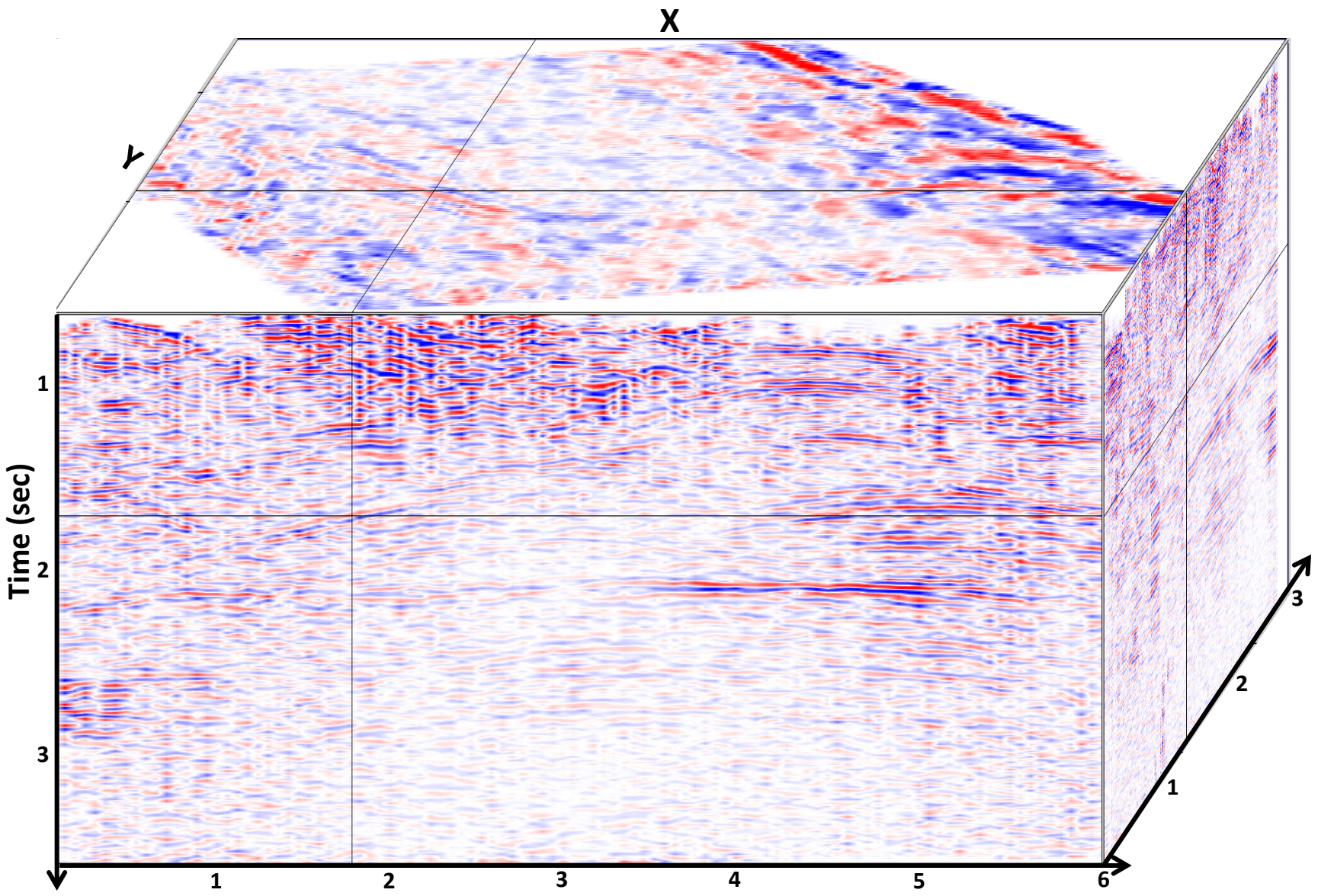

Original sections

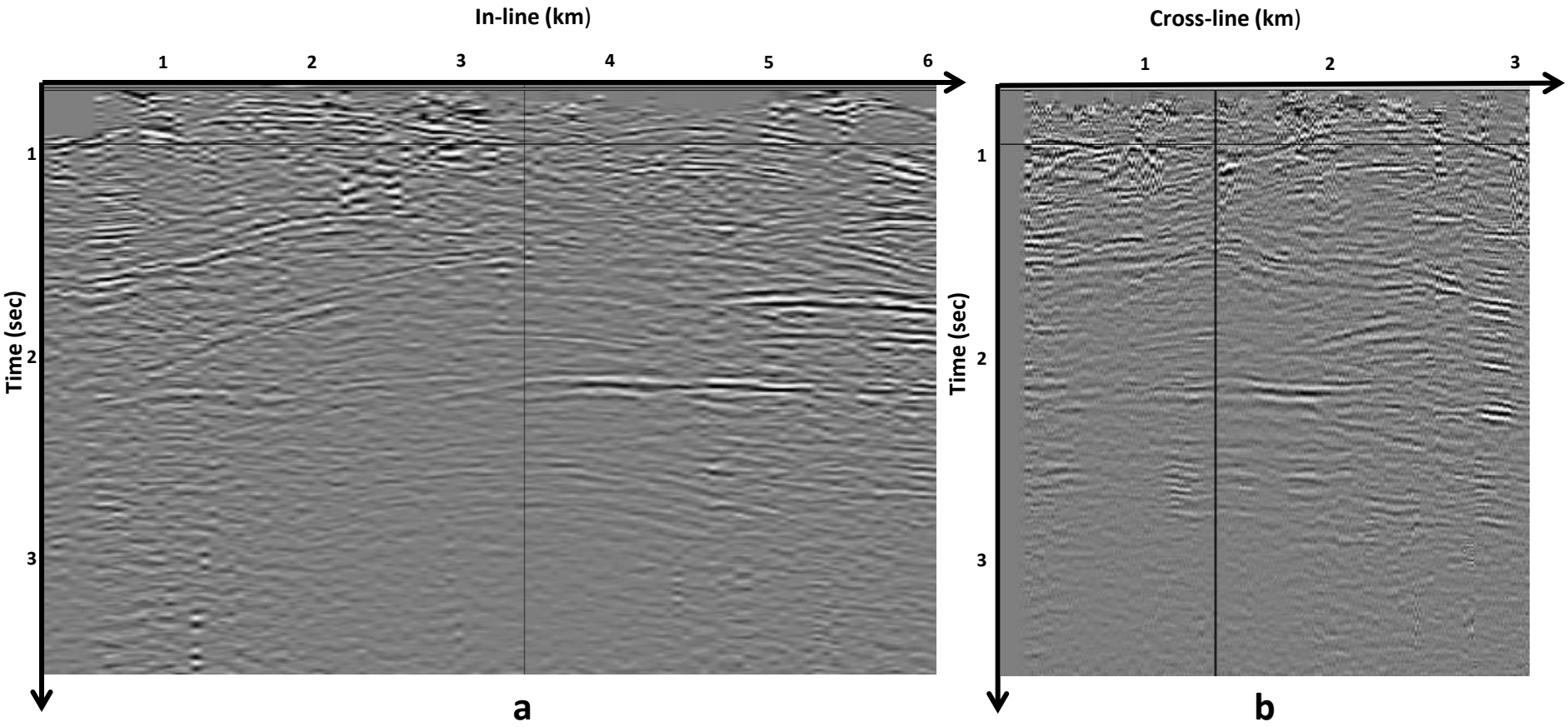

Enhanced sections

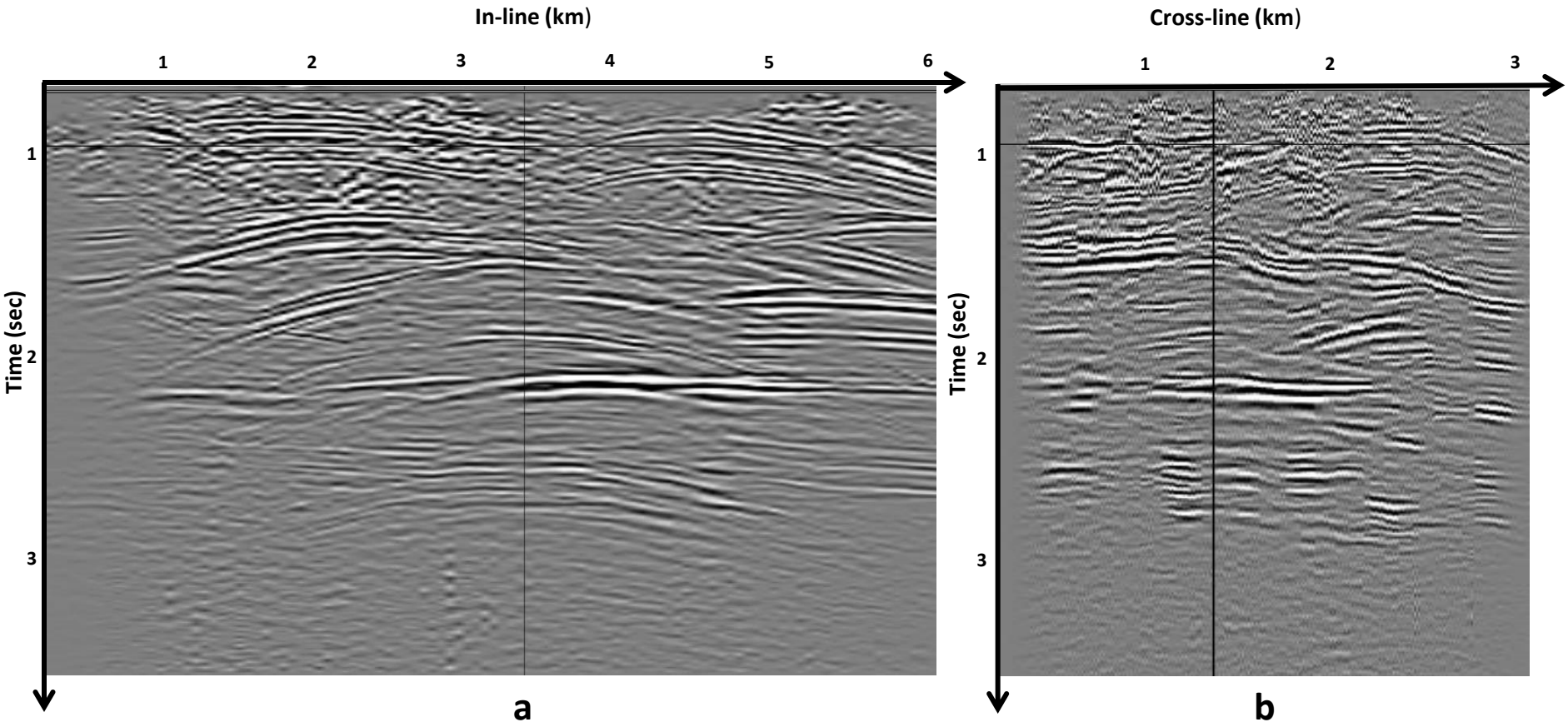

Original sections

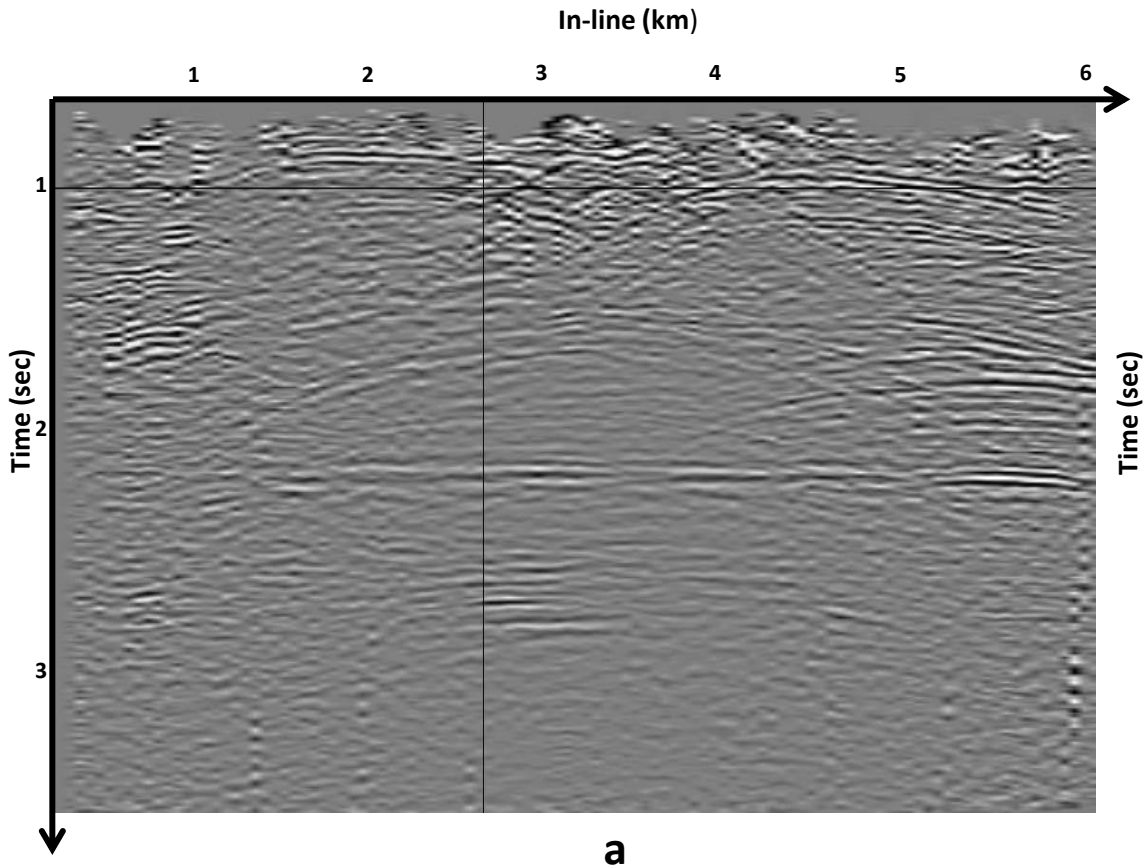

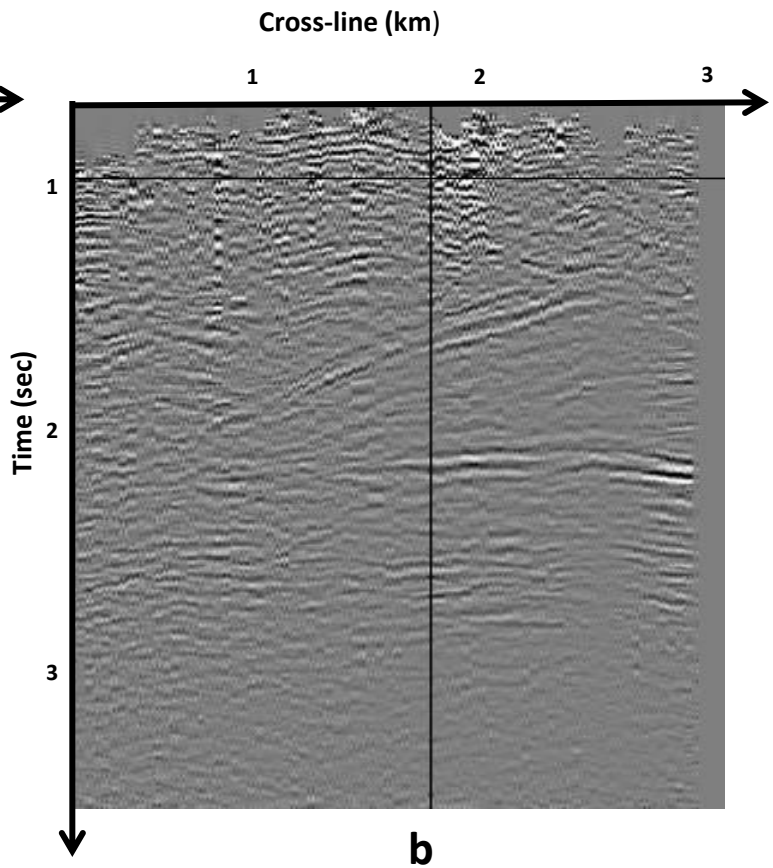

Enhanced sections

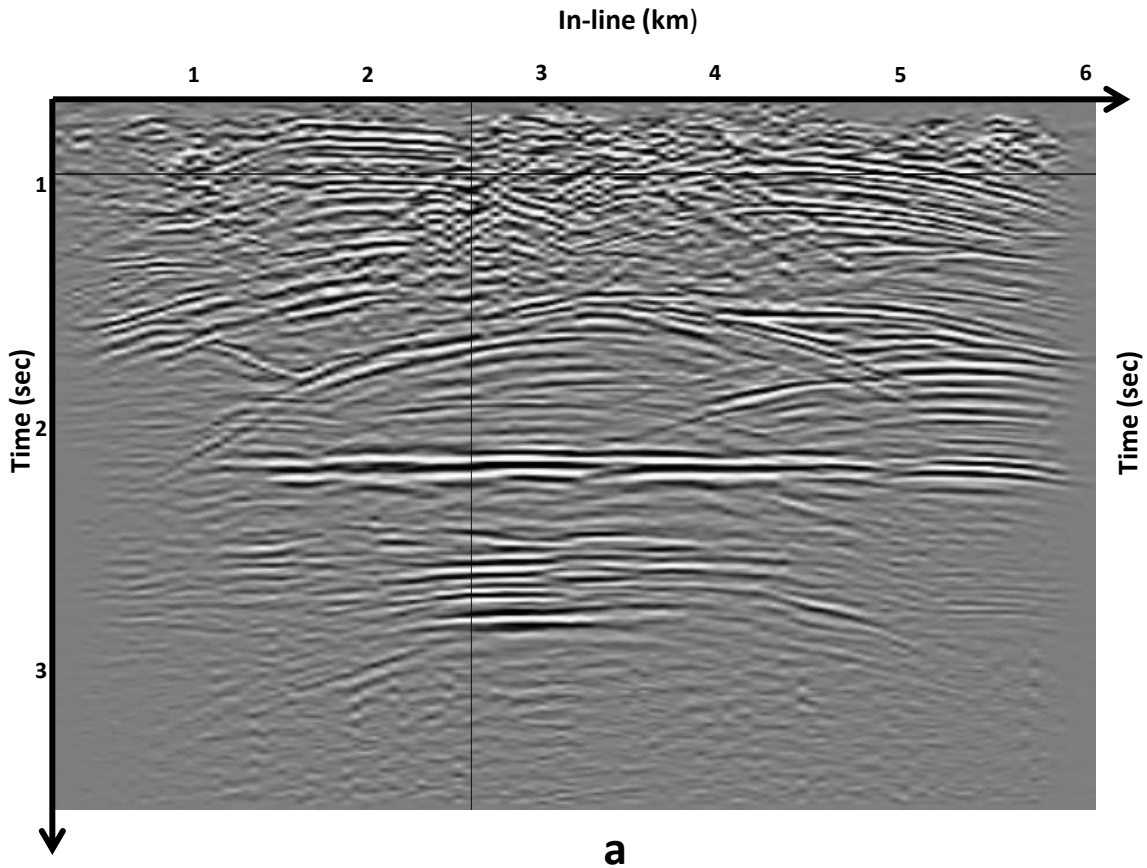

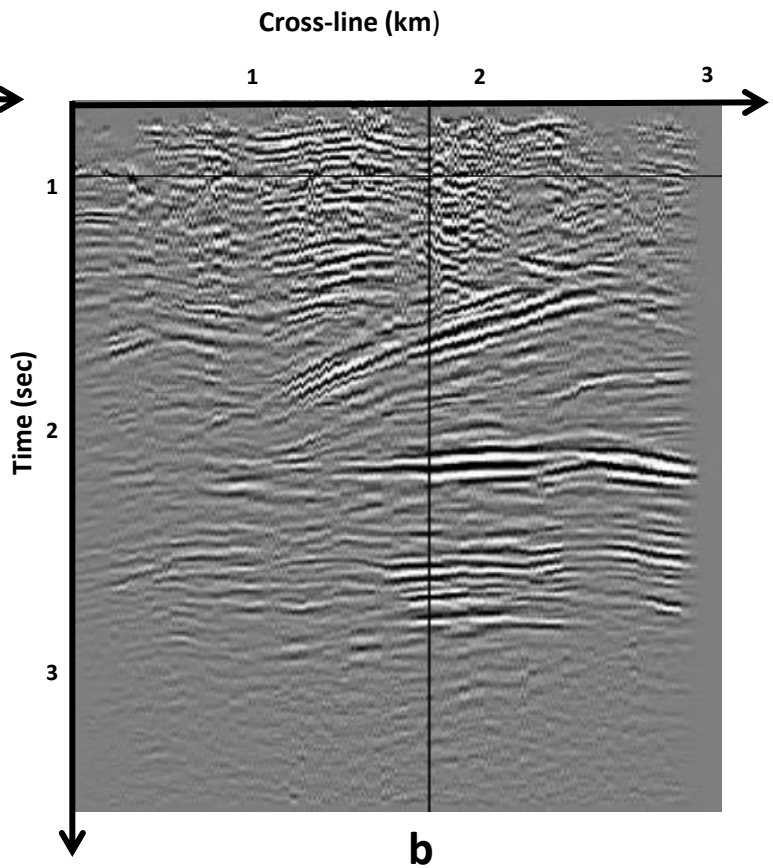

Original time slice

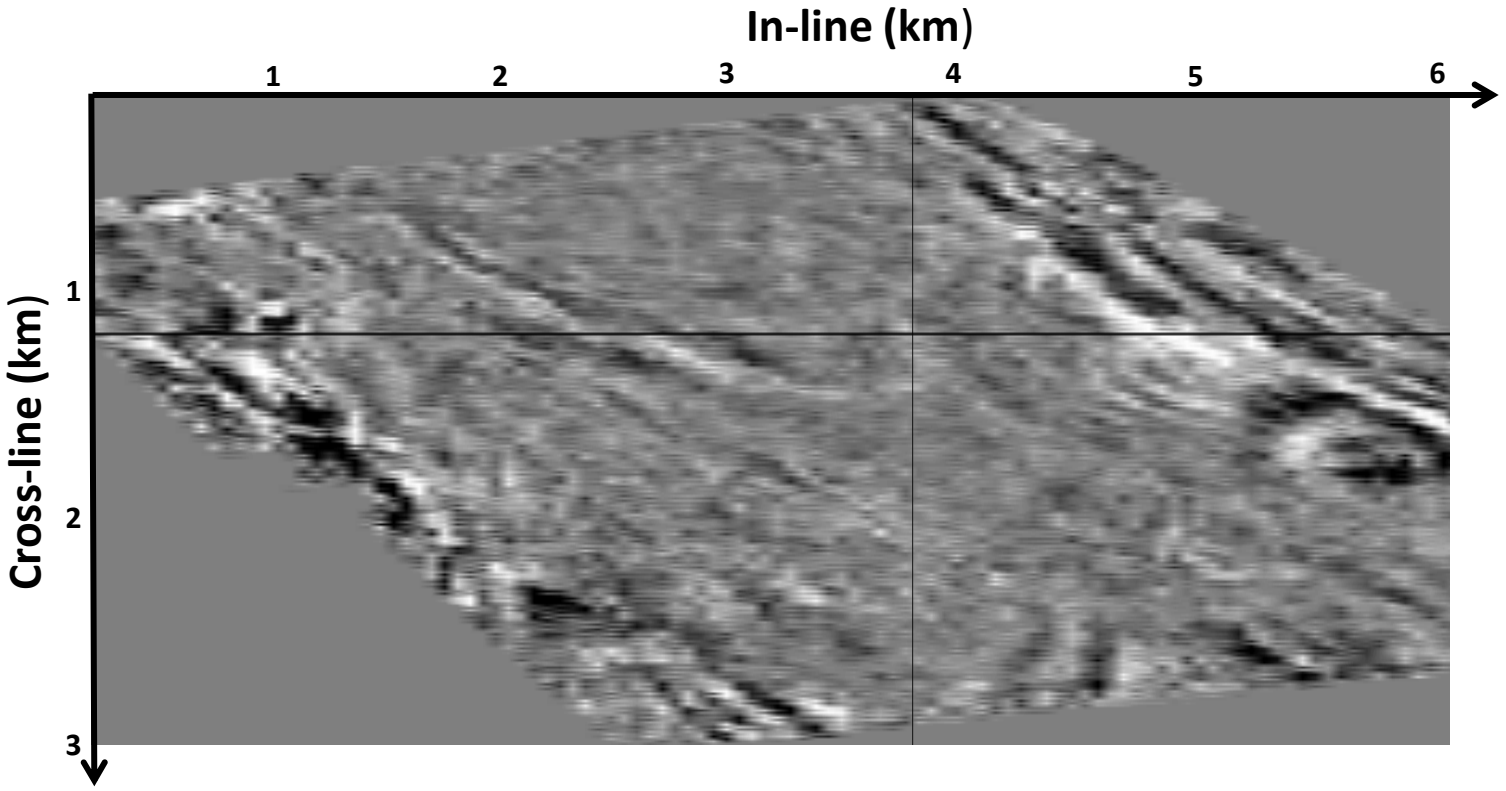

Enhanced time slice

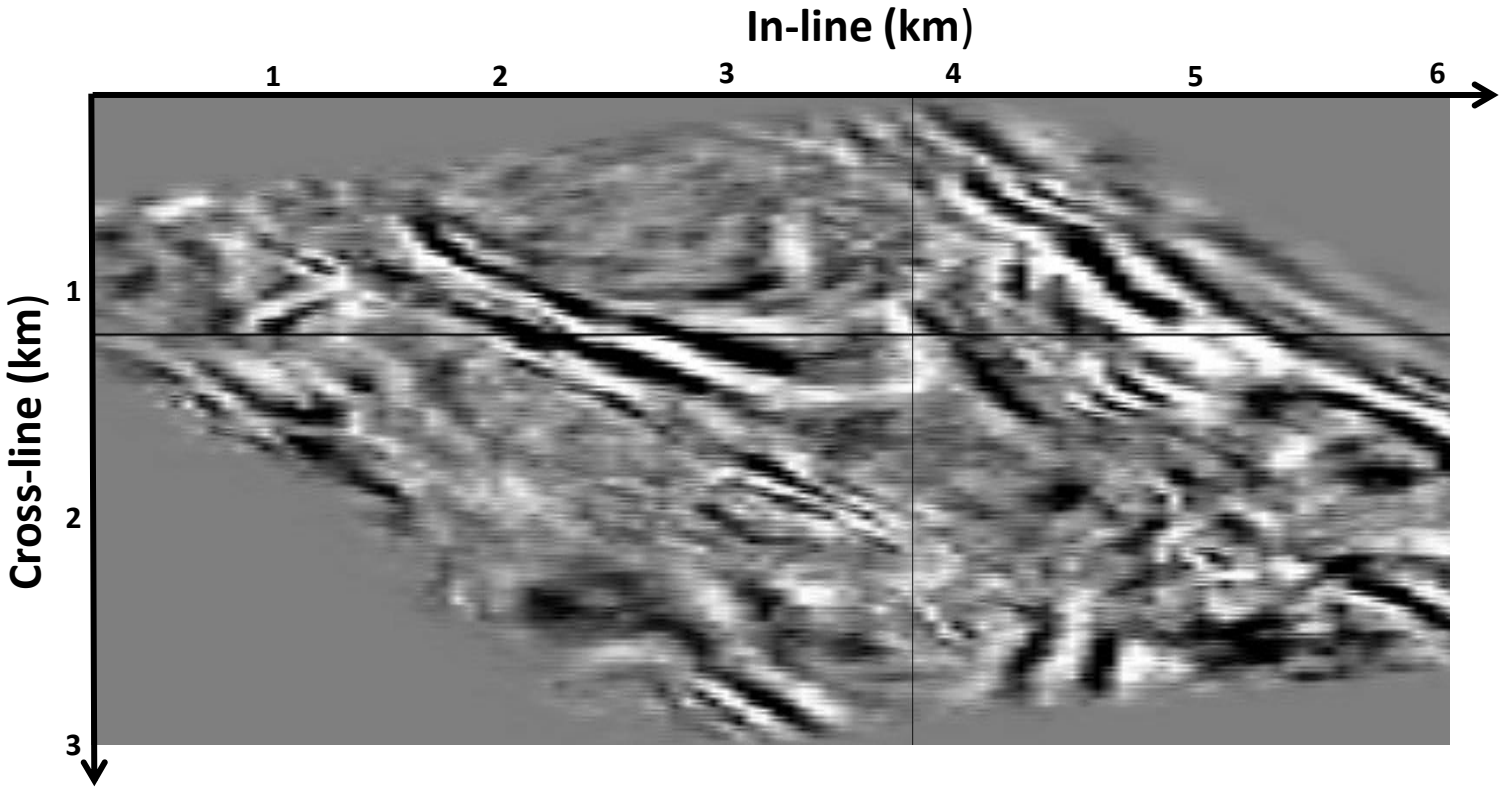

Original time slice

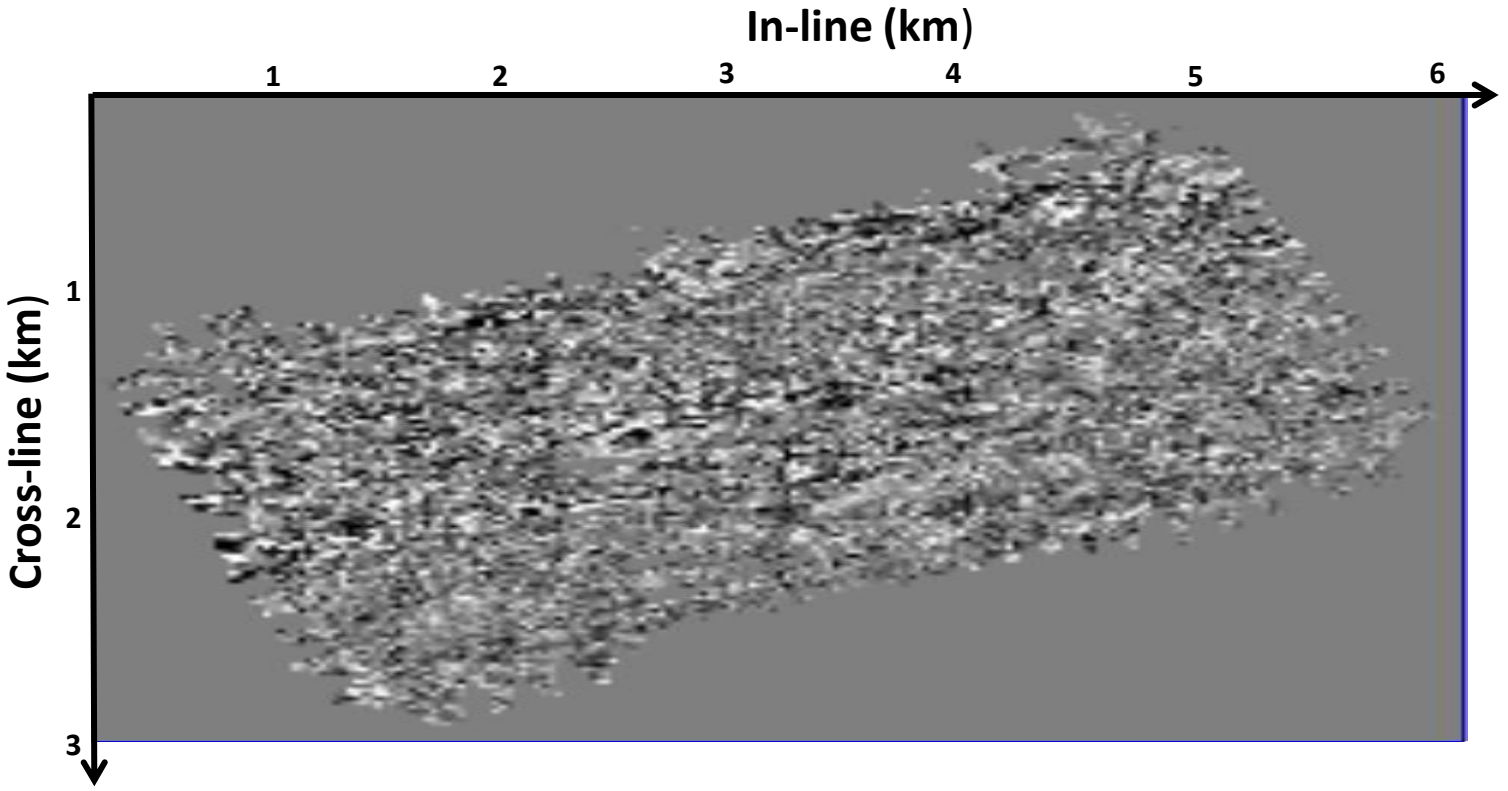

Enhanced time slice

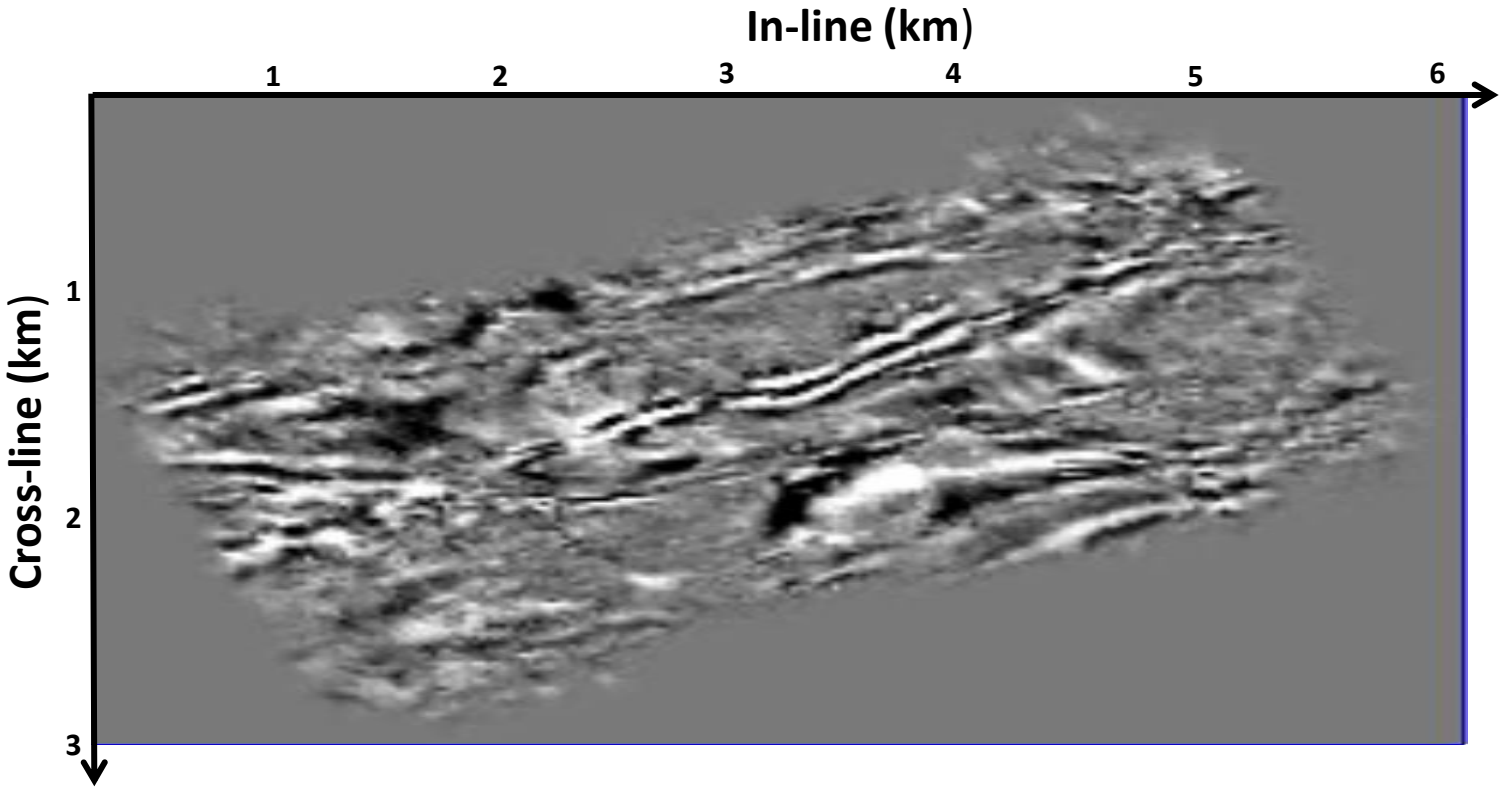

Enhanced stacked cube

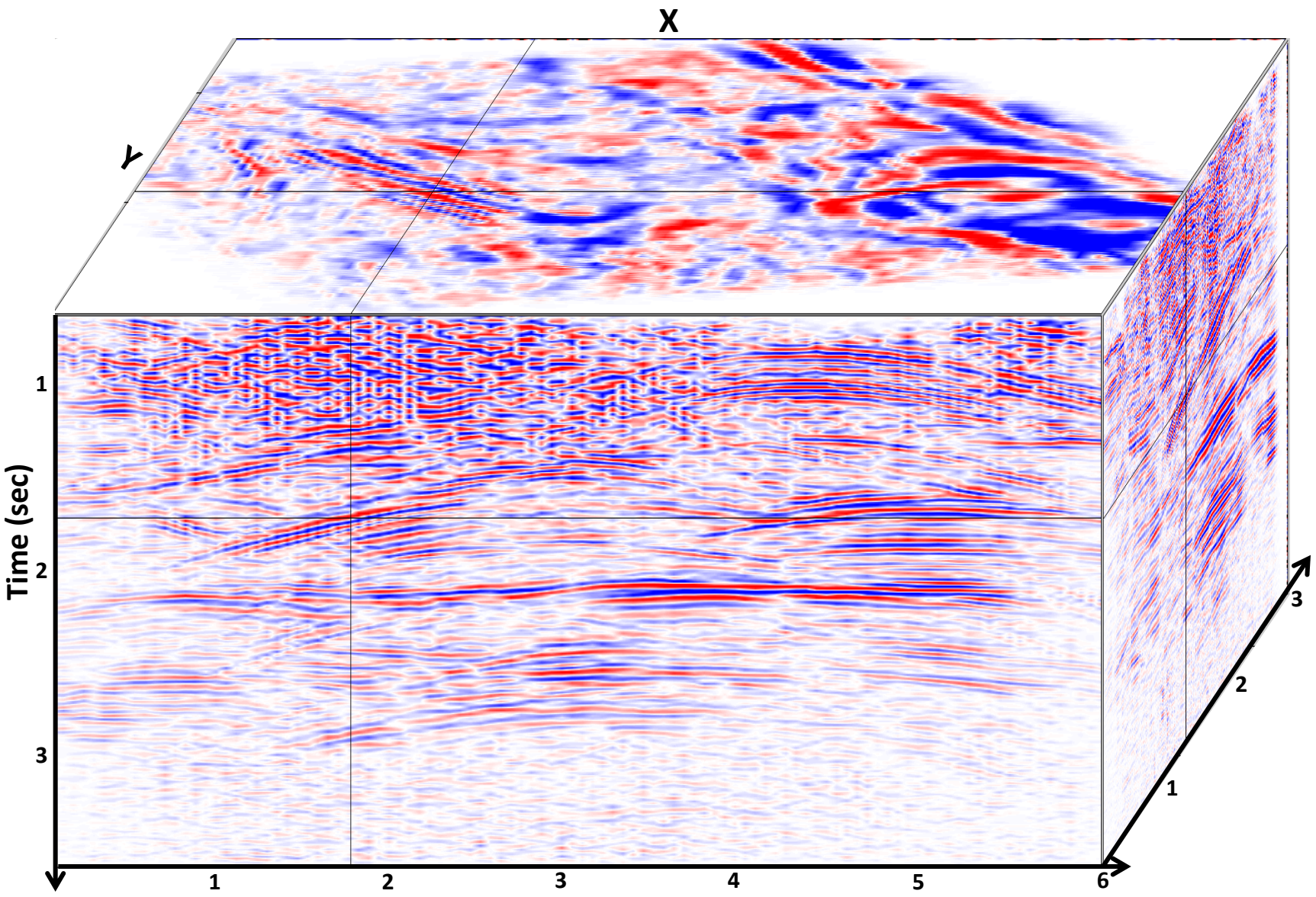

Original stacked cube

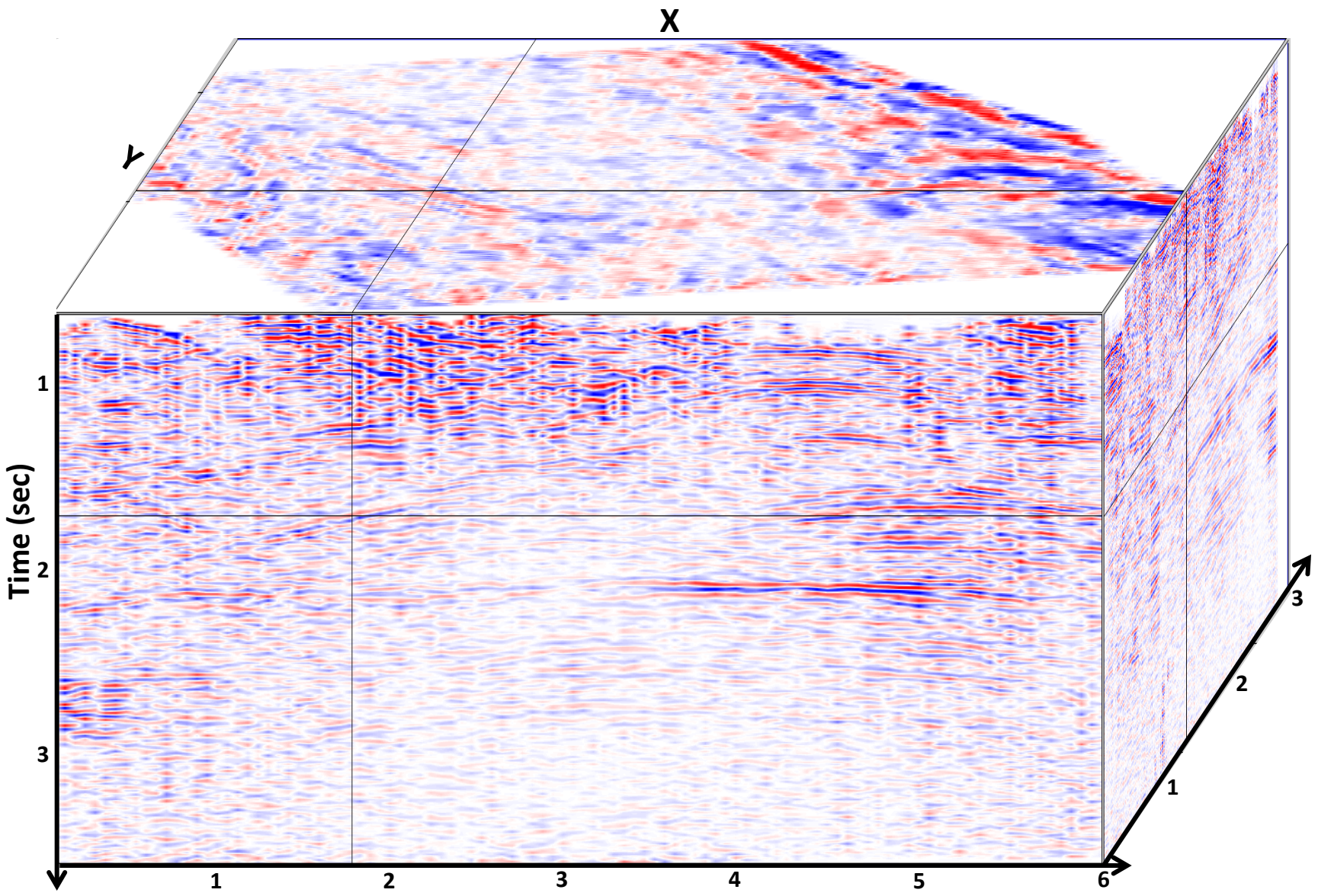

Non-CMP based seismic data analysis, processing and imaging

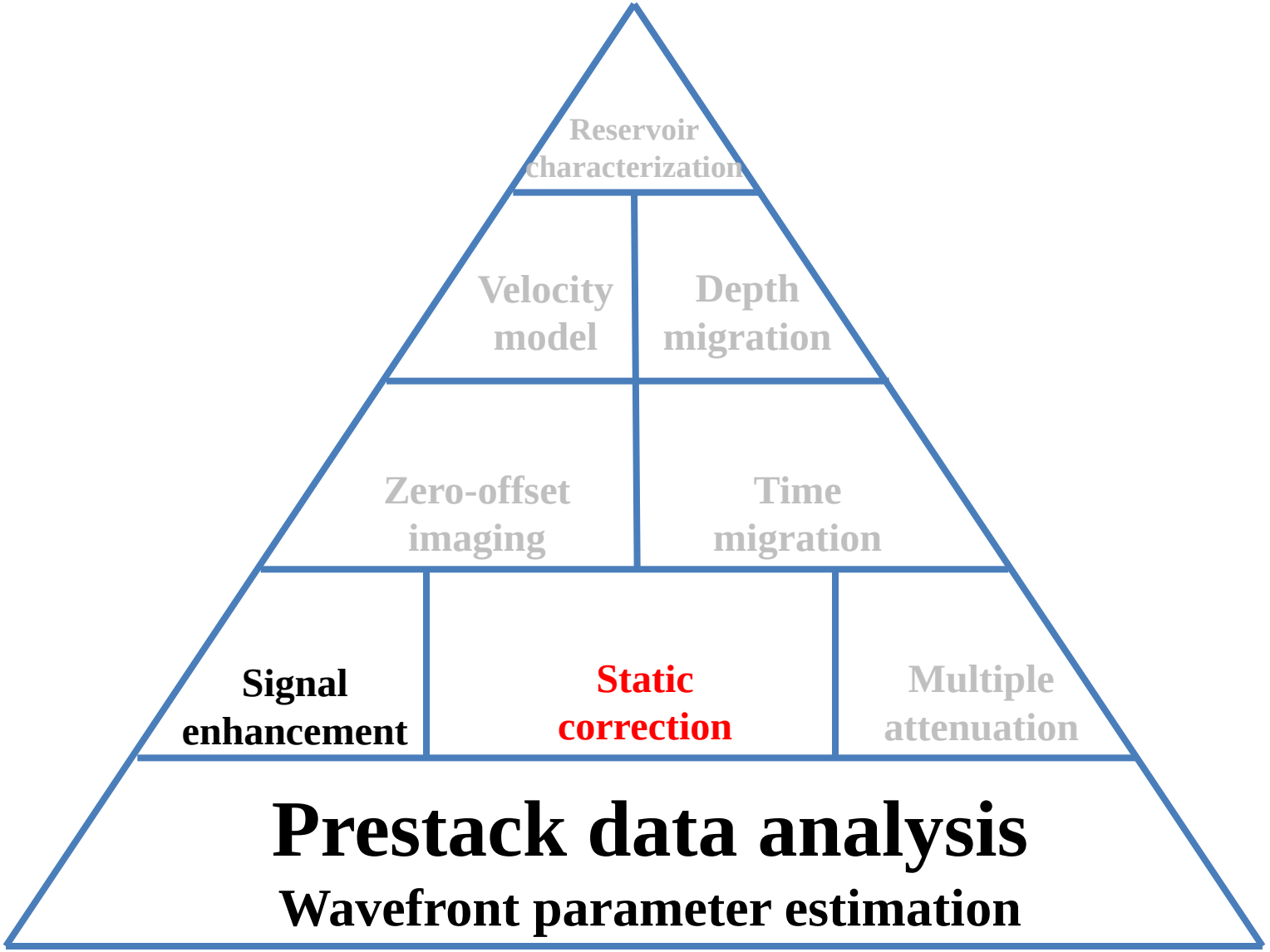

Rugged Topography

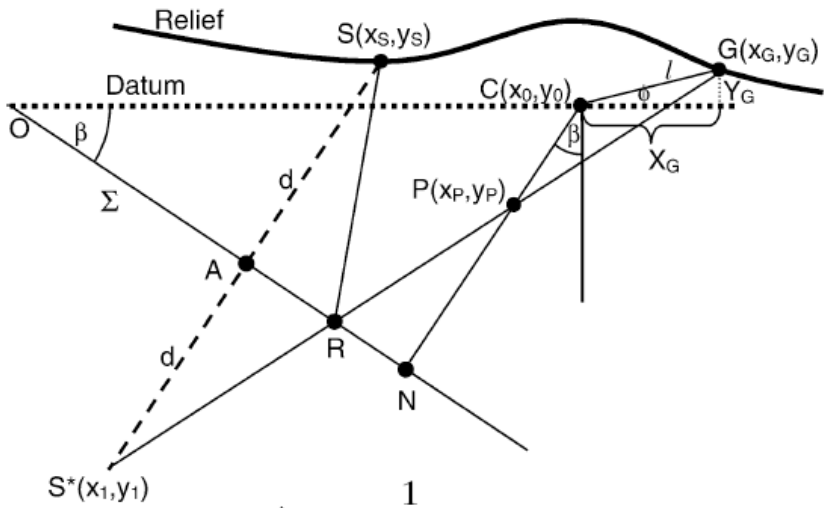

Gurevich et al., 2002

$$\Delta\tau^{-} = \frac{1}{v_0} \times \left[\sqrt{(R^{-})^2 + \left(Y_G^2 + X_G^2\right) + 2(X_G \sin\beta + Y_G \cos\beta)R^{-}} - R^{-}\right].$$

$$\Delta\tau^{+} = \frac{1}{v_0} \times \left[\sqrt{(R^{+})^2 + \left(Y_S^2 + X_S^2\right) + 2(X_S \sin\beta + Y_S \cos\beta)R^{+}} - R^{+}\right]$$

$$\sigma = \frac{X_S - X_G - (Y_S - Y_G)\tan\beta}{X_S + X_G - (Y_S + Y_G)\tan\beta + \dfrac{2(X_S X_G - Y_S Y_G) + (X_S Y_G + X_G Y_S)(\cos^2\beta - \sin^2\beta)}{R_{NIP}}\sin\beta}.$$

RUGGED TOPOGRAPHY

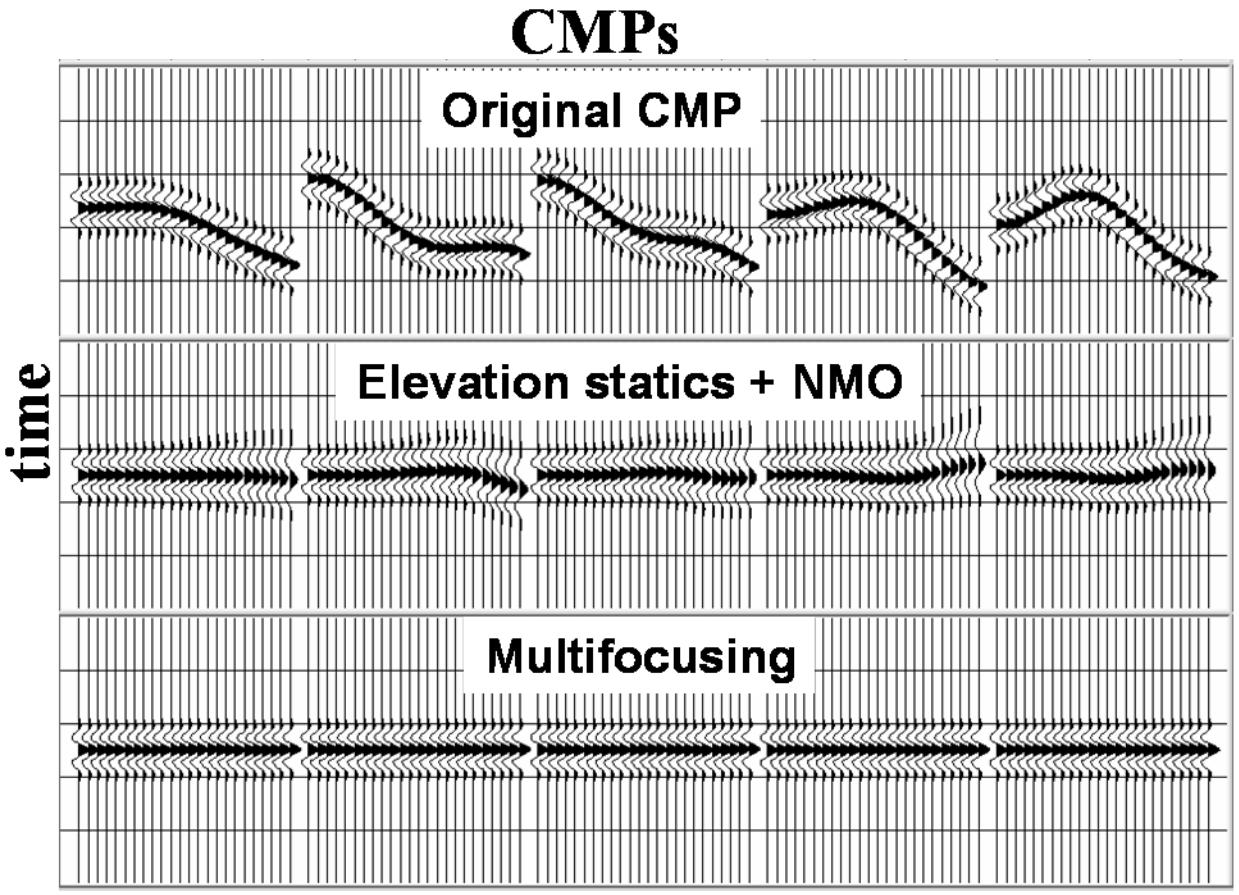

RUGGED TOPOGRAPHY

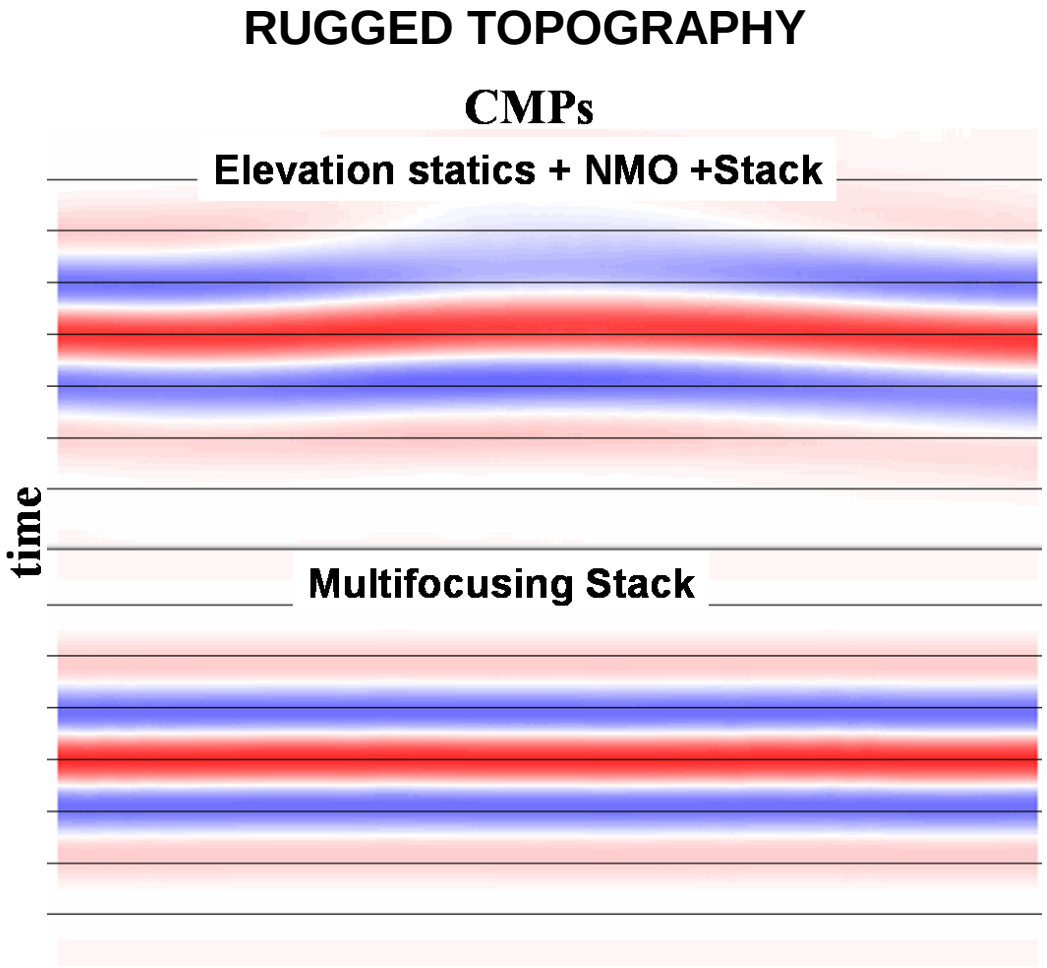

MF

Statics solution

- Multifocusing statics correction solution is based on the surface consistent concept and prestack signal enhancement.
- It overcomes a hyperbolic assumption for arrival traveltimes

MF

Stack with standard statics solution

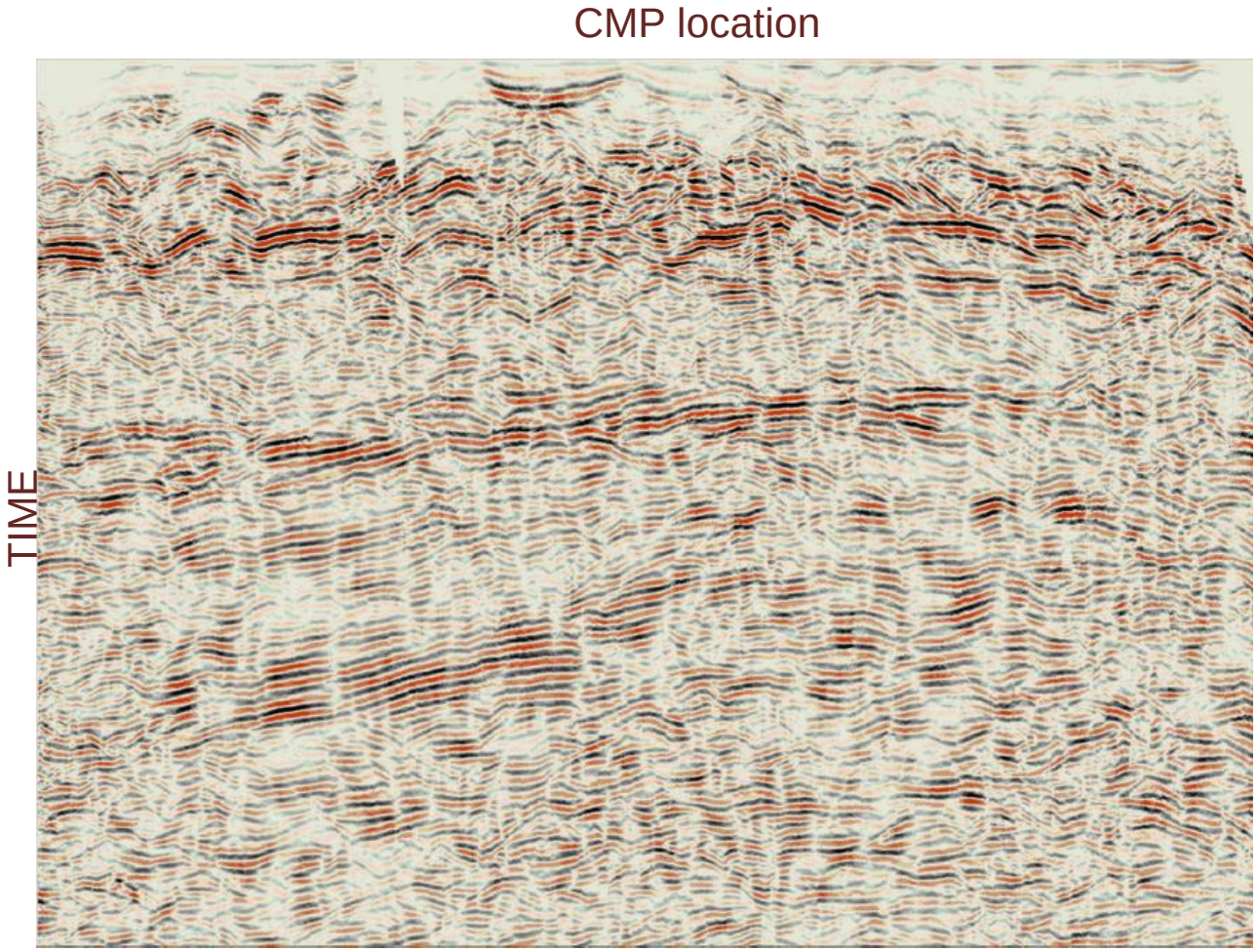

MF

Stack with MF statics solution

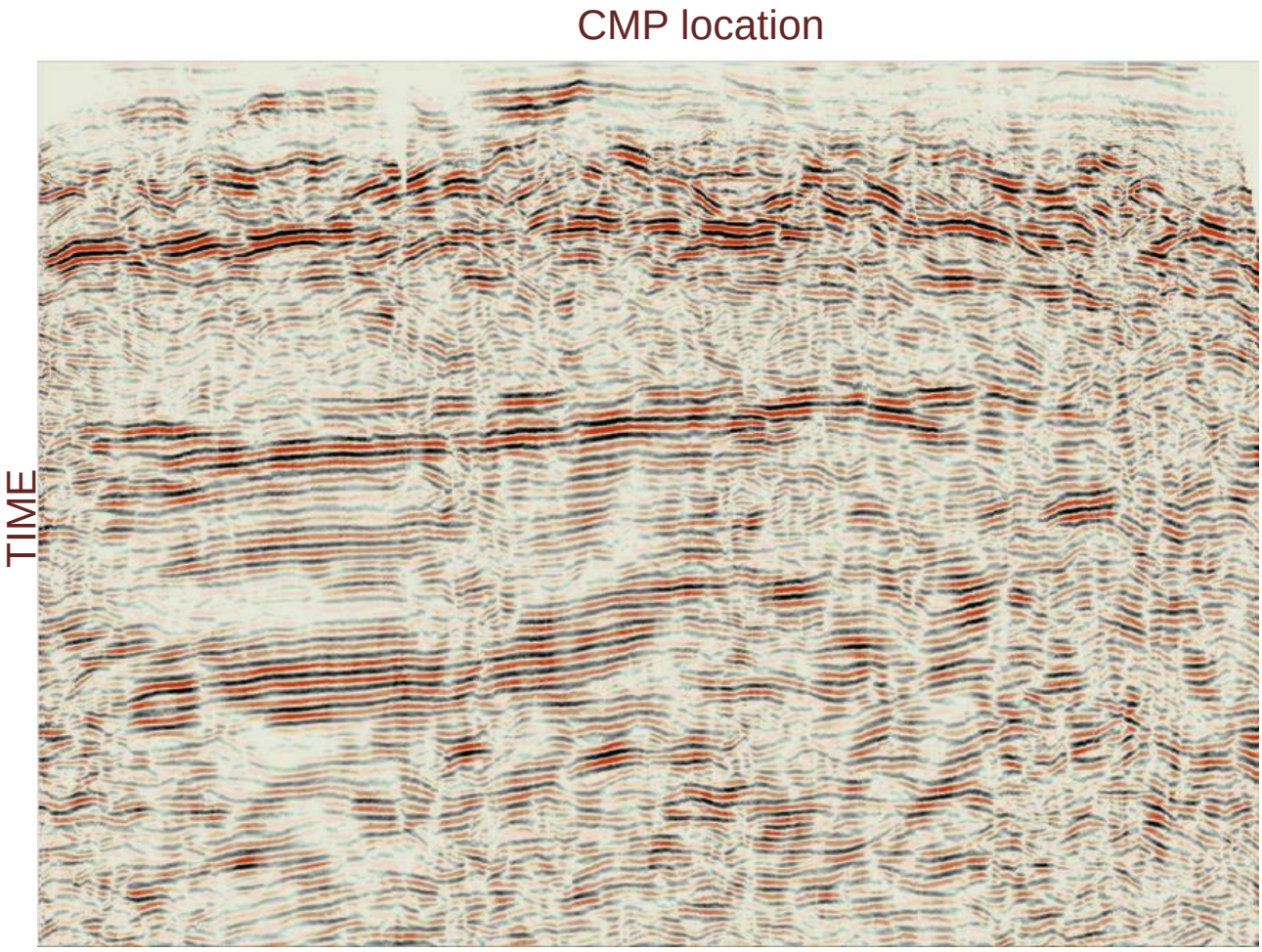

Non-CMP based seismic data analysis, processing and imaging

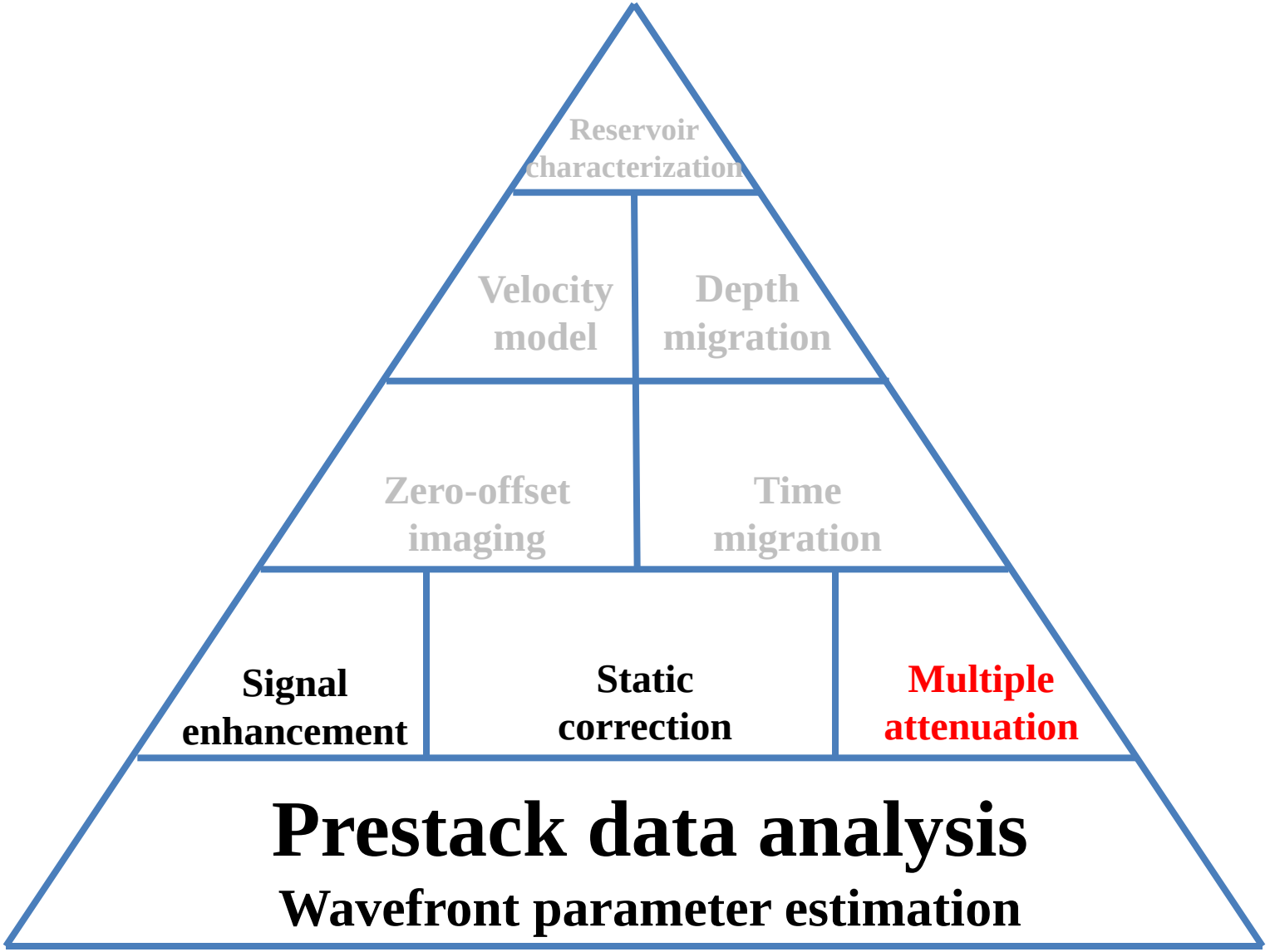

Multiple Attenuation

- The timing of any multiple event, no matter how complicated its raypath, consists of segment that are primary events

- Parameters obtained in prestack wavefield analysis allow prediction and better separation between primary reflections and multiples in the wavefront parameter domain resulting in computing an accurate “multiples model” and better subtraction from the total wavefield

MF

Multiple Attenuation

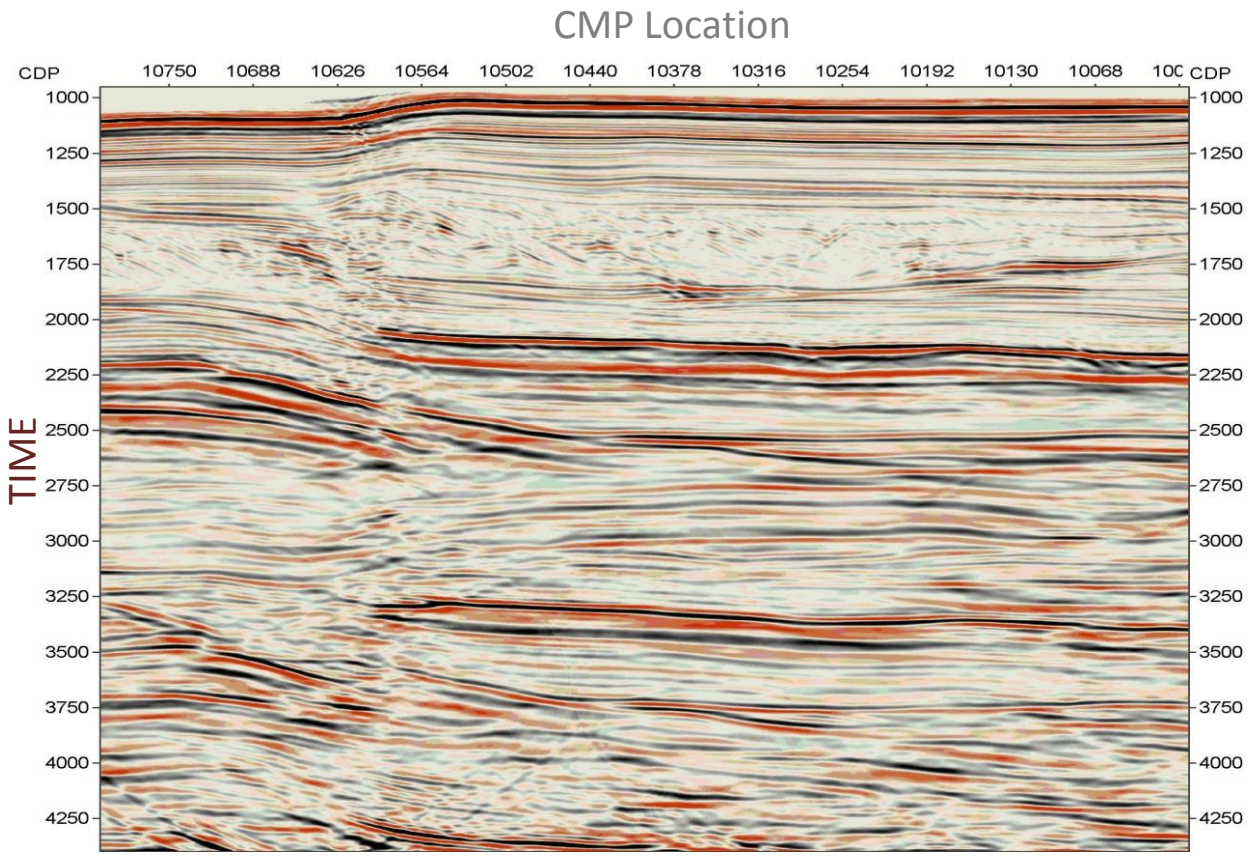

Stacked section

MF

Multiple Attenuation

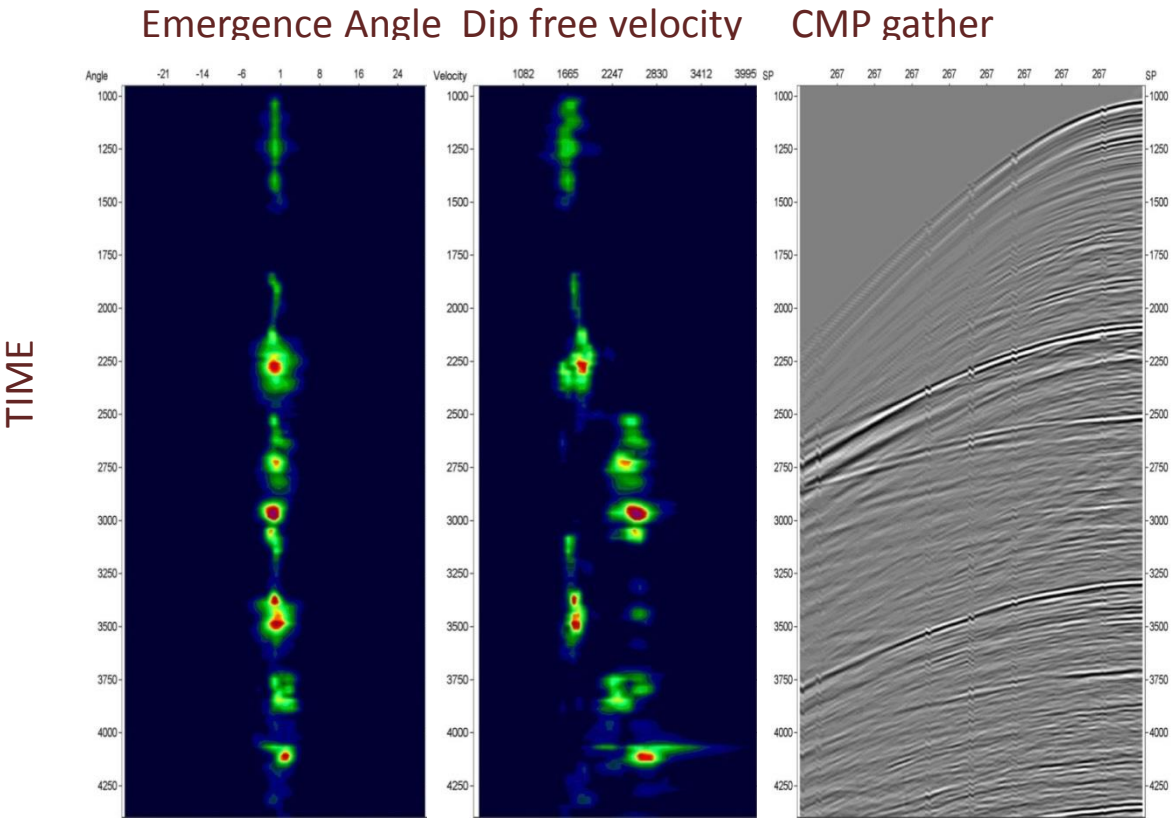

MF

Multiple Attenuation

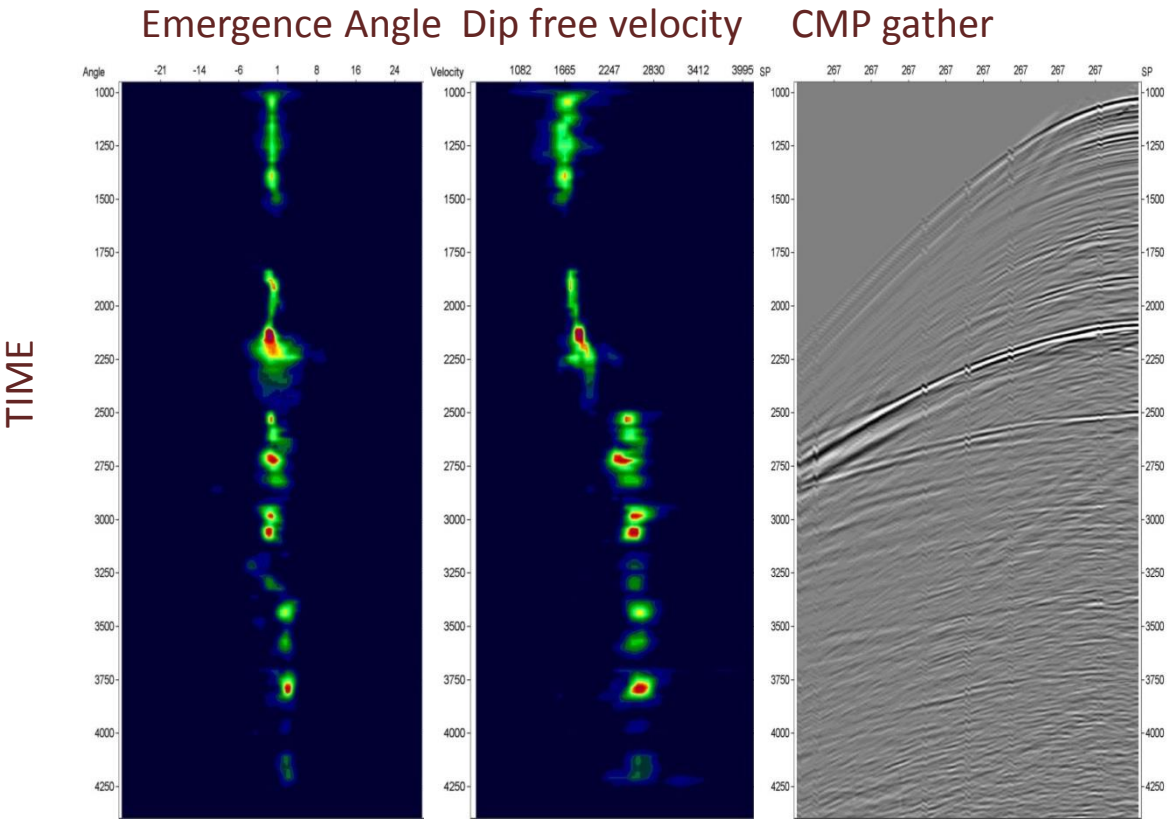

MF

Multiple Attenuation

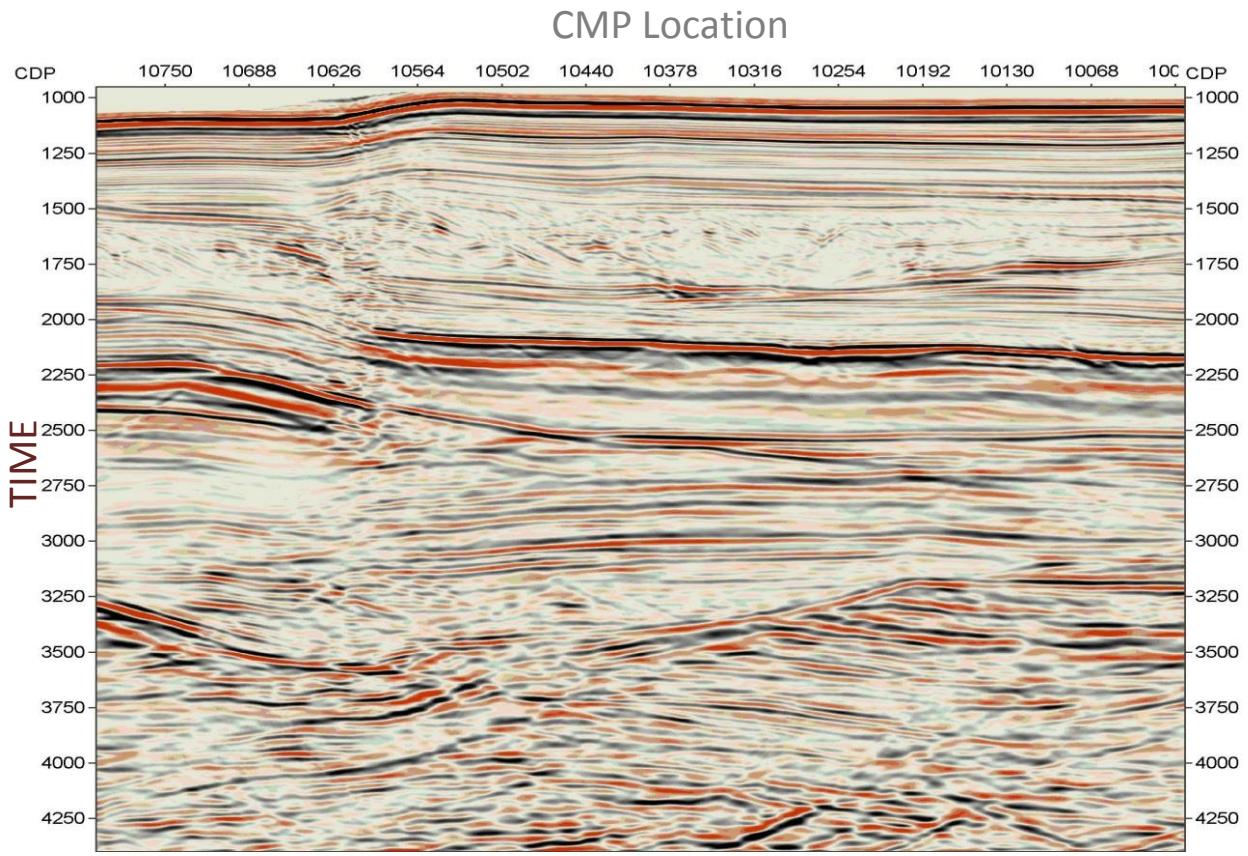

Stacked section after multiple attenuation

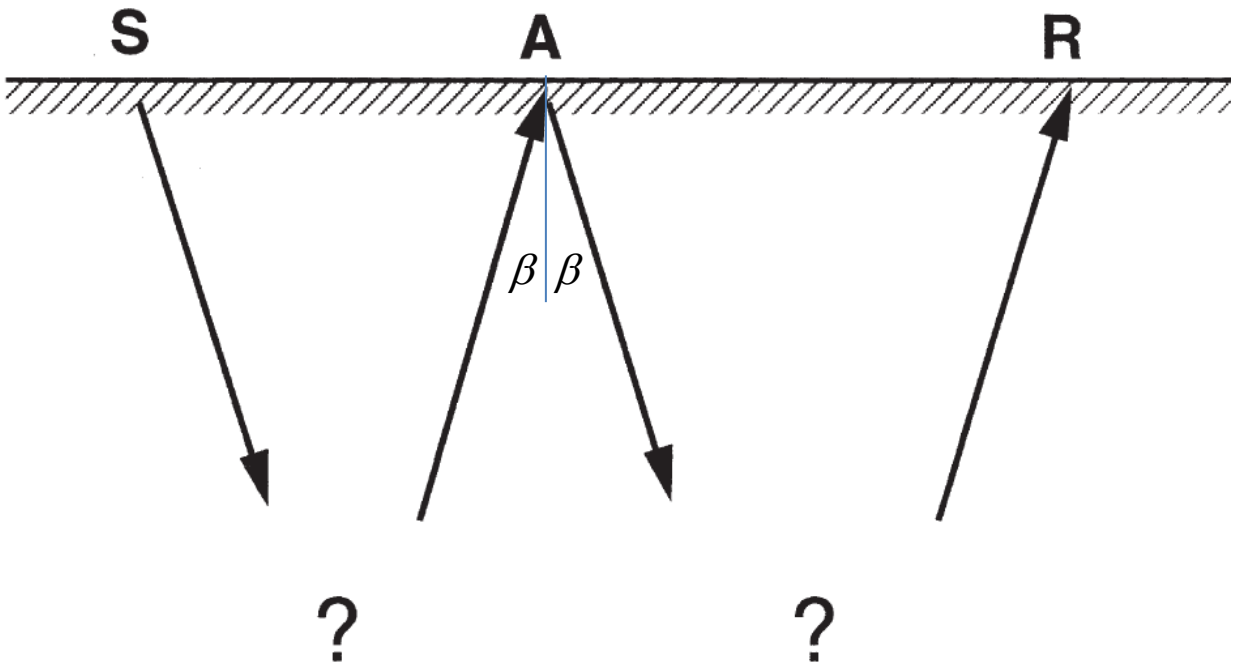

In order to predict multiple SAR from two primaries SA and AR we must find intermediate point A

Multiple attenuation using wavefront characteristics of multiple generating primaries

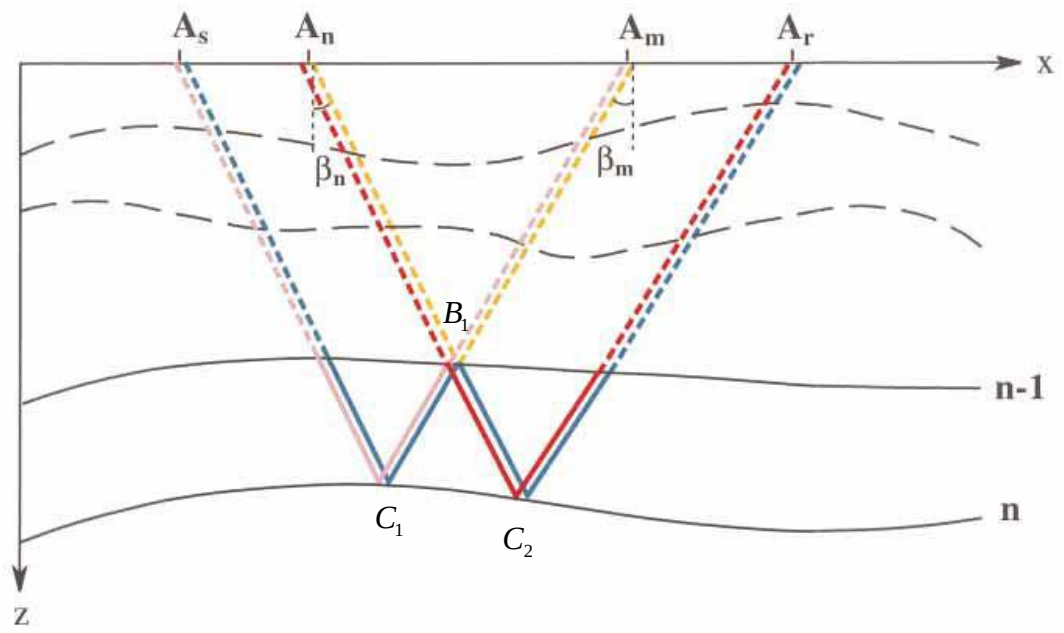

Kinematic properties of multiples. The inter-bed multiple $A_sC_1B_1C_2A_r$, can be represented as a combination of three primary events reflected from the interfaces n — 1 and *n,* namely $A_sC_1A_m$, $A_nC_2A_r$, and $A_nB_1A_m$

$$T_m = T_{p1} + T_{p2} - T_{p3}$$

Thus, to predict the multiple for a given source and receiver positions *As* and *Ar* , we need to find locations of intermediate points *An* and *Am. It* is evident that:

1) The emergence angle, β_m is identical for the wave emitted from source *As* , reflected from the interface n at point C1 and emerging at point *Am* , and the wave emitted from source *A n,* reflected from interface n —1 at point *B*1 and recorded at the same point *Am.*

2) The emergence angle β_n is identical for the wave emitted from source *Ar,* reflected from the interface n at point *C2* and emerging at point *An*, and the wave emitted from source *A*m , reflected from interface n —1 at point *B*1 and recorded at the same point *An.*

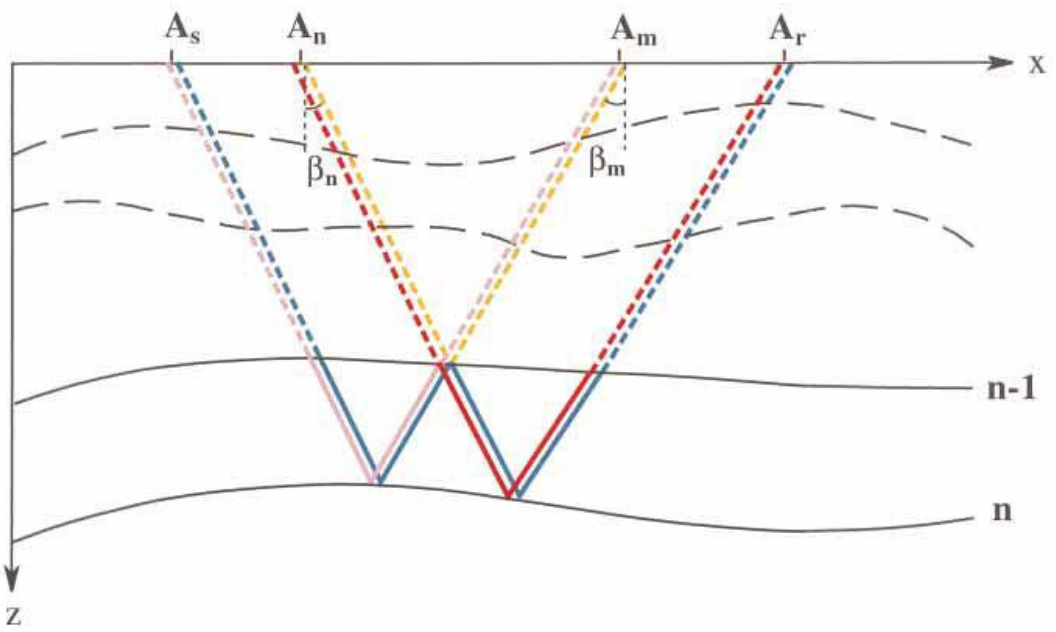

The crucial step in our prediction procedure is the estimation of the angle of emergence of the reflection wavefront.

These conditions ("multiple conditions") are used to determine the segments of primary events generating the multiple. The prediction procedure consists of three steps:

1) The angle of emergence of the primary reflections from multiple generating interfaces is estimated for every trace of each common shot gather

2) For a given source-receiver location, primary reflections that satisfy the multiple conditions are selected (thereby defining the points *Am* and *An, (*in Figure)

3) The arrival times for multiple events are calculated from known primary reflections

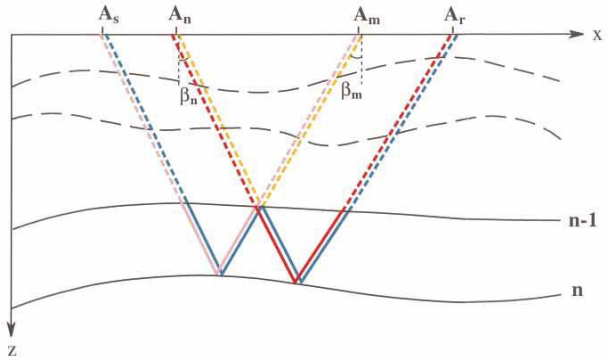

SYNTHETIC EXAMPLE

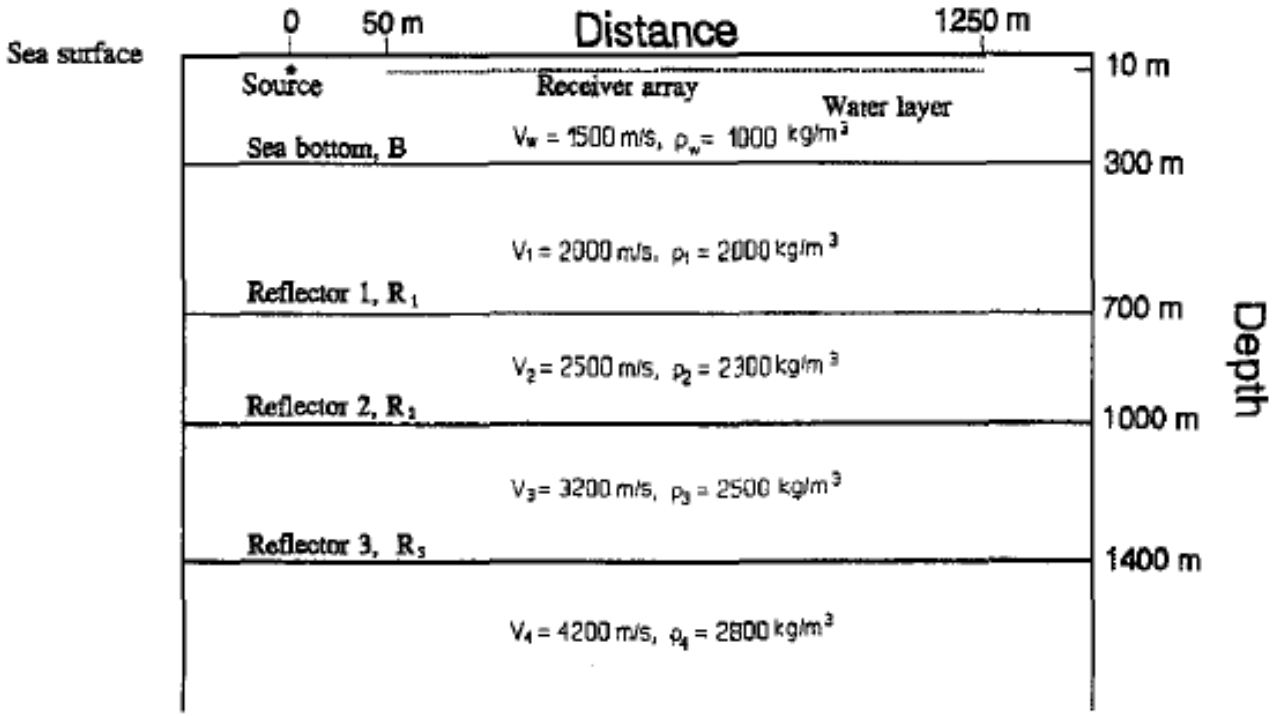

1) For a given multiple code (in our case water-bottom or surface-related peg-legs), the angles of emergence and the radii of wavefront curvatures were estimated for primary reflections for each receiver in the CSP gather. This was done using the wave correlation procedure and local NMO correction.
2) For each shot-receiver pair, the intermediate points participating in the composition of a specified multiple event were determined using the multiple conditions.
3) The traveltimes of the multiples were calculated.

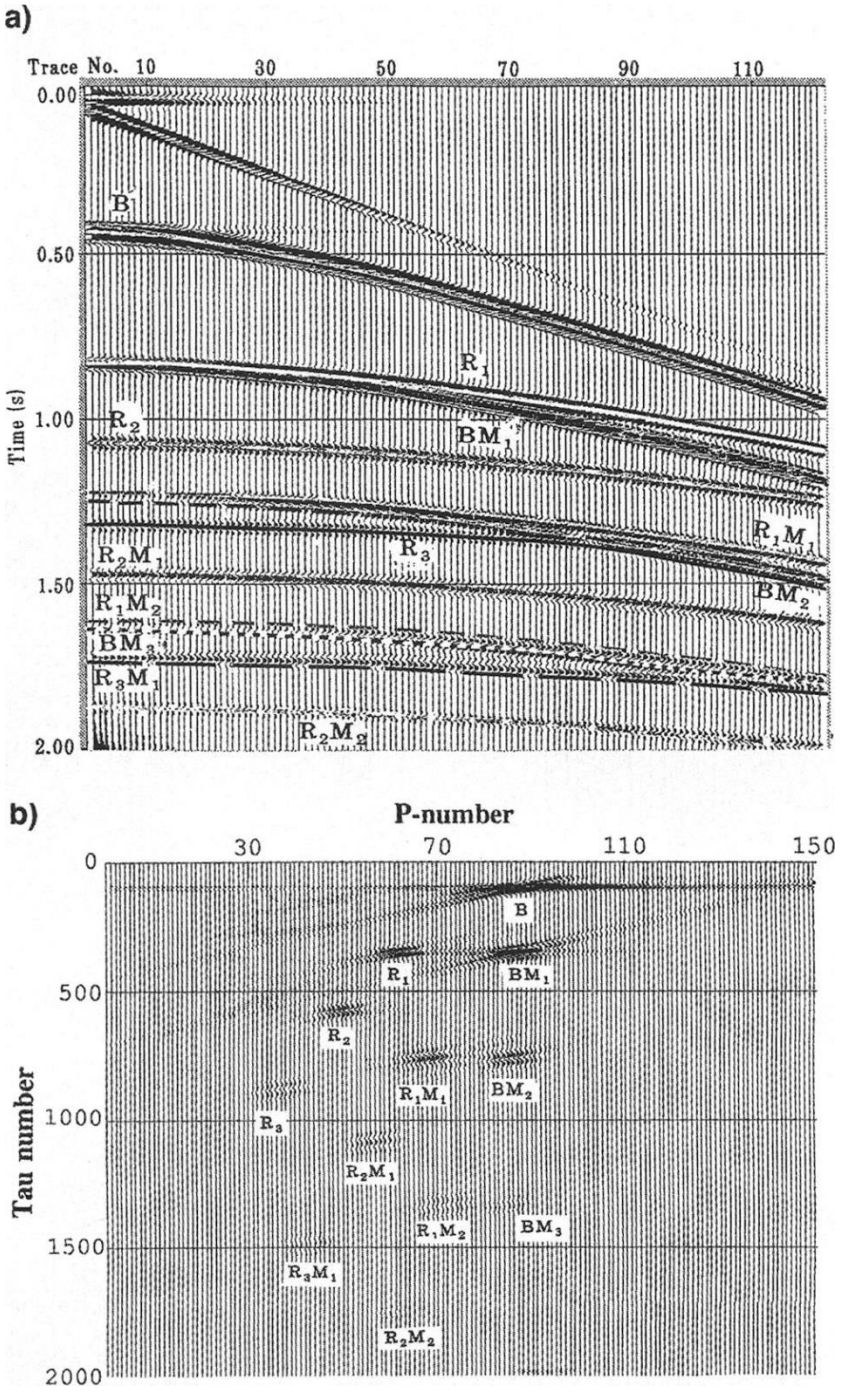

(a) Synthetic CSP gather calculated using the FD method. The primary reflectors, B, R1 , R2 , and R3, are labeled on the gather. The water-bottom multiples of the first, second, third, and fourth orders are labeled *BM, BM2 , BM3 ,* and *BM4 ,* respectively. The symbols R1 M1, *R1M2 ,* and R1M3 represent the first, second, and third order peg-leg multiples from reflector R1 . The peg-leg multiples from R 2 are R2M0 and *R2M2 .* Only the first order multiple R3M1 from R3 can be observed. Multiple traveltimes predicted using our prediction procedure are shown.

(b) the parabolic Radon transform of the seismogram in (a).

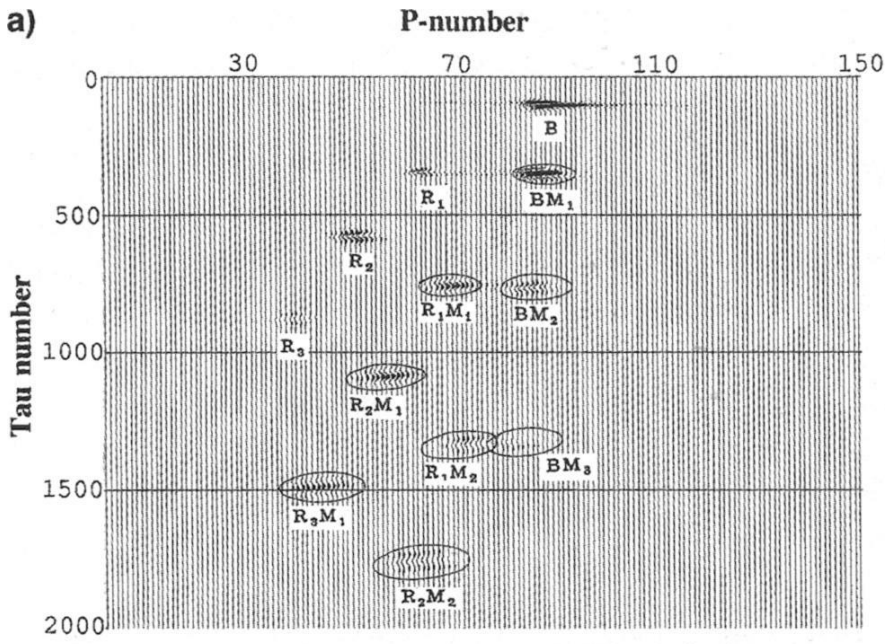

(a) Semblance weighted parabolic *Radon* section calculated for the data set. Results show improved separation of the events. Filter for multiple suppression (muting ellipses) is shown by solid lines.

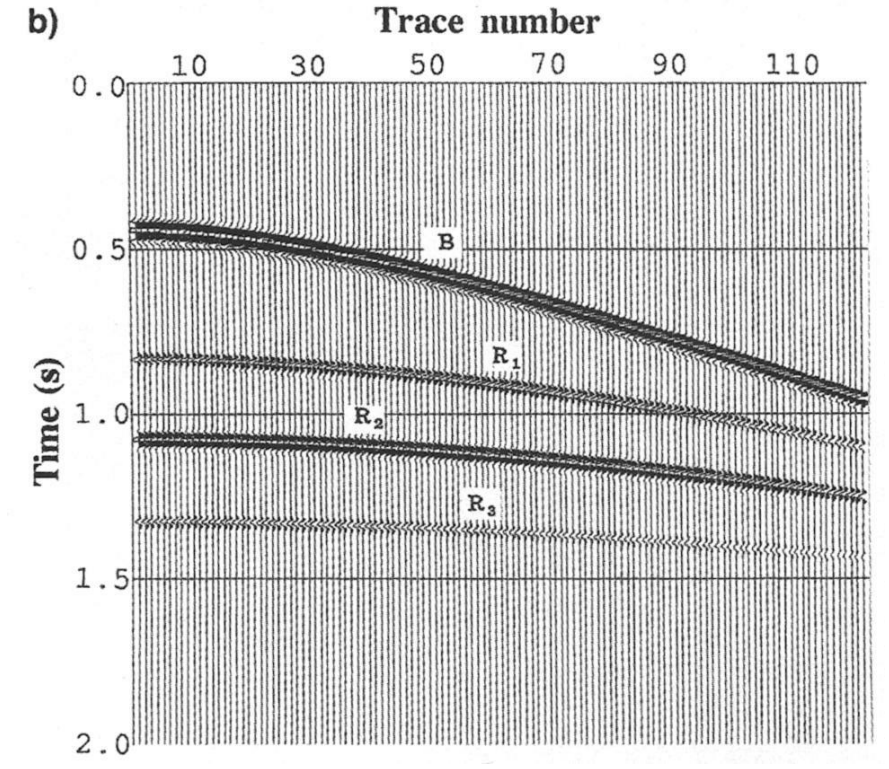

(b) Results of multiple filtering followed by inverse parabolic *Radon* transform.

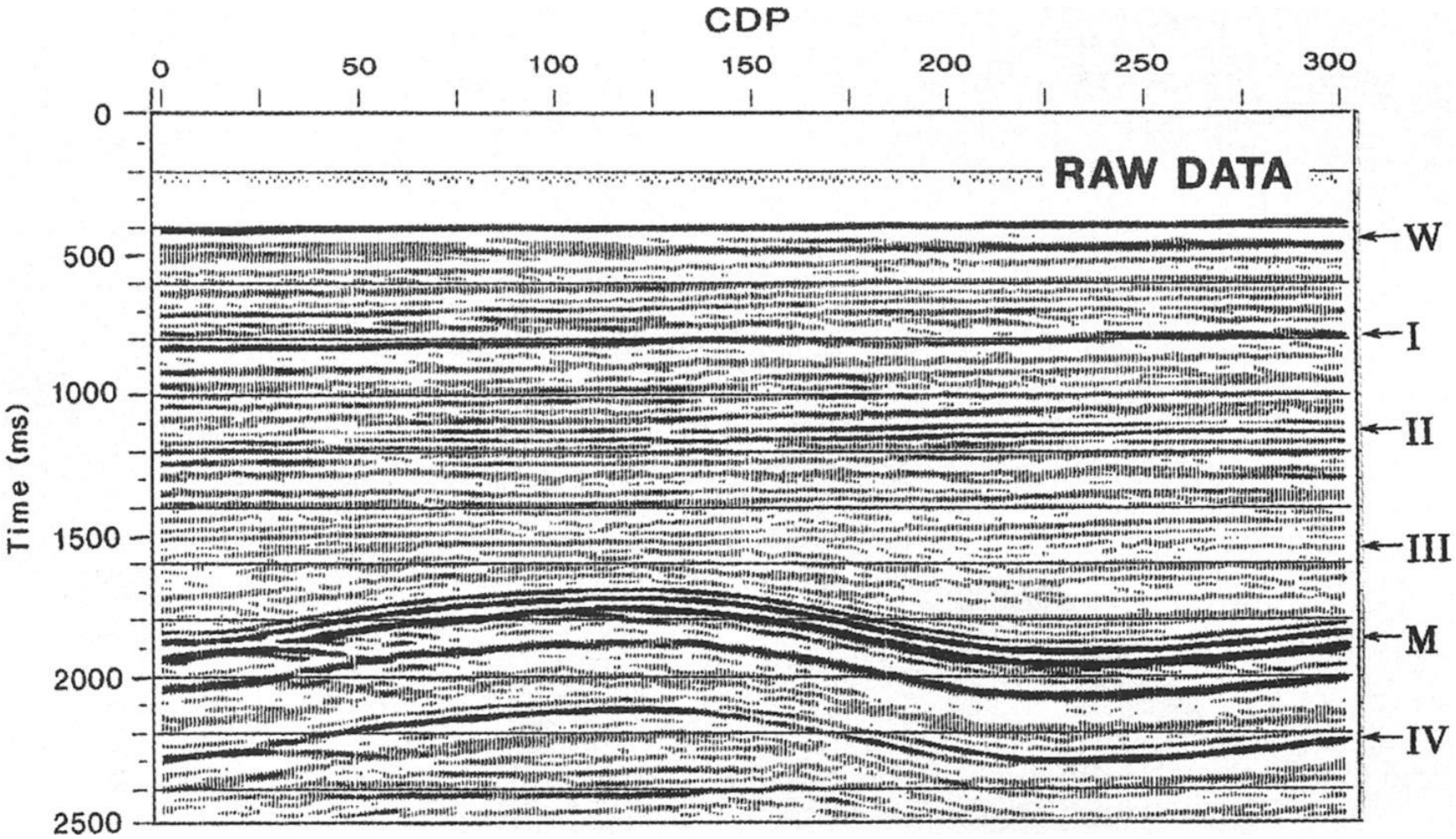

Stacked section containing numerous water-bottom reverberations and multiple reflections. Three orders of water bottom (labeled I, II, and III), and a strong peg-leg (labeled IV) produced by a reflector *M* at about *1.9* s are indicated.

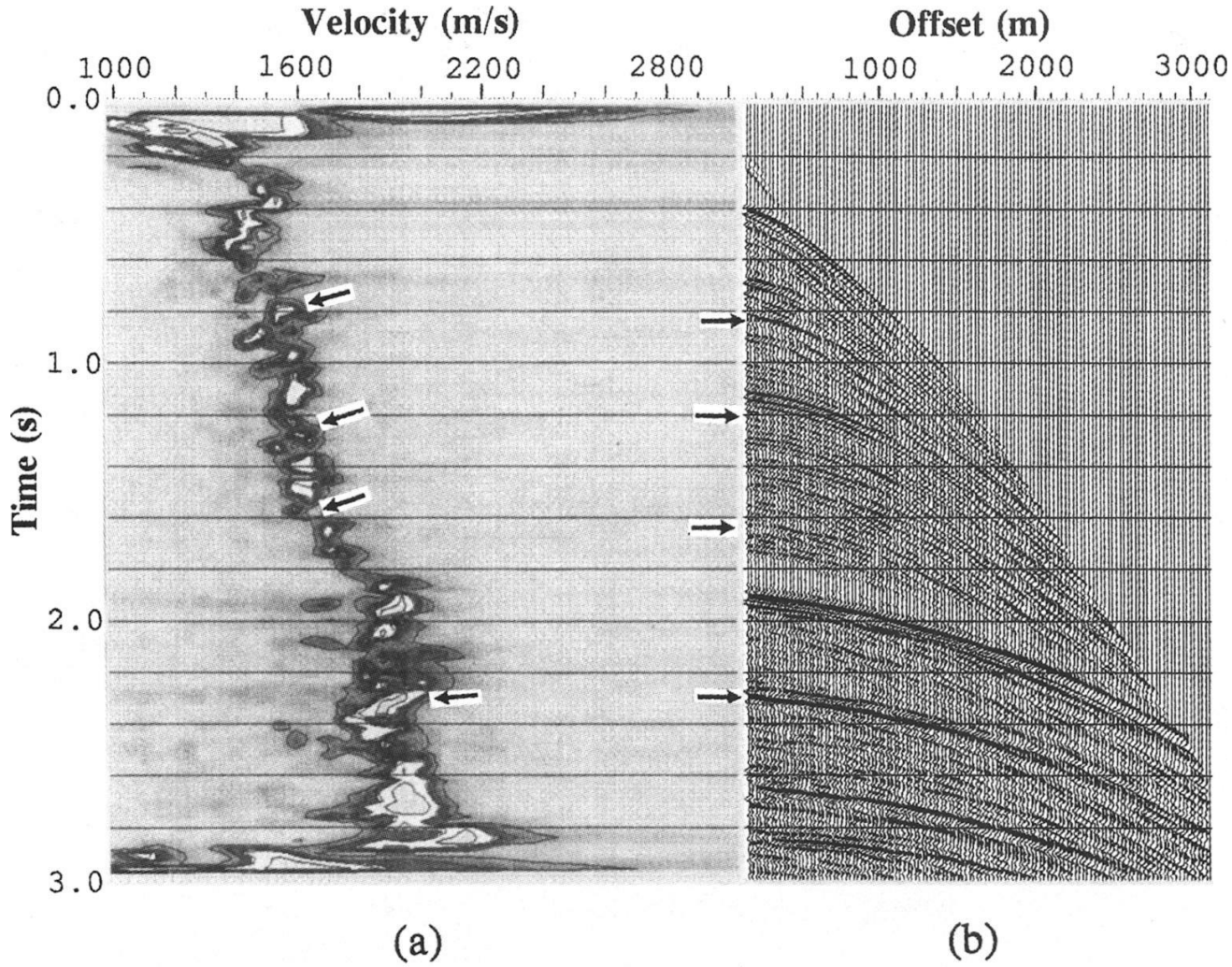

(a) Semblance velocity spectrum. (b) CMP gather acquired in the Mediterranean Sea off Israel. Arrows indicate water-bottom multiples of several orders (times about 0.8, 1.2, and 1.6 s) and a strong peg-leg multiple.

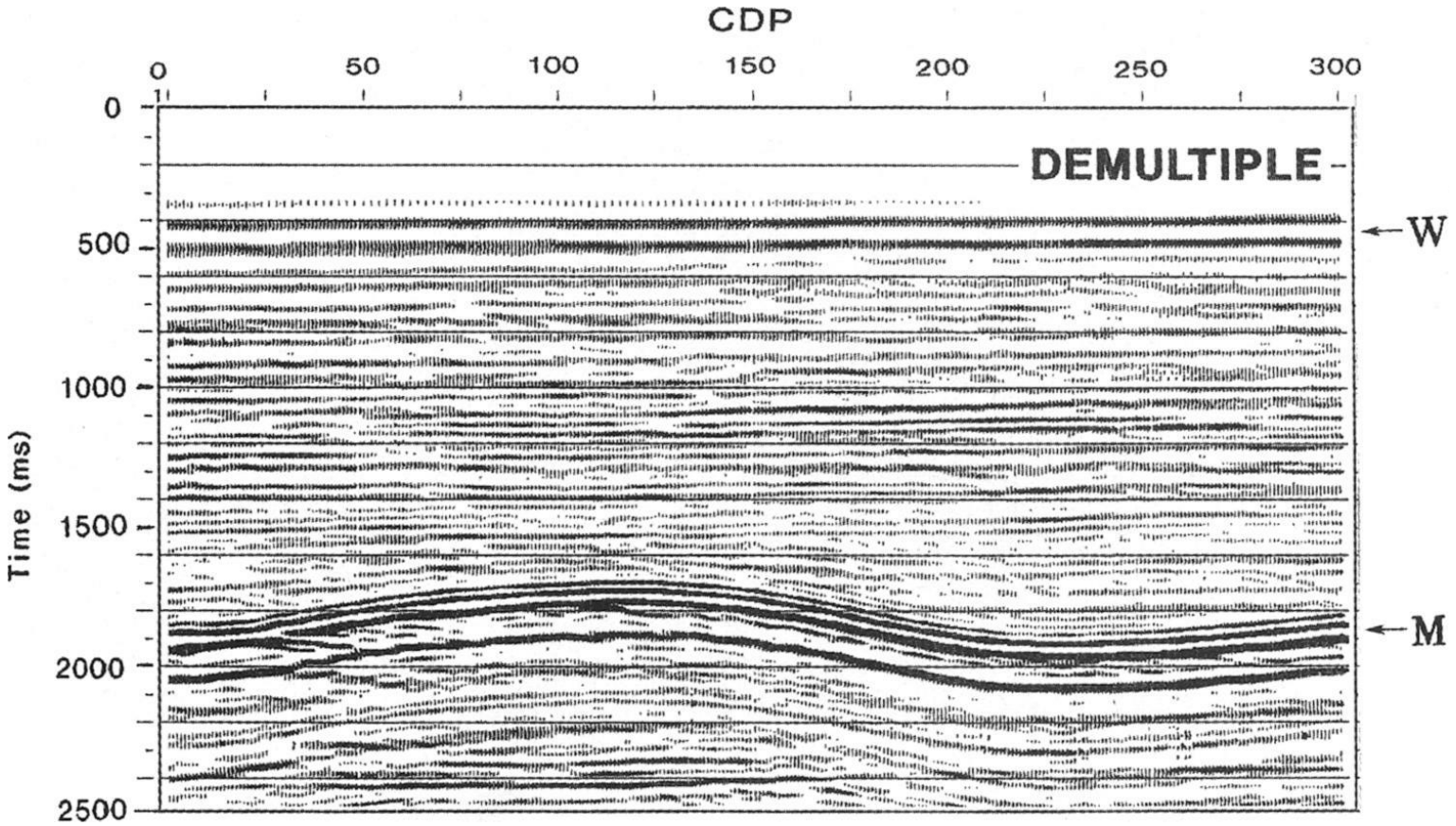

Stacked section after multiple attenuation.

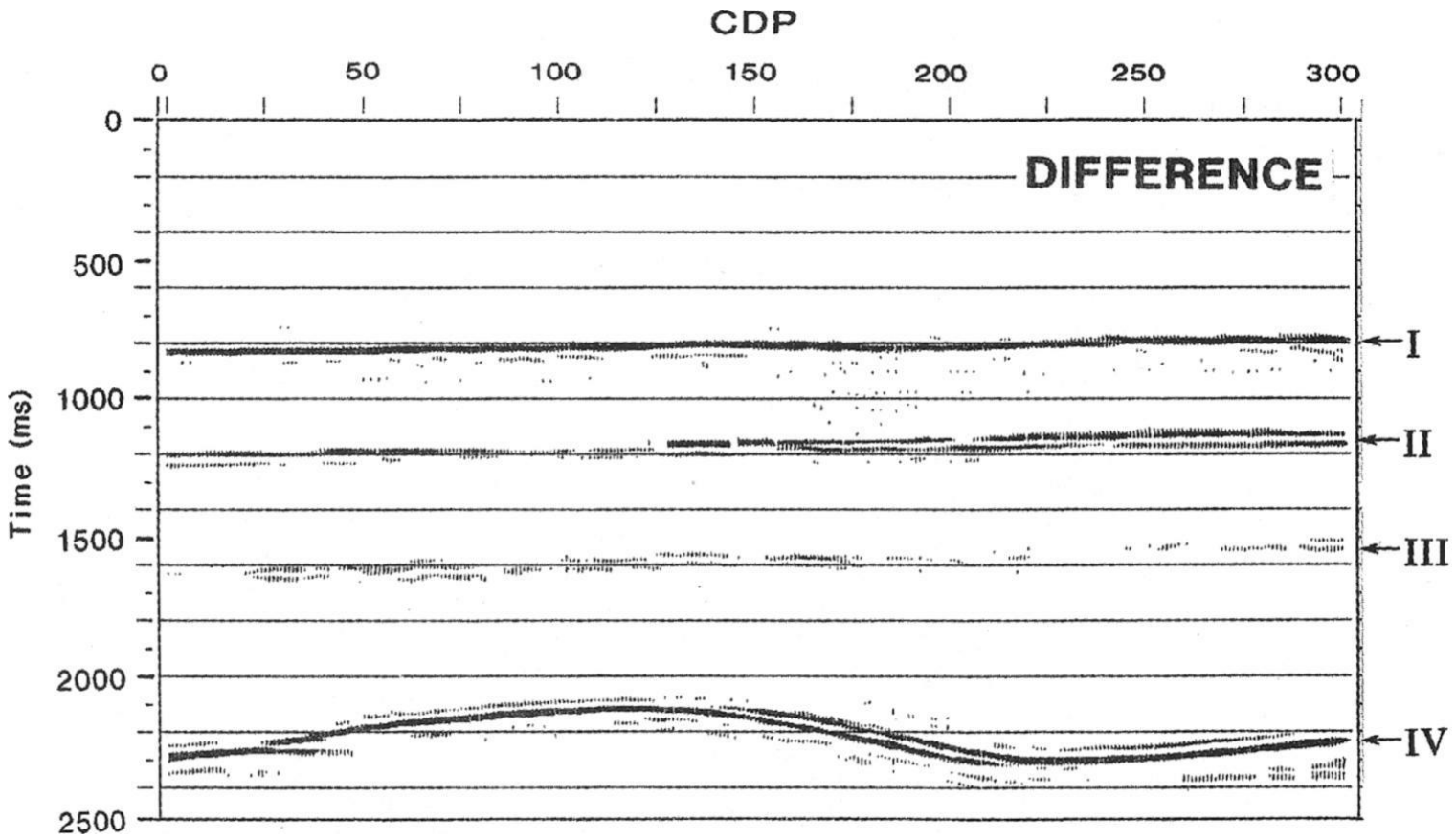

Differential section illustrating exactly what multiple energy has been removed.

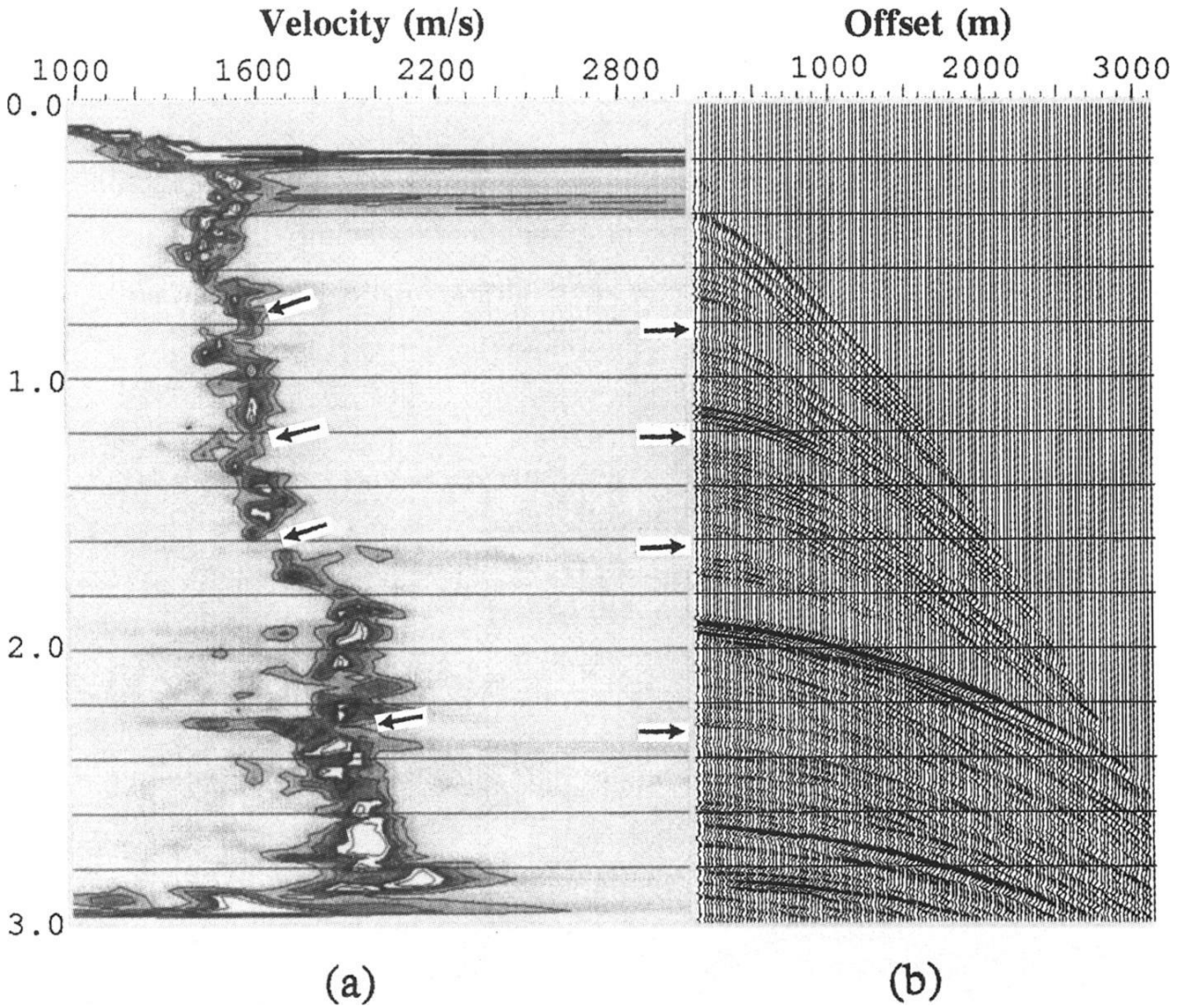

(a) Semblance velocity spectrum after multiple attenuation. (b) CMP gather after attenuation. Arrows indicate places of water-bottom multiples of several orders (times about 0.8, 1.2, and 1.6 s) and a strong peg-leg multiple.

Multiple prediction without prestack data: an efficient tool for interpretive processing

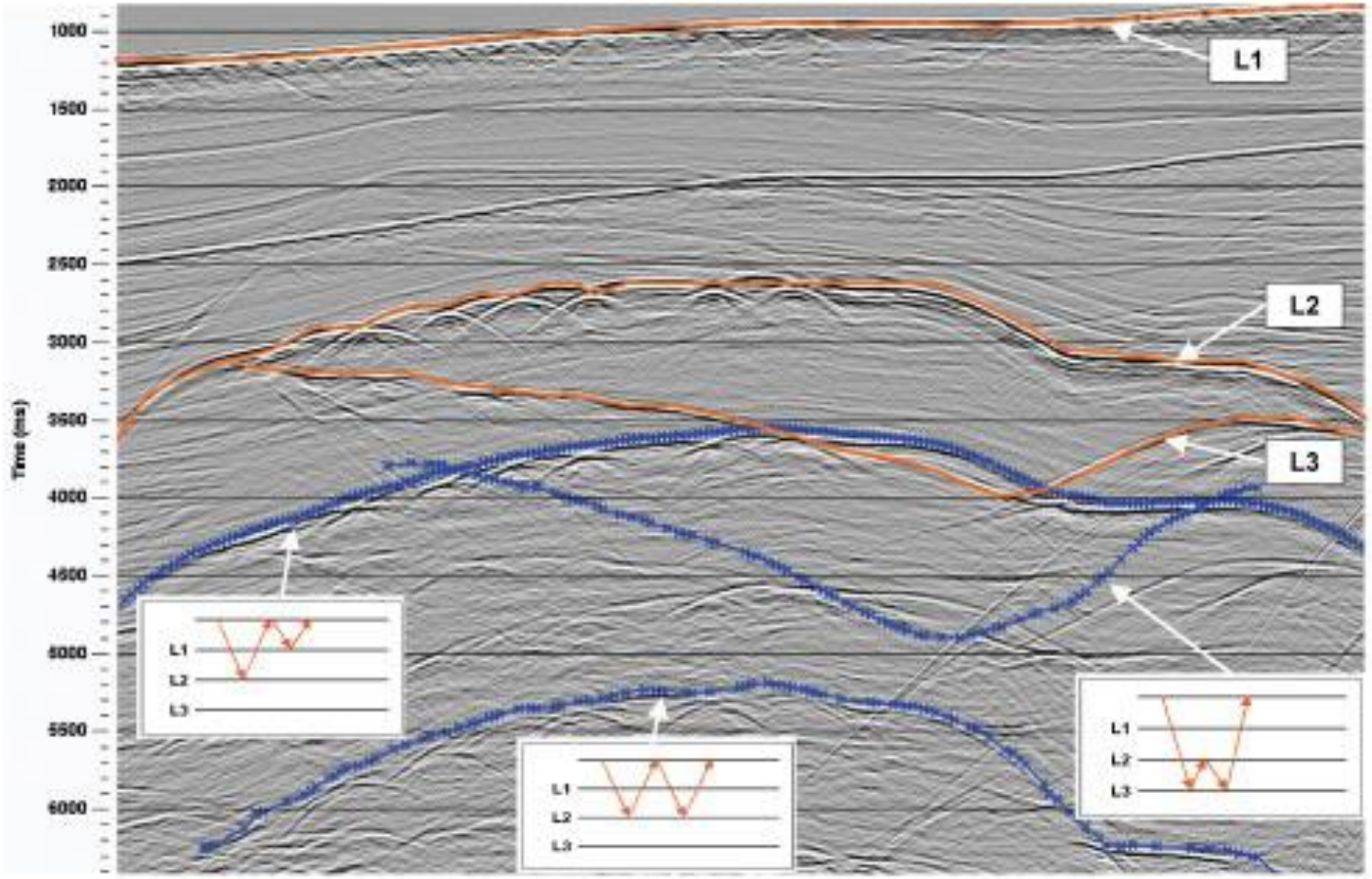

Post-stack multiple prediction. Picked horizons (L1–L3) in red, predicted multiples in blue. Multiple paths are schematically represented in the white boxes.

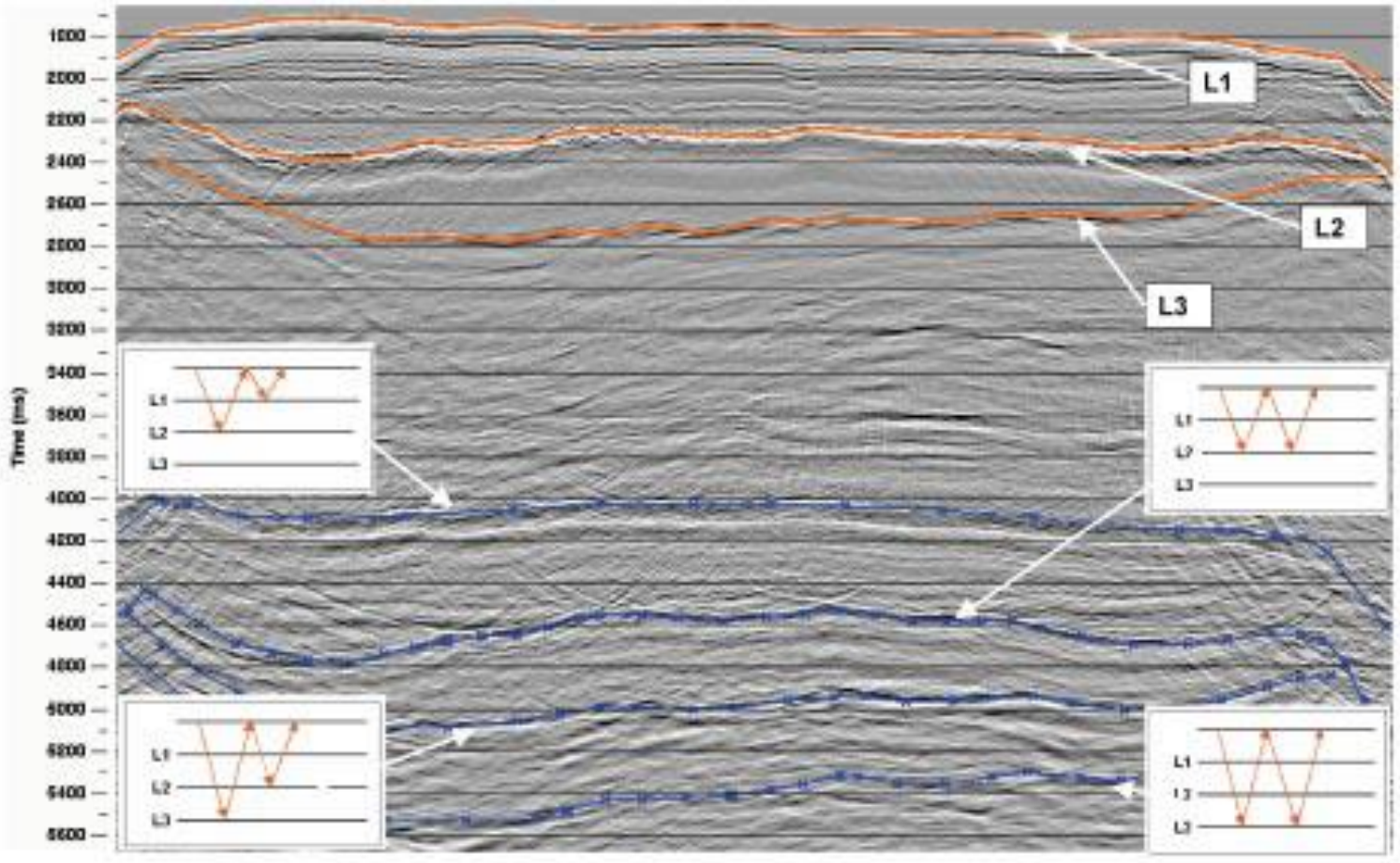

Post-stack multiple prediction. Picked time-migrated horizons L1–L3) in red, predicted (and time-migrated) multiples in blue. Multiple paths are schematically represented in the white boxes.

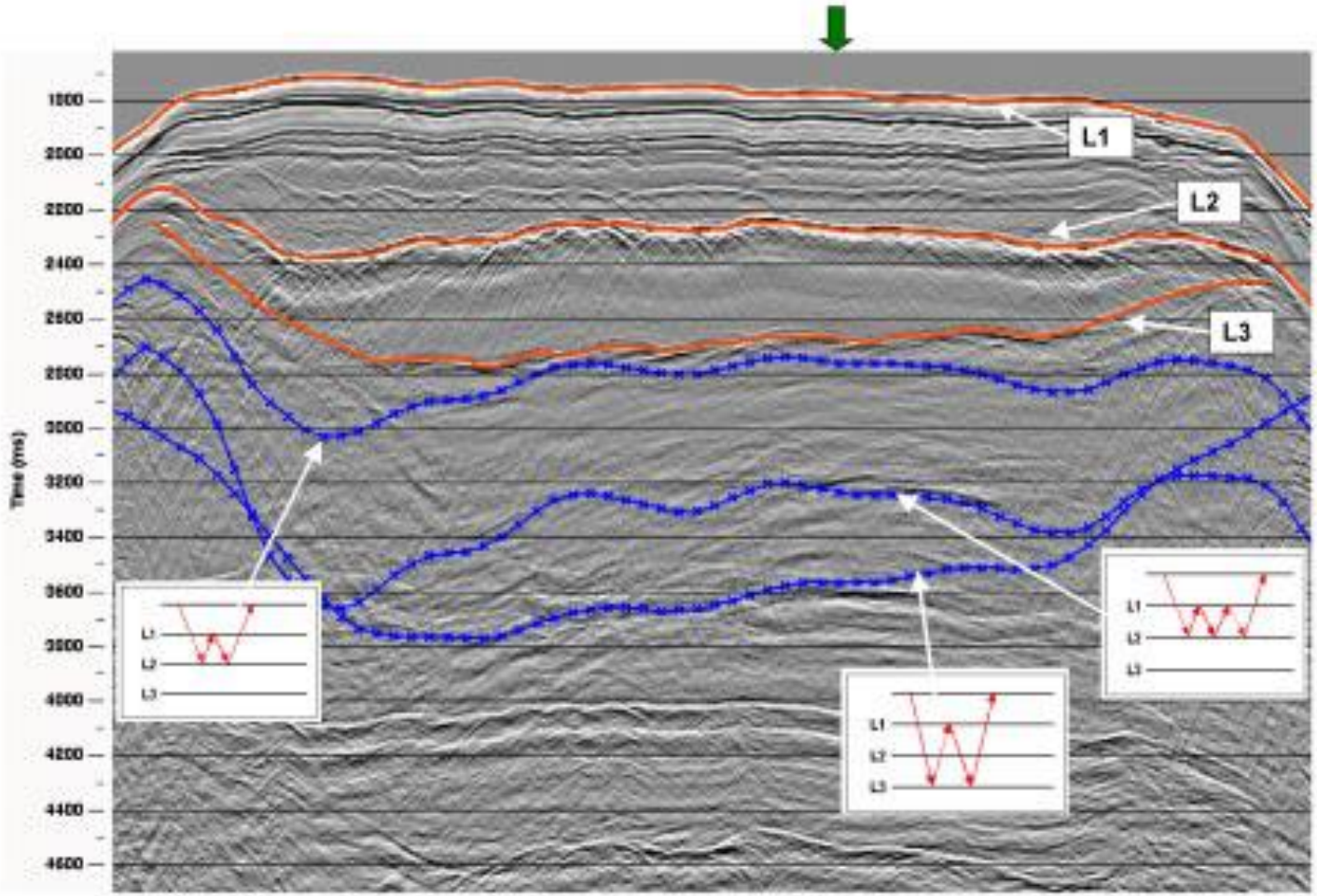

Interbed multiples. Picked horizons (L1–L3) in red, predicted multiples in blue. Multiple paths are schematically represented in the white boxes. The green arrow on top marks the location of the velocity analysis shown in the next slide.

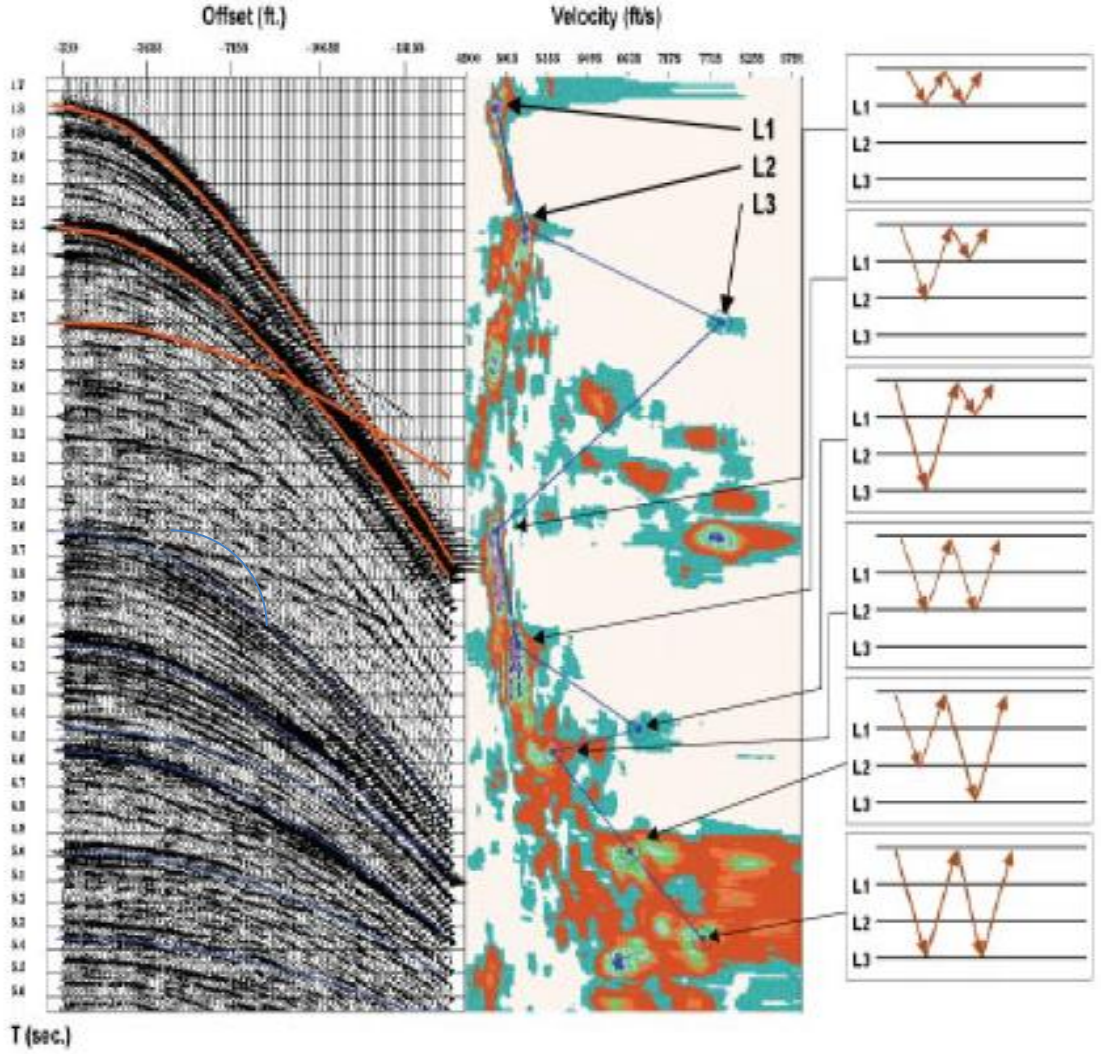

Three primaries and a few predicted surface-related multiples are shown in blue. The multiple paths are graphically represented in the white boxes on the right.

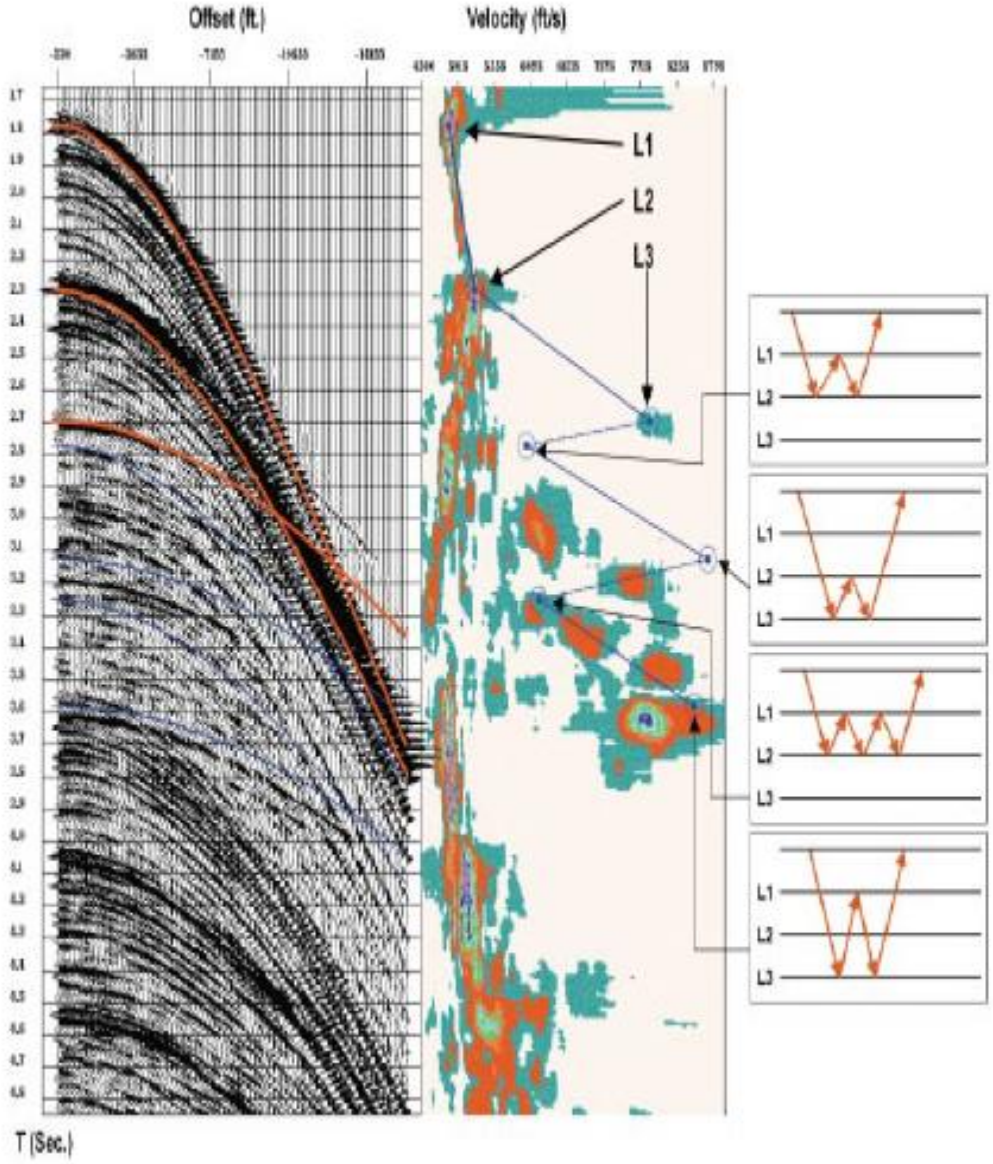

Three primaries and a few predicted interbed multiples are shown in blue. The multiple paths are graphically represented in the white boxes on the right.

3D prediction of surface-related and interbed multiples

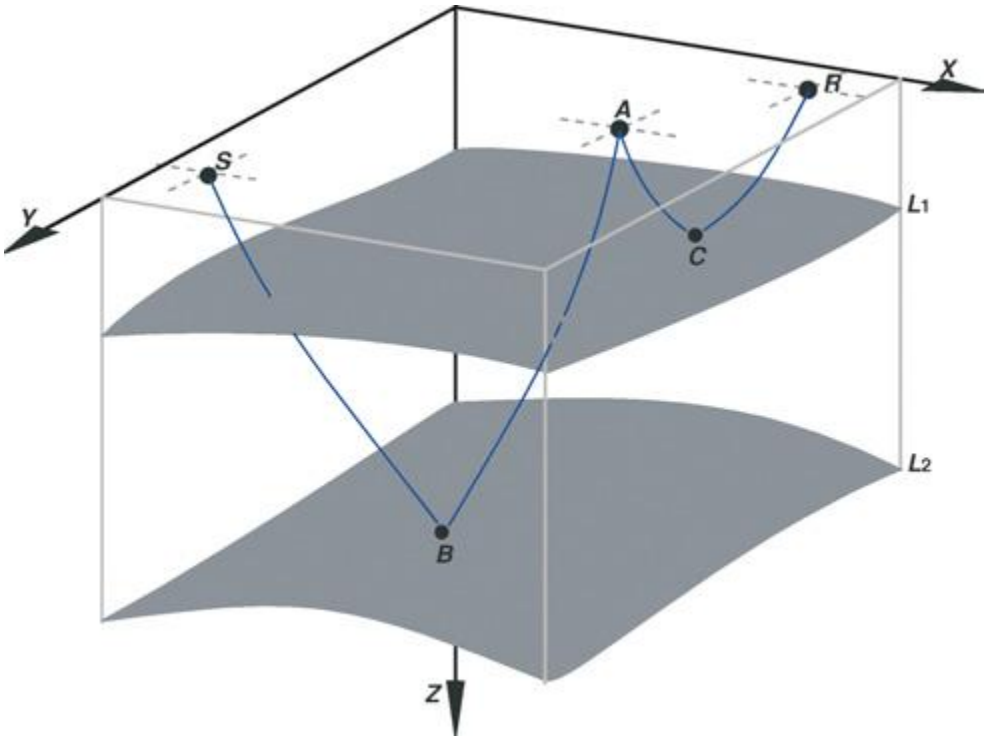

Schematic raypath of a peg-leg multiple for a given shot *S* and receiver *R* pair. The surface reflection point *A* does not have to lie on the line connecting *S* and *R*.

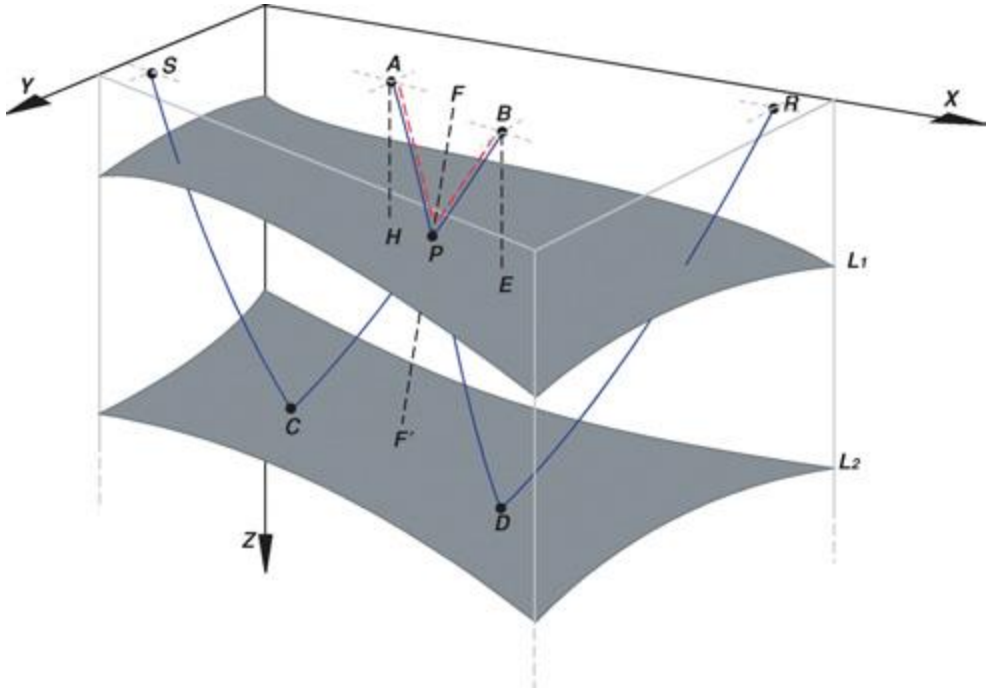

Schematic raypath of an interbed multiple for a givenshot *S* and receiver *R* pair

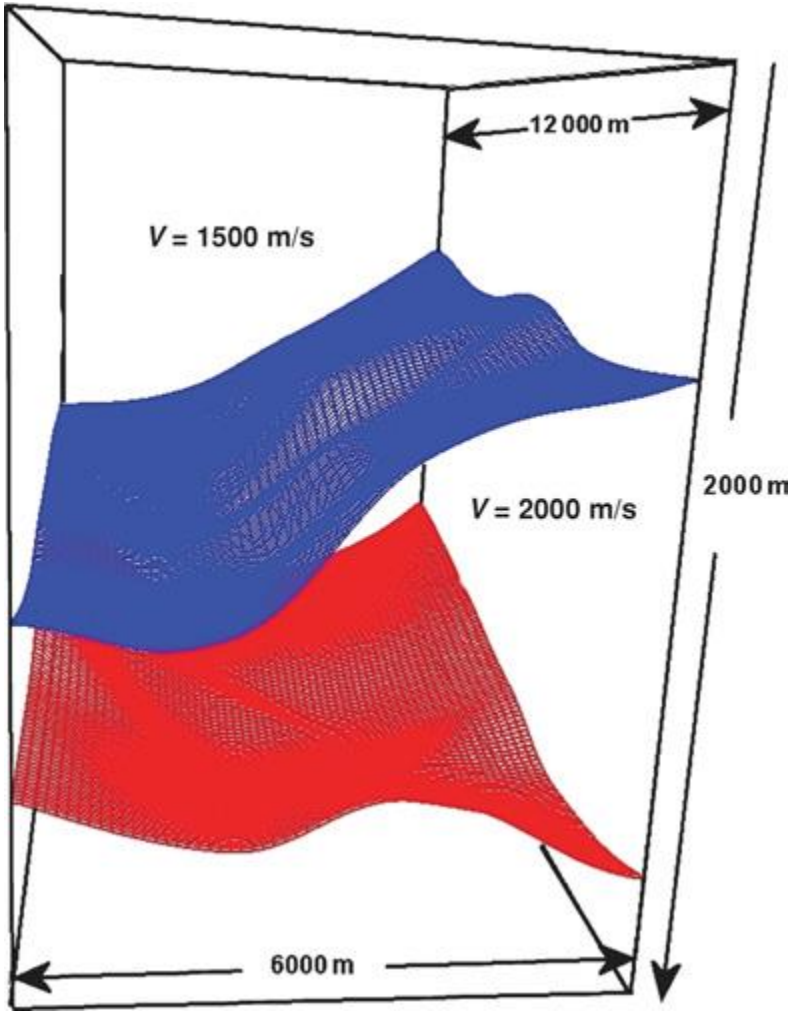

A 3D synthetic model. The horizontal size is 12 × 6 km; 1500 m/s is the velocity *V* above the first interface, 2000 m/s is the velocity between the first and second interfaces, and 2500 m/s is the velocity in the lower half-space.

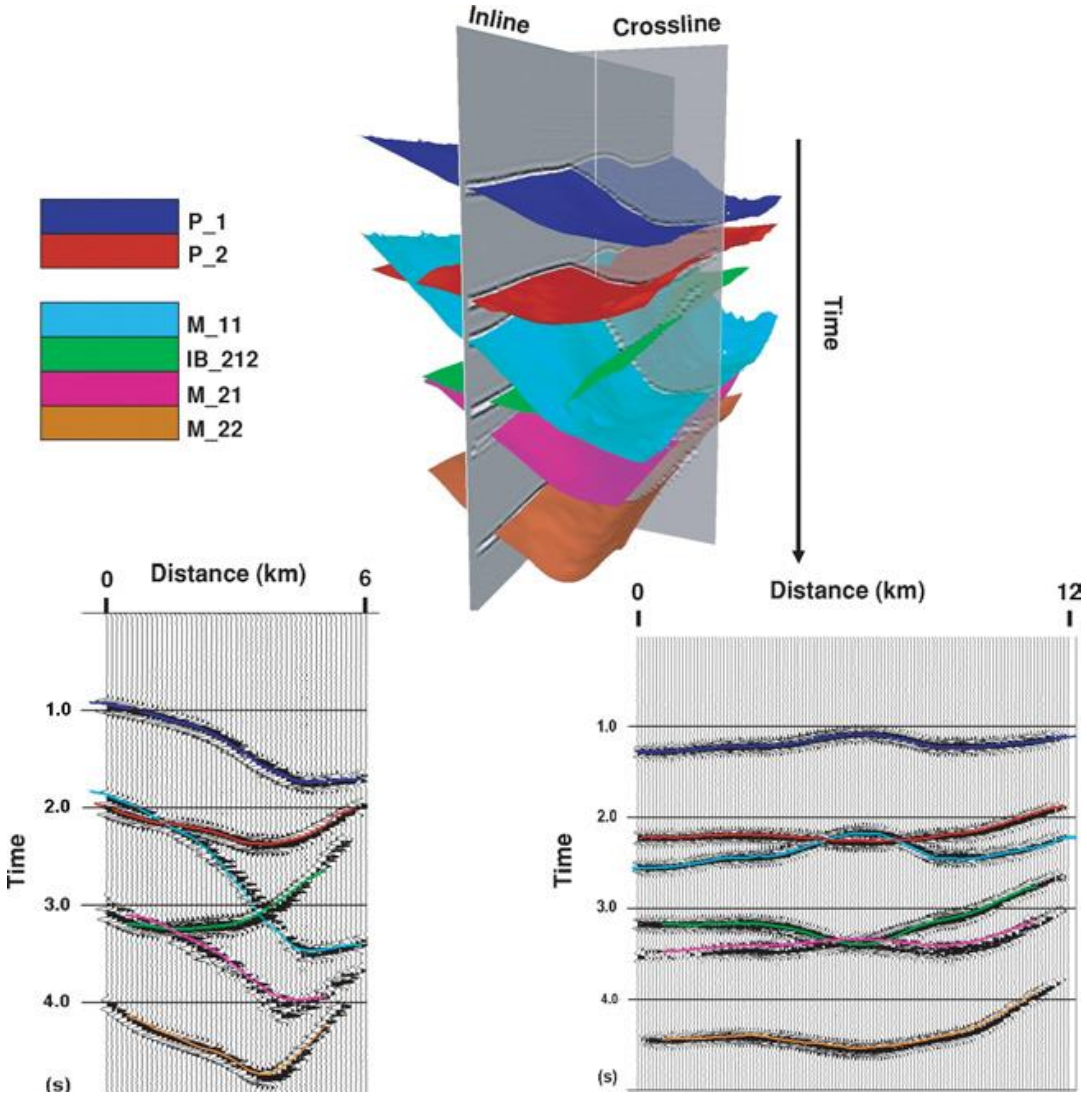

Multiple prediction, synthetic example. (Top) A 3D view of the two primaries and four predicted multiples. (Bottom) Inline and crossline displays from the central part of the cube. The picked primaries and the predicted multiples are color coded according to the table on the upper left

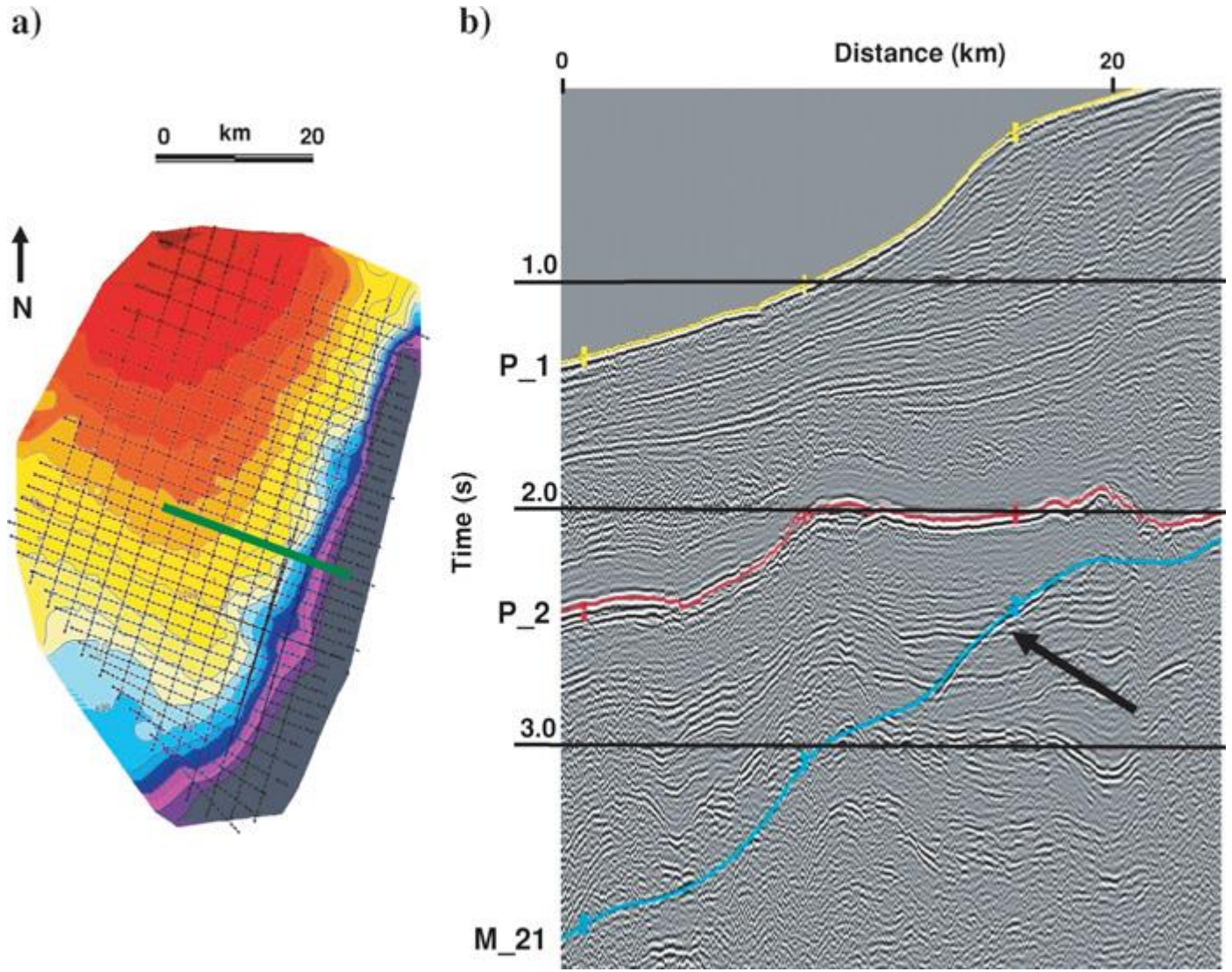

Three-dimensional multiple prediction from a 2D survey. (a) Survey map showing the 2D acquisition pattern overlain by a *T*0 map of the first primary reflector.
(b) Portion of a 2D line [location marked by the green line on (a)], showing two picked primaries (*P* 1 and *P* 2) and a predicted peg-leg (*M* 21). The arrow points to significant multiple energy in the section.

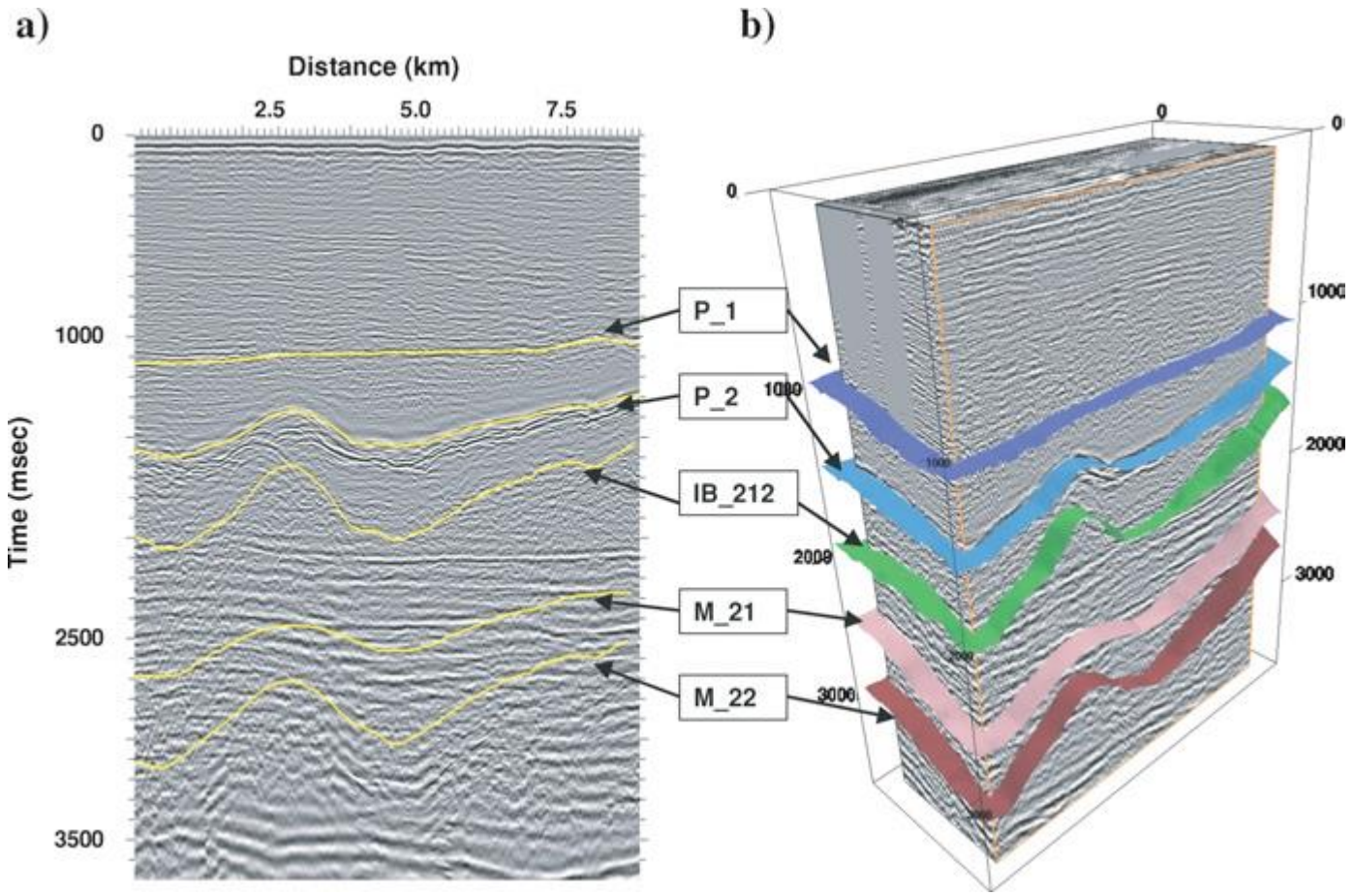

Marine data QC. (a) Two primaries (*P* 1 and *P* 2), two surface-related multiples (*M* 21 and *M* 22), and an interbed multiple (*IB* 212) are shown on top of a central inline taken from a stacked cube (b). No coherent events exist along the predicted multiples' horizons.